Aus der Klinik für Strahlentherapie

Direktorin: Frau Prof. Dr. med. R. Engenhart-Cabillic

des Fachbereichs Medizin der Philipps-Universität Marburg

Titel der Dissertation:

Optimization of high precision stereotactic body radiotherapy with photons and ions for non-small cell lung cancer

Inaugural-Dissertation zur Erlangung des Doktorgrades der Medizinwissenschaften

(Dr. rer. med.)

dem Fachbereich Medizin der Philipps-Universität Marburg

vorgelegt von

Alina Santiago García

aus Ávila, Spanien

Marburg 2016

Angenommen vom Fachbereich Medizin der Philipps-Universität Marburg am:

Gedruckt mit Genehmigung des Fachbereichs.

Dekan: Herr Prof. Dr. H. Schäfer

Referentin : Frau Prof. Dr. A. Wittig

1. Korreferent: Herr Prof. Dr. W. Sauerwein

2. Korreferent: Herr Prof. Dr. A. Burchert

Die vorliegende kumulative Dissertation stellt eine Zusammenfassung der Forschungsergebnisse dar, welche wie folgt in Fachzeitschriften publiziert wurden:

[1] **Santiago A**, Jelen U, Ammazzalorso F, Engenhart-Cabillic R, Fritz P, Mühlnickel W, Enghardt W, Baumann M, Wittig A. Reproducibility of target coverage in stereotactic spot scanning proton lung irradiation under high frequency jet ventilation. Radiother Oncol. 2013 Oct;109(1):45-50.

[2] **Santiago A**, Fritz P, Mühlnickel W, Engenhart-Cabillic R, Wittig A. Changes in the radiological depth correlate with dosimetric deterioration in particle therapy for stage I NSCLC patients under high frequency jet ventilation. Acta Oncol. 2015;54(9):1631-7.

[3] **Santiago A**, Barczyk S, Jelen U, Engenhart-Cabillic R, Wittig A. Challenges in radiobiological modeling: can we decide between LQ and LQ-L models based on reviewed clinical NSCLC treatment outcome data? Radiat Oncol. 2016 May 6;11(1):67.

Anmerkung:

Die Publikationen werden im Text, entsprechend der oben definierten Reihenfolge, mit den Nummern 1-3 referenziert.

Zusammenfassung

Die Arbeit untersucht Aspekte, die vor einer klinischen Implementierung einer Partikelstrahlentherapie mit einem gescannten Strahl zur Behandlung von Lungentumoren berücksichtigt werden müssen.

Im ersten Teil der Arbeit wurde die Reproduzierbarkeit der berechneten Dosisverteilung mit einem gescannten Partikelstrahl zur Behandlung nicht-kleinzelliger Lungentumore (NSCLC) im Stadium I in einem klinischen Szenario untersucht. Die Berechnungen basieren auf einem Datensatz von Patienten, die unter High-Frequency-Jet-Ventilation (HFJV) zur Tumorfixation mittels einer Einzeitbestrahlung mit Photonen behandelt wurden. Bestrahlungspläne für eine Bestrahlung mit Protonen oder Kohlenstoffionen wurden berechnet und bzgl. klinischer Planungsparameter optimiert, um die bestmögliche Dosisabdeckung im Zielgebiet zu erreichen. Inter-fraktionelle anatomische Veränderungen innerhalb einer kurzen Zeitspanne wurden simuliert durch Berücksichtigung der anatomischen Veränderungen zwischen dem Bestrahlungsplanungs-CT und dem Lokalisations-CT vor der Einzeitbestrahlung. Die dosimetrischen Auswirkungen dieser anatomischen Veränderungen (u.a. durch Änderung der Tumorposition und Lagevarianz des Patienten) wurden berechnet. Diese anatomischen Veränderungen wurden mittels Berechnung der water equivalent path length (WEPL) im Eintrittskanal des Strahls quantifiziert und mit der Dosisabdeckung im Zielgebiets korreliert. Zudem wurden Strahl- und Planungsparameter identifiziert, die die dosimetrischen Auswirkungen solcher anatomischer Veränderungen reduzierten, z.B. die Einstrahlrichtung, die Anzahl der Einstrahlrichtungen und die Spotgröße des gescannten Strahls. Wir konnten eine reproduzierbare Tumorfixation durch die HFJV nachweisen. Die Technik garantierte bei den meisten Patienten eine exzellente Dosisabdeckung des Zielgebiets bei einer Einzeitbestrahlung mit Protonen. Bei einer geringen Anzahl von Patienten wurden allerdings nicht akzeptable Abweichungen der Dosisverteilung zum berechneten Bestrahlungsplan beobachten, was die Notwendigkeit einer Kontrolle der Tumorposition und der Patientenlagerung vor jeder Bestrahlungsfraktion mittels Bildgebung verdeutlicht. Hierbei sollten dezidierte Protokolle für die Bildführung einschließlich Interventionsschwellen entwickelt werden, die die Auswirkung anatomischer Veränderungen auf die Dosisverteilung berücksichtigen. Die HFJV scheint Interplayeffekte zuverlässig zu vermeiden. Neuere Beatmungstechniken, die keine Narkose erfordern, können auch bei einer fraktionierten Behandlung eingesetzt werden.

Die biologische Bestrahlungsplanung für die Behandlung mit Kohlenstoffionen erfordert ein biophysikalisches Modell strahlenbiologischer Effekte einer Strahlqualität mit hohem linearen Energietransfer (LET). Ein Modell, das momentan klinisch Anwendung findet, ist das local effect model (LEM). Das Modell beschreibt die Strahlensensitivität und den biologischen Effekt der Ionenbestrahlung im Vergleich zu einer fraktionierten Photonenbestrahlung im Tumor- und Normalgewebe. Das Modell benötigt Inputparameter, u.a. das α/β Verhältnis, das momentan fast ausschließlich aus in vitro Studien bekannt ist. Es besteht daher die Notwendigkeit, tumorspezifische und klinisch realistische Werte für das α/β Verhältnis zu erforschen. Solche tumorspezifische und klinisch realistische Werte für das α/β Verhältnis sind aber auch für eine hypofraktionierte Photonestrahlentherapie hoch relevant. Für solche Dosierungskonzepte wird zudem seit langem diskutiert, ob das Linear-quadratische Modell (LQ) oder das Linear-quadratisch-lineare Modell (LQ-L) solche Dosiseffekte am besten beschreibt und welches α/β Verhältnis für NSCLC adäquat ist, um Fraktionierungseffekte vorherzusagen.

Für den zweiten Teil dieser Arbeit wurde daher ein Review publizierter lokaler Kontrollraten von NSCLC im Stadium I nach einer Strahlentherapie erstellt. Die lokalen Kontrollraten nach Radiatio mit unterschiedlichen Fraktionierungskonzepten wurden mathematisch modelliert, wobei Berechnungen mit dem LQ und dem LQ-L Modell durchgeführt wurden. Mit beiden Modellen ließen sich klinische Kontrollraten nach normo- und hypokraktionierter Bestrahlung vorhersagen. Das LQ-L Modell ergab einen signifikanten Wert für Dt von 11.0 Gy bei Berechnung der biologisch effektiven Dosis (BED) im Isozentrum bei einem α/β Wert von 10 Gy bei hypofraktionierter Bestrahlung. Das Modell sagte eine ähnliche Tumorkontrollwahrscheinlichkeit voraus (TCP), wie das LQ-Modell. Es bestand eine klare Dosis-Effekt-Beziehung, die in der Hochdosisregion allerdings etwas schwächer ausgeprägt war, da hier die Daten stärker streuten. Für die Applikation einer biologisch effektiven Dosis (α/β=10 Gy) von 100-150Gy in 3 oder mehr Fraktionen waren die Unterschiede bzgl. der Isoeffektvorhersage mit beiden Modellen zu vernachlässigen. Die Ergebnisse zeigen somit keine Verbesserung der Vorhersage der lokalen Tumorkontrolle nach einer hypofraktionierten Bestrahlung durch das LQ-L Modell im Vergleich zum LQ Modell. Eine Analyse, um das optimale α/β Verhältnis bei Berechnungen mit dem LQ Modell über den gesamten Fraktionierungsbereich zu finden, ergab keine signifikanten Wert, allerdings einen Trend zu einem α/β Verhältnis unter 10Gy.

Summary

This work presents a contribution in two different aspects required for the implementation of scanned-beam particle therapy for lung tumors.

The first part of this work investigates the reproducibility of the calculated particle therapy dose distribution for early stage non-small cell lung cancer (NSCLC) tumors in a clinical scenario. These calculations were carried out based on data sets of patients treated with single dose photon stereotactic body radiotherapy (SBRT) under high frequency jet ventilation (HFJV) in order to achieve near-total tumor fixation. A dosimetric evaluation of calculated proton and carbon ion plans was performed, to fulfill clinical plan acceptance criteria with emphasis on target coverage. By simulating the inter-fractional anatomical changes in a short time scale between planning and delivery-time anatomies as imaged by the planning and localization computed tomography (CT) data sets, we carried out an investigation of the deterioration in target coverage. The anatomical changes (e.g. tumor position, patient setup) were quantified through water equivalent path length (WEPL) calculations within the beam entrance channels and correlated with the loss in dosimetric coverage. In addition, we identified beam and planning settings, which also help to reduce dosimetric deterioration, such as best choice of beam angle, higher number of beams, larger spot sizes and larger allowances for beam spots outside the target. We demonstrated reproducible tumor fixations through HFJV. Such technique warranted excellent target coverage in proton SBRT in the majority of the investigated patients. However, for a minor number of cases, unacceptable dosimetric deviations were observed, illustrating the need for imaging prior to each dose delivery with dedicated protocols, together with the development of intervention thresholds in case of anatomical discrepancies based on their potential impact on the dose distribution. HFJV seems a suitable technique to reduce interplay effects. Newer assisted ventilation techniques which do not require use of anesthesia might be more suitable for fractionated radiotherapy.

Biological treatment planning for carbon ion therapy requires a model of the radiobiological effects of high linear energy transfer (LET) radiation. One approach in the context of scanned beam ion therapy is built upon the local effect model (LEM). Within this approach, the description of the radiosensitivity and the behavior versus fractionated photon radiotherapy of both tumor and normal tissue requires input of α/β ratios, usually obtained from in vitro studies. Obtaining tumor-specific, realistic, clinical α/β values is urgently required. This topic is also relevant in hypofractionated photon radiotherapy, where there is

an ongoing discussion, if the linear-quadratic (LQ) model represents adequately dose responses at high doses per fraction or if the linear-quadratic-linear (LQ-L) correction is necessary, and which α/β ratio describes better the fractionation effect for NSCLC tumors.

The second part of this work presents a review of local control data of early stage NSCLC and models of these dose response data using the LQ and LQ-L approaches. Both, the LQ and LQ-L models can be fitted to clinical normo- and hypofractionated NSCLC outcome data. The LQ-L model yielded a significant value for the D_t of 11.0 Gy for the model based on biologically effective dose (BED) at the isocenter with α/β equal to 10 Gy for the full hypofractionation range; it produced a comparable tumor control probability (TCP) fit to the LQ model. We found a clear dose-effect relationship, which in the high BED region was weaker due to considerable dispersion in the data. For the application of BED (α/β=10 Gy) in the range of 100–150 Gy in three fractions or more, the differences in isoeffects predicted by both models can be neglected. Our findings therefore do not allow us to suggest use of the LQ-L model for an improved fitting compared to the LQ model of local control data in case of hypofractionation. A tentative analysis to establish the optimal α/β ratio in the frame of the LQ model for the full fractionation range did not produce significant estimates, although it showed a trend for α/β values lower than 10 Gy.

Table of Contents

Abbreviations

3D	Three-Dimensional
4D	Four-Dimensional
BED	Biologically effective dose
BP	Bragg Peak
CBCT	Cone Beam Computer Tomography
CF	Conventionally Fractionated
CNAO	Centro Nazionale di Adroterapia Oncologica (CNAO), Pavia, Italy
DNA	DeoxyriboNucleic Acid
FWHM	Full Width Half Maximum
GSI	Helmholtzzentrum für Schwerionenforschung, Darmstadt, Germany
HF	HypoFractionated
HFJV	High Frequency Jet Ventilation
HFPV	High Frequency Percussion Ventilation
HIMAC	Heavy Ion Medical Accelerator in Chiba, Chiba, Japan
HIT	Heidelberger Ionenstrahl-Therapiezentrum, Heidelberg, Germany
HU	Hounsfield Unit
IGRT	Image-Guided RadioTherapy
IMPT	Intensity Modulated Particle Therapy
IMRT	Intensity modulated RadioTherapy
ITV	Internal Target Volume
LBNL	Lawrence Berkeley National Laboratory
LC	Local Control
LEM	Local Effect Model
LET	Linear Energy Transfer
LINAC	Linear Accelerator
LQ	Linear Quadratic model
LQ-L	Linear-Quadratic-Linear
LTC	Local Tumor Control
MIT	Marburger Ionenstrahl-Therapiezentrum, Marburg, Germany
MKM	Microdosimetric Kinetic Model
MRI	Magnetic Resonance Imaging
MV	MegaVolt
NIRS	National Institute of Radiological Sciences, Chiba, Japan

NSCLC	Non-Small Cell Lung Cancer
OAR	Organ At Risk
OER	Oxygen Enhancement Ratio
PET	Positron Emission Tomography
PSI	Paul Scherrer Institut, Villigen, Switzerland
PTV	Planning Target Volume
RBE	Relative Biological Effectiveness
SBRT	Stereotactic Body RadioTherapy
SFUD	Single Field Uniform Dose
SOBP	Spread Out Bragg Peak
TCD50	Tumor Control Dose 50%
TLD	Thermo-Luminiscence Detector
WHO	World Health Organization

1 Introduction

1.1 Current approaches for radiotherapy of lung cancer

According to the World Health Organization, 8.2 million people die each year of cancer, representing 13% of all deaths worldwide [WHO 2016(a)]. From among all cancers, lung cancer is the most common disease worldwide, contributing with 1.2 million new cases per year and being responsible for 17.8% of all cancer deaths [WHO 2016(b)]. Non-small cell lung cancer (NSCLC) accounts for about 85% of all lung tumors [Molina 2008]. The first therapy option for early, non-metastatic lung tumors is surgery. In patients who are not eligible for surgery due to impaired lung function or secondary diagnoses, studies have shown high local tumor control after high-dose photon radiotherapy for stage I disease. Radiotherapy, together with surgery and chemotherapy, is an essential tool in a multimodal treatment approach for advanced NSCLC. In these advanced cases, radiochemotherapy reaches however a 2-year survival rate of only 50% [Bradley 2015]. In addition, radiotherapy has proven great value in providing many non-curative patients with palliation. Altogether, the optimal radiotherapy utilization rate for lung cancer has been estimated as high as 76% [Delaney 2012].

Ionizing radiation causes cell death mainly as a result of damage to the DNA. The ultimate goal of radiation therapy is to achieve cure without complications by destroying all tumor clonogenic cells with the lowest rates of side effects possible [Joiner 2007]. Radiotherapy advances aim at a broadening of the therapeutic window, which can be achieved with technical improvements such as the refinement of dose delivery, optimized dose distributions such as with intensity modulated radiation therapy (IMRT), or enhanced precision by incorporation of daily imaging into the clinical workflow. Advances can additionally be delivered by core radiobiology research, such as innovative irradiation protocols modifying the timely dose distribution or a combination with drugs.

Modern external beam radiotherapy is mostly delivered with high energy photons provided by linear accelerators (linacs). Conformal techniques aim at an excellent sparing of the normal tissue while increasing the dose in the tumor volume. In conventional radiotherapy this is usually achieved with an increased number of overlapping radiation fields, as for example in stereotactic body radiotherapy (SBRT) and IMRT techniques, in order to redistribute the dose given to the surrounding normal tissue. SBRT is a high precision technique characterized by steep dose gradients, which enable the prescription of ablative doses with excellent sparing of neighboring normal tissue structures [Guckenberger 2014].

Specifics of the radiotherapy approaches of both early and advanced stages of NSCLC are defined by their different goals and technical challenges. In the case of early stage NSCLC, radiation treatments were firstly imparted by means of 3D-conformal fractionated techniques. In recent years, hypofractionated photon SBRT in one to five fractions is has been established as the standard choice in the irradiation of medically inoperable early stage cases [Palma 2011, Vansteenskiste 2014]. For such small tumors, a trend towards hypofractionation has become standard on one hand due to better outcomes of schedules with a shorter treatment time, and on the other, due to better cost-effectiveness of these treatments and greater patient convenience. In inoperable advanced NSCLC stages, multimodal approaches are required which include radiotherapy as an essential tool. To achieve loco-regional control with limited treatment associated morbidity remains to be the major challenge. For local tumor control, doses above 100 Gy biologically equivalent dose (BED) to the macroscopic tumor are required, and this is not always possible with conventional approaches due to critical structures located nearby the tumor. For this reason, various strategies for local treatment intensification with equal or even reduced toxicity are being investigated [Chang 2014, Chi 2014, Kim 2014, Eberhardt 2015, Rodrigues 2015].

1.2 Particle therapy with protons and carbon ions: origins and development

Particle therapy was first proposed in 1946 by Wilson [Wilson 1946], was started in the 1970s with a pioneering ion-therapy program at the Lawrence Berkeley National Laboratory (LBNL) in Berkeley, California [Blakely 1980, Castro 1993] and continued with pilot carbon ion programs at GSI Helmholtz Centre for Heavy Ion Research in Darmstadt, Germany, and at National Institute of Radiological Sciences (NIRS) in Chiba, Japan [Schardt 2010] and continued with numerous proton centers today. In the first experimental experiences at Berkeley, most patients had tumors of the pituitary gland and were treated with helium or neon beams [Castro1993]. Current clinical particle therapy centers are based on protons and/or carbon ions. A worldwide expansion of the number of proton therapy centers is taking place, whereas carbon ion facilities increase slowly in numbers, partly due to their higher size and costs [Peeters 2010]. At the end of 2014, almost 16.000 patients had been treated with carbon ions and more than 118.000 with protons [PTCOG 2016(a)]. As of July 2016, 65 particle therapy centers are operating worldwide, from which five centers are carbon ion therapy facilities and five centers count with both carbon ion and proton beams [PTCOG 2016(b)].

1.3 Physical advantages of particle beams

The inverse dose deposition profile of particles can potentially allow for highly conformal radiation. In contrast to photons, whose dose depth profile shows a maximum close to the surface and an exponential decrease with depth, the dose delivered with particles increases with penetration depth and presents a flat dose profile at the entrance plateau, a maximum of deposited dose at the so-called Bragg peak (BP) and a sharp distal fall-off at the end of the finite particle range [Wilkens 2008, Weber 2009, Suit 2010]. This profile is a result of the Coulomb interaction of charged particles with the electrons present in the tissue, and it allows a good sparing of the adjacent organs at risk (OAR), especially of those located behind the tumor.

In order to irradiate uniformly a finite volume, the BP needs to be enlarged to a spread out Bragg peak (SOBP). Two technical solutions are deployed: passive and active beam shaping. Passive scattering techniques need first to produce both lateral and in-depth beam spreading. The modulation depth remains constant through the whole volume which results in a high dose area upstream of the target. Active scanning beam delivery techniques rely on a pencil beam which is deflected with magnets in horizontal and vertical directions to scan the whole irradiation field and with in-depth modulation of the beam by means of beam energy switches. This way excellent dose conformity is achieved, also in the proximal edge of the tumor. However, active beam shaping systems are considered to be more prone than passive systems to dosimetric deterioration resulting from organ movement [Bert 2011, Knopf 2011].

Range straggling is the widening of the BP of a monoenergetic ion beam due to stochastic fluctuations in the energy loss and therefore in the range. This effect is larger for lighter ions and the BP width is therefore larger for protons than for carbon ions. These differences are smaller in the case of an extended SOBP in comparison to a single BP [Weber 2009].

Lighter carbon ion fragments at the same speed as the original carbon ion projectiles fly larger distances, and therefore, carbon ion beams present a so-called fragmentation tail with a non-negligible contribution to dose deposition, which is not present in the case of protons [Suit 2010]. Some of these projectile fragments are radioactive isotopes and can be used for PET imaging for ion range monitoring [Enghardt 1999]. Still, the fragmentation of carbon ion projectiles is lower than for other heavier ion species and can be handled with adequate treatment planning [Castro 1993, Suit 2010]. Other species such as helium or oxygen are under examination for future clinical use [Krämer 2016, Tommasino 2016].

Concerning the lateral profiles, scanned ion beams are continuously enlarged by multiple Coulomb scattering when traveling through the final elements of the beam line (vacuum window, monitor chambers, passive energy modulators) as well as inside the patient [Schardt 2010]. This effect is 3.5 times more pronounced for protons than for carbon ions and therefore more critical for proton treatments [Weber 2009]. By bringing the patient closer to the nozzle the beam widening in the air gap between the nozzle and the patient stemming from the scattering in the beam line can be reduced [Weber 1999, Jelen 2013].

1.4 Potential biological advantages of carbon ion beams

Protons do not present, in a first approach, an enhanced relative biological effectiveness (RBE) [Paganetti 2002], unlike heavier ions. The biological effects of ionizing radiation result mainly from damage to the DNA, the most critical being DNA double strand breaks. DNA radiation damage can be direct or indirect. Direct DNA damage takes place when the atoms within the DNA molecule are ionized or excited by incident charged particles. Indirect damage occurs when the radiation interacts with other chemical species present in the tissue to produce free radicals. The oxygenation status of the tissue at the moment of irradiation enhances the severity of the indirect damage [Gray 1953, Hall 2006]. In addition, cellular radiosensitivity is modulated also by the cell cycle phase and the repair capability of the cell. A certain absorbed dose imparted either with photons or electrons with energies within the clinical MV-range will yield similar amounts of cell damage. In contrast, charged particles may produce a greater biological effect per dose unit as compared to photons. This is due to their different energy deposition patterns in the tissue, [Scholz 1997, IAEA 2008, Wambersie 2015]. The ionization events of charged particles are tightly concentrated along the particle trajectory, leading to clustered DNA damage, which is more difficult to repair and therefore more prone to cause cell death. Cell response is thus driven by direct damage and as a result, there is a reduced dependency of the radiosensitivity on other factors [Hall 2006, Kraft 2000, Joiner 2007].

The linear energy transfer (LET) was defined to describe these different ionization patterns as the energy transferred by an ionizing particle and secondary electrons to the material per track length unit of the incident particle, and it is usually measured in keV/μm. Radiation types are classified in sparsely and densely ionizing with low and high LET, respectively. The RBE was introduced to quantify the different biological effects of different radiation types, and it is defined as the quotient between the dose of the reference radiation (usually

^{60}Co sources, or 250 kVp X-rays), and the dose of the radiation under study required to produce the same biological effect on a certain biological system [IAEA 2008].

1.5 Planning for particle therapy: modeling of the RBE

The RBE is a complex quantity to model due to its many dependencies: LET, particle type and energy, dose per fraction, dose rate, degree of oxygenation, cell or tissue type, biological endpoint under study, etc. [Weyrather 1999, Friedrich 2013(a)]. In the case of irradiation of a target with a SOBP, it is also a function of the particle and energy spectra at every point in the tissue. The RBE of protons also varies along the proton track inside the tissue, although to a much lower extent than the carbon ion RBE. The current consensus is to apply a fixed value for the RBE of 1.1 to the whole proton Bragg curve, based on reviewed experimental and clinical data [ICRU 2007, Carabe 2012, Paganetti 2014]. For carbon ions, this simplification is not possible since great LET variations occur within the SOBP. Experimental RBE values may vary between 1.5 in the entrance channel and 3 just before the end of the particle range. As a consequence of this, biological plan optimization aiming at achieving a uniform biological effect and not a homogeneous physical dose is required. RBE estimations have to be carefully performed and included in all steps of the carbon ion treatment planning [Schardt 2010]. The biological effect is thus commonly taken into account with the distribution of the absorbed dose in Gray [J/kg] weighted with the estimated RBE values at each point [IAEA 2008, Kraft 2000, Wambersie 2011, Krämer 2004, Jäkel 2007]. Currently many different RBE models exist [IAEA 2008, Schardt 2010, Giovannini 2016] to achieve this.

The local effect model (LEM) was first developed to obtain RBE estimations for carbon ion radiotherapy at GSI, the first facility using active energy variation and raster scanning. It has been implemented in the TPS used clinically for carbon ion therapy in Europe. This model requires the attribution of radiobiological properties to both tumor and normal tissues. The main assumption of the LEM is that the biological damage arising in a small subvolume of the cell nucleus is independent of the specific radiation type which deposited that energy and the biological damage is solely determined by the size of the energy deposition taking place in that specific subvolume. This way, it is possible to use the existing cell survival data, i.e. the LQ coefficients α and β, obtained from in vitro X-ray irradiation experiments (survival curves) to characterize the radiosensitivity of the tumor [Krämer 2000]. For the calculation of RBE values for normal tissue side effects,

estimations of the α/β ratio of the endpoint under study derived from clinical data are used [Scholz 1996, Jäkel 2007]. The LEM also requires the input of further parameters, namely, an estimation of the size of the critical target in the cell (i.e. the cell nucleus), the ion track structure for the calculation of the distribution of local physical doses and the so called dose threshold, D_t, which takes into account the transition from linear-quadratic to linear cell killing beyond a threshold at high local doses [Scholz 1996, Scholz 1997, Kraft 2000, Kramer 2004, Weyrather 2004]. The influence of these parameters on the output of the model, as well as the influence of α and β alone, is lower than that of the α/β ratio [Jäkel 2007]. Verification of the LEM predictions for in vitro cell survival prior to clinical application [Weyrather 2004] and in vitro and in vivo tests of the different LEM versions [Elsässer 2008] have been carried out, as well as the calculation of expected local tumor control based on patient data [Scholz 2006]. Several sensitivity analyses to uncertainties in the input parameters of the LEM have also been carried out in selected tumor entities [Böhlen 2012, Friedrich 2012, Chanrion 2014]. The capability of the LEM for prediction of normal tissue complication was tested in a low number of in vivo experiments [Zacharias 1997]. The LEM is implemented in several commercial treatment planning systems (TPS) for particle therapy planning, including all TPS used for carbon ion radiotherapy in Europe [GSI 2016].

As described above, the modulation of biological effects of particle irradiation is very complex and experimental RBE studies and radiobiological modeling are of great importance in particle therapy to understand their effects relative to photons. Currently some important questions remain open. Most of the present RBE data are based on in vitro studies. In vitro experiments have been used for the development and check of the models and for clinical quality assurance. However, in vivo RBE values for both local tumor control and normal tissue toxicities are still scarce [Kummermehr 2002, Peschke 2011, Sørensen 2015]. Well-designed and systematic large scale research, both in appropriate preclinical and clinical models would be required to improve the RBE estimations obtained in vitro, and if possible, RBE estimations from clinical data should also be obtained [Schardt 2000 and Suit 2010]. In addition to all mentioned parameters with impact on the RBE, clinical factors such as the patient physiology or tumor biology may influence the clinical RBE [Schardt 2000]. Moreover, the employed input parameters for the LEM in clinical planning are so far identical for all tumors, not taking into account the existence of intertumoral differences and differences in normal tissue sensitivity, which probably decreases the accuracy of the RBE estimations [Jäkel 2007].

1.6 Relevance of modeling of tumor outcome for radiotherapy

For the MV photon energies used in external beam photon radiotherapy, the RBE values are known to be nearly 1. For this reason, prescriptions and planning objectives for both tumor and OAR in photon radiotherapy are based on the physical dose. Still, there is a dependency of the radiation effects on other factors such as tumor microenvironment (e.g. oxygenation status) and tumor and patient characteristics, among others. Moreover, in the case of the OAR, so called organ volume effects exist and therefore biological optimization has been proposed also for photon therapy [Allen Li 2012]. In current clinical practice, however, the biological effects of a certain dose distribution are in the majority of cases still estimated *a posteriori*, usually in research contexts. Thus, the main task requiring modeling in clinical practice is the comparison of different fractionation schemes. The LQ approach upon which the LEM is built was firstly developed to describe experimental survival curves of normal and tumor cells after irradiation. In the LQ approach, cell surviving fractions after irradiation are fitted with a second-order polynomial on the dose per fraction. The ratio between the two coefficients, α and β, describes the repair capacity of the cells and their sensitivity to fractionation for tumors as well as for normal tissues [Barendsen 1982, Joiner 2007].

The LQ formalism is accepted to describe the fractionation effects at fraction doses below 8-10 Gy per fraction [Herrmann 2006], however, it loses accuracy for both very low and very high doses. It enables isoeffect calculations in current clinical practice, describing the relationship between the biological effect after irradiation and treatment parameters such as dose per fraction, total number of fractions, and total treatment time, within the BED formalism.

The current expansion of HF treatments gives relevance to the question, whether the description of the radiobiological effects provided by the LQ formalism is adequate for this type of schedules [Fowler 2006, Kirkpatrick 2010, Brown 2014]. Estimations of the clinical α/β values are required to assess the benefit of a HF irradiation scheme [Thames 1990], when it is suspected that the α/β value is lower than 10 Gy. Such schemes would reduce tumor cell recovery between fractions, thus increasing the therapeutic ratio, as it is thought to be the case e.g. in prostate carcinoma. Some recent studies review and model the dose response relationship of NSCLC [van Baardwijk 2008, Stuschke 2010, Zhang 2011, Mehta 2012, Chi 2013]. However, in the case of NSCLC, studies attempting to estimate the α/β ratio are scarce [Stuschke 2010, Chi2013, Guerrero2008]. It is currently under debate if the

improved outcomes of hypofractionated SBRT are a consequence of an α/β ratio lower than 10 Gy, or even lower than the α/β value of the surrounding normal tissue, or alternatively, of a reduced repopulation in a shorter overall treatment time. The first case would add up to existing radiobiological rationale of the use of hypofractionation. For fraction doses larger than 10 Gy, a linear dependance of the cell killing has been observed with dose instead of linear-quadratic. A correction has been proposed, which consists of a dose threshold $D_{t,}$ and is commonly called the linear-quadratic-linear (LQ-L) model [Astrahan2008].

1.7 Indications for particles: tumor resistance and improved dose distribution

Radiotherapy with protons or carbon ions has the potential for improved treatments of both early and advanced stage tumors, based on the physical properties of charged particle beams, radiobiological considerations, and clinical criteria. However, benefits of particle therapy over photon therapy have only been demonstrated for a small number of indications. These are rare, often inoperable tumors, for which traditional approaches show limited efficacy or would be associated with high morbidity. Especially tumors with clear margins without infiltration into healthy surrounding tissue which can be sharply delineated benefit, as they match the good spatial definition of particle irradiation [Wambersie 2004, Schulz-Ertner 2007, Combs 2013(a), De Ruysscher 2012]. Examples are choroidal melanoma and deep-seated tumors that grow in or in close contact with sensitive normal structures, such as chordoma and chondrosarcoma of the skull base. Such tumors present a poor outcome from conventional radiation treatments and in these cases, more conformal particle dose distributions may offer an advantage by helping to spare normal tissue while delivering curative doses to the tumor. In order to maximize the benefit in terms of overall survival, selected tumors must display local failure, but late metastases.

Adding to the rationale for carbon ion therapy is tumor radioresistance through various mechanisms such as hypoxia, slow proliferation or specific repair characteristics. Traditionally, a potential high LET advantage of tumor versus the surrounding tissue has been considered as an additional criterion for carbon ion therapy, since only tumors which exhibit a higher RBE than the normal tissue surrounding them will benefit from carbon ion therapy (e.g. tumors with an observed slow growth pattern) [Wambersie 2004]. Concerning choices between both particle therapy modalities, proton therapy may be preferred instead of carbon ions or IMRT in pediatric cases to minimize side effects to normal tissue and hypothetical higher risk of secondary malignancies [Patel 2014].

At present, the list of indications for particle therapy is under development [Allen 2012, De Ruysscher 2012, Combs 2013(a), Muren 2013]. Established indications for particle therapy are rare, and the rapidly increasing number of particle therapy centers entering operation will require efforts to determine for which frequent cancer diseases particle therapy might bring a significant advantage over current photon treatments. Furthermore, optimal treatment concepts need to be conceived to exploit this advantage. It is to expect that the rapid expansion in this field will require clinical evidence, but at the same it will allow to generate enough proof to answer these questions in the coming years, based on data collected from large patient numbers treated in the frame of clinical trials [Combs 2013(b)].

1.8 Role of particle therapy in the treatment of NSCLC

Particle therapy with its accurate dose deposition could decrease the dose to the lung and other OAR and potentially reduce the risk of treatment-related lung morbidity [Wink 2014]. For early stage NSCLC, SBRT has shown excellent results. For these cases, the dose coverage of photon delivered dose might be superior to that of particles, since the risk of dose deterioration in moving targets is higher for the latter [De Ruysscher 2013, Knopf 2011]. The comparison of both radiation modalities needs to consider this fact as well as the existing range uncertainties which inherently affect both passive and active beam shaping [Seco 2012]. However, after appropriate management of these risks, particle therapy could potentially further reduce the probability of radiation side effects, and the decreased integral dose would also reduce the risk of second cancers. Several cohorts of patients treated with both protons and carbon ions have been reported and generally show good outcomes, although most of these were treated with passive scattering techniques [Wink 2014, Berman 2015].

Radiochemotherapy shows limited efficacy for advanced lung cancer stages. A dose-response relationship has been demonstrated for NSCLC, with higher tumor doses affecting not only local control but also reducing the occurrence of metastases [Kong 2014]. This would motivate dose escalation as a mean to improve both local control and overall survival, however, radiation-related morbidity might be currently masking the benefits of dose escalation, even when high-end photon techniques are used [Wink 2014]. Considering this hypothesis, proton or carbon ion irradiation might be indicated for some advanced stage tumors. Novel treatment concepts are being explored since the dosimetric advantage of particle irradiation might allow dose escalation to increase local tumor control

[Demizu 2014, Wink 2014, Berman 2015] and other more aggressive treatments [Berman 2015]. Additionally, in scenarios where the therapeutic window is narrow such as re-irradiations and post-operative irradiations, particle therapy and specifically proton beams can be of interest [Berman 2015].

It is important to note that almost all irradiation of lung cancer have been performed with more forgiving passive field forming techniques so far [Wink 2014, Knopf 2016] with respect to dosimetric degradation in presence of tumor motion, which on the other hand offer a lower conformity than scanning beam techniques. Scanned beam could lead to improved outcomes over passive scattering techniques, provided that the interplay effects are handled adequately [Bert 2011, Wink 2014, Knopf 2016]. All in all, more evidence is required to determine the value of particle therapy for lung cancer [De Ruysscher 2012, Wink 2014].

1.9 Technical challenges of particle therapy of lung tumors

Their well-defined range makes particles more sensitive to changes in the radiological depth in the beam entrance channels. These changes may originate from residual positioning errors, inter-fractional tumor movement and other anatomical changes which take place within a larger time scale during the radiotherapy course such as tumor shrinkage or tumor baseline shift, fluctuations in patient weight, or filling/emptying of cavities [Britton 2009, Kwint 2014]. Such events can translate into clinically relevant alterations in the particle dose distribution, more critically than for the case of photons [Bert 2011].

The management of anatomic changes requires frequently repeated CT imaging and eventually replanning. For this reason, investigations on optimal image-guidance and adaptive strategies are ongoing. Current strategies for image guidance in particle therapy have been historically derived from photon techniques and usually rely on anatomical landmarks or fiducial markers. In a particle therapy scenario however, relevant dosimetric deviations may occur even if the repositioning of the tumor is geometrically correct, making dedicated methods necessary [Bert 2011, Koay 2012, Seco 2015, Knopf 2016].

1.10 Lung motion consequences for particle therapy

Periodical movement of lung tumors with respiration represents the main challenge to the application of particle therapy in the lung [Bert 2011, Knopf 2016]. Other intra-fractional

movements such as heartbeat and swallowing may influence irradiations in the thoracic region although to a lower extent [Langen 2001].

Four-dimensional (4D) imaging techniques such as 4D-CT, 4D-CBCT, and 4D-MRI can provide information about the tumor movement. Tumor motion patterns are not perfectly periodic, precise motion features are patient-dependent, and for the same patient respiration patterns can differ between fractions [Bert 2011, Knopf 2016]. Motion prediction and development of motion surrogates are complex tasks, and therefore intra-fractional verification of the tumor movement is required [Knopf 2016]. Due to the absence of exit dose, projection imaging is not feasible for particle beams, and since extensive use of X-ray-based imaging significantly increases the integral patient dose, optimized intra-fractional imaging solutions not based on ionizing radiation are needed whenever possible [Knopf 2016]. 4D-CT can currently provide useful motion information which is entered in the target definition through various strategies, but so far, no 4D treatment planning is performed on a clinical basis.

In scattered beam particle therapy, target coverage is typically ensured by extended lateral as well as distal and proximal margins through compensator smearing [Moyers 2001, Seco 2012] to secure target coverage against uncertainties in treatment variables [Flampouri 2014]. In a similar manner for scanned beam therapy, specific internal target volumes (ITV) concepts [Bert 2011] and beam specific approaches for the planning target volume (PTV) have been proposed [Albertini 2011, Knopf 2011, Park 2012], and also robust planning [Pflugfelder 2008]. Both approaches require precise tumor motion characterization not yet available in commercial treatment planning systems . In absence of dedicated solutions, the target volumes used for scanned ion beam therapy are defined according to the recommendations of the ICRU, developed for photon radiotherapy [Knopf 2016]. Specific studies exist in which intra-fractional changes in the radiological depth are quantified based on 4D-CT [Mori 2011]. These type of anatomical changes have been related to dosimetric fluctuations inside the ITV with scanned protons [Casares-Magaz 2015].

1.11 Interplay effects

In passive scattered facilities, the main effect of target movement is dose blurring and larger margins can be applied to cope with it. In scanned beam particle therapy, additionally to anatomy changes, the interplay between target motion and beam scanning adds extra

complexity to the irradiation of lung tumors [Bert 2011]. Severe mis-dosage can occur in form of cold and hot spots in both the target and the surrounding structures. Therefore, a margin-based approach might not be sufficient to assure both the planned target coverage and homogeneity, especially in the case of intensity modulated particle therapy (IMPT). For single-field uniform dose (SFUD), however, margins could still be employed in lung tumors which present a reduced movement with respiration below 5 mm [De Ruysscher 2013, Wink 2014].

The dosimetric severity of the interplay effects depends on tumor movement and on properties of the beam system. A careful selection of plan parameters can help to reduce dose deterioration such as larger spot sizes and smaller grids, more fields, optimized beam angles and changed fractionation schemes. Specific means to counteract motion interplay effects have been developed, and their clinical applicability is currently under investigation, such as tracking, rescanning, gating, as well as combinations of these [Knopf 2016].

In addition, tumor fixation approaches are being investigated [Bert 2011]. Target fixation techniques in particle therapy of the lung have two main potential clinical advantages: to obtain a reduction in the motion and deformation of the target volume while managing the sensitivity of particle range to tissue density changes in the beam entrance channels. The advantage of these methods is that they do not require hardware modifications nor full-fledged 4D treatment planning, and can be implemented with existing devices after careful check of feasibility and development of implementation workflow. Examples of such techniques are breath hold, apnea, and high frequency jet ventilation (HFJV) [Bert 2011, Boda-Heggemann 2016, Dueck 2016, Josipovic 2016]. HFJV is a modality of mechanical ventilatory support, which prevents any movement of the tumor with respiration. It is well known in lung surgery but of novel use in radiotherapy for target fixation [Fritz 2010]. Newer ventilation techniques are being tested in the context of radiotherapy, which do not require use of anesthesia [Péguret 2016].

2 Summary of the results

2.1 Dosimetric Study

Rational exists for the treatment of lung tumors with particle therapy, especially with the more conformal scanning beam techniques. However, important technical issues need to be addressed before clinical application. The main concern is tumor movement originating from respiratory motion. One potential solution to handle this problem is to apply HFJV in order to create reproducible tumor fixation. Through a cooperation, data from early stage NSCLC patients treated with single-fraction SBRT under HFJV were available for this work. CT scans done at both planning and delivery time, were collected for a cohort of 11 patients bearing 12 tumors. For each patient, both clinical datasets were co-registered, and the target and OAR were contoured. The Marburger Ionenstrahl-Therapiezentrum (MIT) in Marburg, Germany has capabilities to irradiate with both scanned protons and carbon ions, therefore plans with both particle types were made with the treatment planning system TRiP98 [Krämer 2000, Krämer 2004]. The RBE for protons was assumed to be 1.1. All carbon ion planning optimization was calculated based on the physical dose as a surrogate of the biologically optimized dose, under the hypothesis that their respective dosimetric behavior in presence of anatomical changes is similar.

2.1.1 Dosimetric quality of the presented plans

Three different beam setups where considered in this study: setup 2FA (compatible with a fixed nozzle facility with lateral and oblique beams at 0° and 45°), setup 2FB (beams at 0° and 90°), setup 2FC (beams at 0° and -45°), MultiF1 (3-4 beams), and MultiF2 (5-7 beams, same directions as for the clinically applied SBRT plans). The main criterion was to reach a PTV $V_{95\%}$ (i.e., a percentage of the PTV receiving a dose of at least 95% of the prescribed dose) of at least 98%. Only plans for both proton and carbon ion irradiation which fulfilled this criterion were included in the study.

For the proton plans, only one set of planning parameters was used: a nominal spot size of 8 mm full width at half maximum (FWHM), a grid size of 3x3 mm^2 and an energy step size of 2 mm. The spot sizes were found to be considerably larger than for the carbon ion plans. For instance, for the plans with beam setup 2FA the spot sizes ranged between 6 and 18 mm. The lateral contour extension (lateral allowance to place beam spots outside the target) was set to 1.5 for all proton plans, expressed in units of the FWHM at the isocenter. The larger value for the contour extension of 1.8 (FWHM) was considered excessive with

regard to the compromise between nominal plan coverage and conformity, and the smaller contour extensions of 0.9 and 1.2 (FWHM) did not yield satisfactory PTV coverage. For this reason, we applied the previously mentioned standard settings to the 2-field proton plans with different beam angles and to the multifield plans. Plans with an energy step of 3 mm were also created, however, they only yielded an acceptable coverage for 6 out of the 12 tumors cases in the plans with beam setup 2FA and therefore these settings were discarded. Target coverage values for the proton plans are presented in ***(table 1 paper 1)***, and ***(table 1 paper 2)***. For the chosen planning settings, the planning objective of PTV $V_{95\%} > 98\%$ was reached for all 12 tumor cases with all field setups.

The proton plans with beam settings 2FA, MultiF1 and MultiF2 presented in ***paper 1*** were additionally evaluated in detail in terms of dose limits to relevant OAR for lung irradiation. Representative dose-volume histogram parameters were summarized in ***(table1 paper 1).*** In this table it can be seen that all planning constraints for single-fraction SBRT treatment according to [Timmerman 2011] could be reached, except dose constraints to the chest wall for some patients. As an example, median V_{22Gy} for the ribs for the whole cohort was 2 cm^3 for the 2FA plans, above the recommended 1 cm^3. The median V_{22Gy} value sank to zero for the multifield plans. For some patients, part of the thorax wall was encompassed by the PTV and for this reason the maximum values remained high (for example, 15.9 cm^3 for the 2FA setup).

For the carbon ion plans, plans with the beam setups 2FB, and 2FC were calculated for one set of planning and raster scan settings, as well as several plan versions for the beam setup 2FA with different planning and raster scan settings. Summaries of the PTV $V_{95\%}$ values are listed in ***(table 2 paper 2)***. Plans with excess contour extension regarding PTV coverage were excluded from the analysis. The plans C12v4 and C12v10, with contour extension 0.9 (FWHM), presented a coverage slightly below the objective ($V_{95\%} > 98\%$) in only 2/12 and 1/12 patients, respectively, which was considered clinically acceptable. PTV $V_{95\%}$ for the clinically accepted plan versions with different raster scan settings are presented in ***(figure 1 paper 2)***.

The early stage, peripheral tumors presented in this study have no critical normal tissue structures in the vicinity of the tumor, except for some patients for which a portion of the thorax wall and the ribs encompassed by the PTV. Therefore, the conformity indexes had a lower priority than a satisfactory PTV coverage. Homogeneity and conformity values for all proton and carbon ion plans are listed in ***(supplement paper 2)***. Changes of the field

configuration alone resulted in small changes in these two indexes. Use of a larger number of fields improved both conformity and homogeneity. Lower values of the conformity indexes $CI_{95\%}$ and $CI_{98\%}$ were seen for larger values of the lateral virtual contour extension, since more dose is placed outside the PTV. However, these values also resulted in increased $V_{95\%}$ values, indicating that there is a trade-off between both quantities. Larger contour extensions also improved homogeneity as did smaller energy steps. The contour extension was the parameter with the largest influence on homogeneity, whereas it did only influence the conformity to a minor degree.

2.1.2 Reproducibility of dosimetric target coverage

Target coverage reproducibility was studied for all clinically accepted plans, based on the GTV $V_{98\%}$ and $V_{95\%}$ indexes. For proton planning, values for the beam setups 2FA, MultiF1 and MultiF2 are summarized in ***(table 1 paper 1)*** and ***(supplement paper 1)***, and for the rest of the beam setups and planning settings in ***(table 1 paper 2)***. For convenience of the reader, these values are also summarized in the table below:

Table R1: Summary of the coverage loss for the proton plans presented in ***paper 1*** and ***paper 2***, all with the same settings of 8 mm (FWHM), grid 3x3 mm^2, energy pitch 2 mm, and contour extension 1.2 (FWHM).

Beam Setup	GTV $\Delta V_{95\%}$ (# Patients with ΔGTV ≥ 3pp)	GTV $\Delta V_{98\%}$ (# Patients with ΔGTV ≥ 5pp)
2FA	0.1 (-0.1 – 8.9) (2/12)	3.9 (-0.6-14.1) (5/12)
2FB	0.0 (-0.3-3.5) (1/12)	1 (-0.8-13.2) (2/12)
2FC	0.0 (-0.6-0.3) (0/12)	1.1 (-0.7-2.8) (0/12)
MultiF1	0.0 (0.1–6.9) (1/12)	0.6 (1.7–12.9) (2/12)
MultiF2	0.0 (0.0–2.9) (0/12)	0.1 (-0.6 – 6.5) (2/12)

As can be seen in the table, all median values of the GTV $\Delta V_{95\%}$ for all plan versions are close to zero, showing that the maxima are originated by a few outliers, indicating good reproducibility in general among the cohort. For beam setup 2FA, the coverage loss ΔGTV $V_{95\%}$ reached a maximum of 8.9 percentual points (pp) and remained smaller or equal to 3 pp for all patients except two. For beam setups 2FB and 2FC, the same index reached lower maximum values of 3.5 and 0.3 pp, respectively, falling below 98% only for 1/12 or

0/12 patients respectively. For the multiple field plans, the maximum values were 6.9 and 2.9 pp, demonstrating that the coverage loss did not depend strictly on the number of beams. For the setup MultiF1 there were some large anatomical variations among the employed beam directions for some patients and the coverage loss was therefore comparable to that of the 2-field plans even though three to four fields were used. The magnitude of the coverage loss was strongly patient related.

2.1.3 Variations in the ΔWEPL with beam angle

For some patients, some anatomic qualitative changes were observed in the entrance channels. Very frequently this was linked to the reproducibility of the arm position see ***(figure 1(b) paper 1)***. In ***paper 2*** a method was developed to quantify changes in tissue density and thickness in the beam entrance channels between the planning and the irradiation time. For this, a software tool was created to calculate variations in water equivalent path length (WEPL) along different coplanar beam angles. We correlated the measure for ΔWEPL described in detail in ***paper 2*** with the dose deterioration to find beam directions which could minimize such changes.

The mean WEPL values measured within the PTV in this patient cohort ranged, for instance, from 25 mm to 88 mm in the lateral direction and from 22 mm to 100 mm at -45°. Concerning the variability among patients, the lowest ΔWEPL averaged among all angles corresponds to patient 1 with 1.5 ± 0.6 mm (mean with standard deviation), in contrast to patient 10A, which shows a maximum averaged ΔWEPL of 3.6 ± 3.9 mm. For six patients the ΔWEPL reached values larger than 5 mm in specific beam directions. These high values concentrated for three patients at angles around the ventrolateral direction (-45°). Two of these specific patients presented considerable anatomical changes between the repeated CT scans in the beam entrance path, and therefore the ΔWEPL reaches extreme values of up to 10 mm and 19 mm, see ***(figure 3 paper 2)***.

2.1.4 Influence of raster scan settings on robustness to anatomical changes

Eighteen carbon ion plan versions were made and from these, eleven were considered clinically acceptable regarding PTV coverage. For these plans an analysis was performed of the influence of the different raster scan settings on the preservation of the target coverage. A qualitative comparison suggested that a larger spot overlap contributed to preserve the target coverage, and also provided better PTV $V_{95\%}$. The smaller energy steps led to better coverage preservation in presence of anatomic discrepancies. Similarly, a visual

comparison of plans with identical planning settings up to the value of the contour extension, which was varied between 0.9 and 1.2, evidences a large improvement in coverage for larger values of this parameter. Results can be visualized in ***(figure 1 paper 2, (a) and (b))***, where the trends of the different planning settings can be seen. It is furthermore observed that the coverage loss was again patient-dependent, since the datasets for the specific patients presented marked anatomical differences between the planning and the delivery anatomy. A summary can be found for all beam setups and beam settings used in this study in ***(table 2 paper 2)***.

In order to quantify the influences of the different carbon ion plan settings and the calculated ΔWEPL as described in ***paper 2*** on the coverage loss, a multivariate analysis of the subset of clinically acceptable carbon ion plans was carried out. The linear model which explained best the fluctuations in the GTV $\Delta V_{95\%}$ was given by ΔWEPL, the PTV volume and the contour extension (Rsquared of 0.58, $p<0.05$), with ΔWEPL being the strongest predictor (R-square of 0.40, $p<0.05$, in a univariate analysis).

2.1.5 Effect of the number of fields

In ***paper 1***, plans with 3-4 and 5-7 fields (MultiF1 and MultiF2) were additionally calculated and compared with the 2-field plans with beam setup 2FA. As mentioned, the MultiF2 plans were created using the same beam directions as for the SBRT with which the patients were originally treated. It was observed that a higher number of beams helped in coverage conservation ***(table 1 paper 1)*** and ***(supplement paper 1)***. The plans with a larger number of beams displayed a higher conformity ***(figure 2 paper 1)*** but as a tradeoff, they also presented an enlarged low dose region. No significant correlation existed between the global mean ΔWEPL and the coverage loss for the plans using more than two beams. The maximum loss in GTV $V_{95\%}$ of the proton plans with more than two fields remained in all cases below 3%. However, for some patients, adding more fields did not always maintain nor improve the dosimetric reproducibility of the 2-field plans. For three patients the GTV $\Delta V_{95\%}$ for the MultiF2 setup worsened with respect to the MultiF1 plans. For patient 3, the GTV $\Delta V_{95\%}$ increased from 0.1 to 2.7 pp with the use of seven fields with respect to the 2-field plan. For this patient, the ΔWEPL value increased from 2.3 mm on average in the PTV to 2.5 mm for the field directions in MultiF1 and MultiF2. This particular case shows that an increased number of fields alone does not always lead to improved coverage preservation, but, in addition, it is important to carefully select the beam directions.

2.1.6 Influence of the different beam directions

Total ΔWEPL values for each plan were calculated as the averaged ΔWEPL for each beam direction and this was correlated with the coverage loss in the GTV. For the plans with field setup 2FA, the median decrease in the GTV $V_{95\%}$ between the plan and the recomputation was 0.1 pp, ranging from 0 pp to 8.9 pp. Two patients in the series presented an unacceptably high decrease, patient 7 with 4.5 pp and patient 10A with 8.9 pp, both representing the largest differences in the mean absolute value of the WEPL at the combined beam directions 0° and -45° of 4.7 and 4.5 mm, respectively. The Spearman's correlation for the ΔV95% and the ΔWEPL was 0.701 (p=0.02), and after removing the afore-mentioned two worst cases, the correlation decreased to 0.670 (p=0.034).

Assuming a fixed beamline from the vertical direction, new 2-field proton plans were prepared with the beam setups 2FB and 2FC. For 2FB, the GTV $\Delta V_{95\%}$ values were reduced to 1.3 and 0.0 pp in the problematic cases, reflected also in lower WEPL differences of 3.3 mm and 1.5 mm, respectively. The median (range) GTV $\Delta V_{95\%}$ was 0.0 (-0.3-3.5). The correlation between $\Delta V_{95\%}$ and ΔWEPL was not significant. The 2FC plans also showed generally low ΔWEPL values for all patients with a median (range) $\Delta V_{95\%}$ of 0 (-0.6-0.3). Again, no significant correlation was found between $\Delta V_{95\%}$ and ΔWEPL. The same trends were seen for the carbon ion plans.

2.1.7 Effects of CT calibration uncertainties

For two representative patients with the deepest and shallowest PTV in the cohort, the proton plans presented in ***paper 1*** were additionally recalculated introducing 3.5% over- and underrange estimations in the CT calibration table in order to assess the dosimetric consequences of possible errors in the proton range calculation of a realistic size on a modified anatomy [Moyers 2001]. The interest of this check lies in estimating the performance of the 5 mm isotropic margins that were used in this study, versus range uncertainties. CT calibration uncertainties of ±3.5% led to moderate GTV $V_{98\%}$ reductions below 1.5 pp in most plans with field setups 2FA, MultiF1, and MultiF2. Beam undershoot leads to larger coverage reductions than the overshoot of up to 3 pp for the 2FA plans.

2.2 Modeling of the dose response relationship of NSCLC

In ***paper 3***, the dose response relationship of early stage NSCLC tumors was studied based on published outcome reports after fractionated treatment, modeled both with the LQ and

the LQ-L approaches. We selected reports on 3-year local control (LC) of cohorts treated with curative radiotherapy as single treatment. Details of the reviewed studies can be found in (***table 1***, ***table 2***, ***table 3***, and ***suppl 1*** from ***paper 3***). The main characteristics of the cohorts included in this study have been summarized in the table below for convenience of the reader, in two groups, namely, patients treated with conventionally fractionated (CF) and hypofractionated (HF) treatments (dose per fraction < or ≥ 6 Gy per fraction):

Table R2: Summary of the patient characteristics.

	CF treatments	**HF treatments**
Patient features	8 studies, 344 patients	23 studies, 1975 patients
	treated between 1976 - 2010	treated between 1996 - 2012
	no routine PET-CT staging	PET-CT staging routine
	86.3% inoperable	55.2% inoperable
	median age 72 [range: 35-90] years	median age 75 [range: 29-94] years
Treatment features	Margins 1.0-1.5 cm around the GTV	GTV-to-CTV margins in 5/23 series
		ITV concepts in 13/23 series
	dose at isocenter in 5/8 series	9/23 report dose to isocenter
		11/23 to PTV edge, usually 80% isoline
	median BED10 @iso:	median BED10 @iso:
	82 [67.2-93.5] Gy	89.9 [56.8-211.2] Gy
	fraction dose < 6 Gy	fraction dose ≥ 6 Gy
Reported outcomes	3-y LC: 63 [50-91]	3-y LC: 86 [55-100]
	median follow up: 28.5 months	median follow up: 27 months

Based on this data collection we fitted a logistic dose response relationship with nonlinear least squares of the 3-year LC versus BED, both for doses at the isocenter and at the PTV edge. The logistic model was coupled with BED definitions given by the LQ and the LQ-L approaches. These two models include three and four parameters, respectively: TCD_{50}, k, α/β, and additionally D_t in the case of the LQ-L model. TCD_{50} is the dose necessary to obtain a local tumor control of 50%, k is a parameter related to the slope of the sigmoid curve, and D_t is an additional parameter describing the dose per fraction from which the effect from a certain fraction dose is not linear-quadratic but purely linear with dose. We compared the LQ- and LQ-L-based fits with the maximum likelihood ratio since they are nested models. A summary of all the models is presented in ***(table 5 paper 3)***. Our first case

was to assume the commonly accepted value of 10 Gy for the α/β ratio. We fitted either the whole data set or the subsets of CF and HF data under this α/β assumption. The models based on dose at the isocenter and the PTV edge showed a similar behavior but with the models based on dose at the isocenter showing consistently higher TCD_{50} values than the models based on the dose at the PTV edge. Thus, here only the models based on the values at the isocenter will be commented. For the fits based on the CF data, both the steepness of the curve and the TCD_{50} values are closer to the values that might be expected clinically, whereas for the data sets including HF data the TCD_{50} is displaced towards lower values and the steepness is consistently lower. The values of the parameters were only significant ($p < 0.05$) in the case of the full dataset. For the LQ-L fit a significant value of D_t (standard error) was found of 11.0 ± 5.2 Gy. Similar values for D_t, in the range between 9.8 Gy and 12.4 Gy, were also consistently found for the subset of HF data alone and for the models based on doses at the PTV edge as well, with both the full and the HF datasets (see ***table 5 paper 3***). None of the D_t values estimated under any of the different assumptions were statistically significant. The LQ and LQ-L fits did not differ significantly, neither according to the maximum likelihood ratio test nor visually (see ***figure 1a*** and ***1b*** in ***paper 3***). Differences in isoeffect prediction with the LQ and LQ-L models are small beyond 3 or more fractions. For instance, for a BED of 100 Gy according to the LQ-L or LQ with α/β equal to 10 Gy and D_t of 11.0 Gy the BED differences remain equal to or below 3.3 Gy, as presented in (***figure 4 paper 3)***.

For an estimation of the α/β ratio, two logistic fits were made based on the BED description of the LQ model both based on the full and the CF datasets with the α/β ratio as a fit parameter as well. The value obtained from the direct LQ fit for the complete fractionation range was 3.9 [68% CI: 2.2–9.0] Gy ($p > 0.05$) for the doses at the isocenter ***(figure 3a paper 3)***. The value from the fit based on the CF dataset only was 3.8 Gy (no 68% CI calculation was possible in this case). These values were not statistically significant, and neither were the equivalent values considering doses at the PTV edge. Nevertheless, the values found for the fits with a free α/β ratio were consistently lower than 10 Gy.

3 Aim and Contribution

Particle therapy is still an evolving technique which can potentially offer improved lung cancer treatments. Prior to clinical use for this location, tumor motion needs to be addressed, in particular for scanned beam delivery. One straightforward solution is tumor fixation, for instance through HFJV. The present work aims, firstly, at performing a dosimetric comparison of the target coverage with both proton and carbon ion planning between planned versus recalculated dose on the anatomy at delivery time and to investigate the influence of various treatment parameters on the dosimetric coverage. Secondly, the dose response relationship according to the LQ approach and an estimation of the α/β value for early stage NSCLC were obtained based on LC reviewed data using state of the art modeling methods.

Publication 1

Reproducibility of target coverage in stereotactic spot scanning proton lung irradiation under high frequency jet ventilation

This publication estimates the reproducibility of the dosimetric target coverage between the planning and the application of the proton radiation treatment under assumption of target fixation through HFJV. The study was designed by me and U. Jelen with advice from A. Wittig and P. Fritz. I performed the treatment planning, extracted and analyzed the data. P. Fritz and W. Mühnickel provided the patient datasets for the study. A. Wittig carried out the patient contouring and the image co-registration and I prepared extra contours for the dosimetric analysis and exported and processed all the DICOM data. U. Jelen and F. Ammazzalorso supported all questions related to the treatment planning with TRiP98 and the DICOM handling, and contributed to the drafting of the manuscript. U. Jelen contributed to the interpretation of the results. R. Engenhart-Cabillic contributed with corrections to the manuscript. All authors read and approved the manuscript.

Publication 2

Changes in the radiological depth correlate with dosimetric deterioration in particle therapy for stage I NSCLC patients under high frequency jet ventilation

This work broadens the previous study to include carbon ion and further proton planning, quantifies the anatomical changes between planning and irradiation, correlates them with the dose deterioration, and assesses the influence of various planning parameters on the

dosimetric reproducibility. I conceived the study, developed the tools for the analysis of the radiological depth, analyzed and interpreted the results and drafted the manuscript. P. Fritz and W. Mühnickel provided patient datasets. A. Wittig helped with the case selection, did the contouring and the image co-registration. A. Wittig and R. Engenhart-Cabillic revised the manuscript and contributed to the result interpretation. All authors read, corrected, and approved the final manuscript.

Publication 3

Challenges in radiobiological modeling: can we decide between LQ and LQ-L models based on reviewed clinical NSCLC treatment outcome data?

This work investigated the dose-response of NSCLC tumor control data from conventionally fractionated and hypofractionated radiotherapy treatments, based on a review of published outcome results, evaluating the validity of the LQ and LQ-L models for both conventional and SBRT treatments, and obtaining an estimation of the clinical α/β ratio of NSCLC. A. Wittig, S. Barczyk, U. Jelen and R. Rita Engenhart-Cabillic conceived the study. I designed the search strategy, collected and assembled the data, analyzed and interpreted the results and drafted the manuscript. A. Wittig and S. Barczyk contributed to design the search strategy and supported the data collection. U. Jelen also contributed to the search strategy. A. Wittig and U. Jelen revised the manuscript and contributed to the interpretation of the results. All authors read and approved the final manuscript.

Hiermit bestätige ich die Richtigkeit der gemachten Angaben bezüglich des Eigenanteiles von Alina Santiago García an den aufgeführten Publikationen.

Marburg, 13. October 2016

Alina Santiago García (Autorin)

Prof. Dr. Andrea Wittig (Betreuerin)

4. Discussion

A strong rationale exists for treatment of lung tumors with particle therapy, as potentially the risk of normal tissue damage can be reduced with equal or improved LC rates as compared to photon radiotherapy. Recent meta-analyses suggest that the optimal total dose for advanced stage NSCLC has yet to be reached, however, investigation into modern treatment methods is required in order to reduce the high toxicity of chemoradiation [Kong 2014, Ramroth 2016]. A recent phase III trial on dose-escalation in chemoradiotherapy for advanced stage NSCLC found that higher total radiation dose, PTV volume, grade of esophagitis, and heart V5 and V30 were negative predictors for overall survival in a multivariate analysis [Bradley 2015] showing the potential of optimizing the target volume definition and OAR sparing through advanced delivery techniques. Carbon ion radiotherapy may offer clear clinical advantages through optimized dose distribution and a higher biological effectiveness in the BP [Karube 2015, Takahashi 2015].

4.1 Potential strategies for decreased tumor movement in particle therapy

To date, clinical data are sparse and mainly limited to facilities using the passive scattering technique, which is due to the still small number of facilities available worldwide but also due to technical and dosimetric challenges related to the scanned beam technique. In addition, especially for heavy ion therapy, uncertainties in the biological effect complicate the use of the technique within clinical trials. Until now, the majority of lung tumors treated with particle therapy have been irradiated with passive scattering. In absence of interplay, different approaches for ITV construction coexist and are commonly used, combined with gating and breath hold to reduce the ITV size and reduce anatomical variation in the entrance channels. Field specific safety margins achieved normally through hardware design help to compensate range uncertainties and range variations produced by anatomical changes and setup errors [Knopf 2016]. Few clinical experiences with scanned beam particle therapy for lung tumors have been published so far. However, this situation might change rapidly in the coming years since many of the upcoming particle therapy centers are utilizing this technique [Knopf 2016]. Active scanning leads to more conformal dose distributions and does not require the fabrication of patient specific hardware. Concerning dosimetric reproducibility, tumor motion in the lung represents the main difficulty as this may cause target miss as well as shifts in the BP positions. This is partly caused by density changes in the lung and the surrounding anatomy. Dose deterioration caused by tumor

motion is even more pronounced in actively scanned beam particle therapy than in passive scattering due to interplay effects. HFJV is a known method for tumor fixation in radiotherapy, which has successfully been implemented for ITV reduction in photon SBRT. Active beam delivery together with motion mitigation techniques such as gating, breath hold or rescanning, alone or combined, seems to be the preferred option for treatment of moving targets. So far, there are however no guidelines for crucial questions such as the optimal motion mitigation approach, for margin definition, for evaluation of dosimetric motion consequences, for motion monitoring, and for quality assurance of moving targets [Knopf 2016, Chang 2016]. Research aiming at an optimal implementation of solutions for active beam scanning particle therapy for moving targets is thus warranted.

Gating has been successfully implemented in photon radiotherapy of moving tumors, often in combination with other methods aiming at reduction of tumor motion such as breath hold techniques. Breath hold is mature for use in conventional radiotherapy [Boda-Heggemann 2016] and it is under current investigation for use in particle therapy treatments in the lung [Stuschke 2012, Dueck 2016, Knopf 2016].

HFJV has proven to have some clear advantages for use in radiotherapy. It is a ready-to-use solution, which allows for an immediate clinical translation without the need of specific hardware development. It is also appropriate even for patients with poor lung function who cannot comply with breath hold. The main limitation of this technique is that it requires to be applied under anesthesia. Therefore, it is only suitable for oligofractionated treatments. A new variant of the jet ventilation technique, the so called high frequency percussion ventilation (HFPV) does not require anesthesia and therefore it might allow a broader spectrum of fractionated treatments. It is currently undergoing test for application in photon radiotherapy, where it showed average apnea-like breath hold times for the first three treated mixed-indication patients of 7.6 minutes, with no beam-off time as in conventional breath hold approaches [Péguret et al 2016]. Another non-invasive mechanical ventilation technique for assisted breath hold has proven breath holds of more than 5 minutes in average to be possible [Parkes 2016(a)]. These techniques might be regarded with interest in the future for integration in the conventional radiotherapy work flow, and even more in a scanned beam particle therapy context due to the higher needs for tumor motion management solutions [Baumann 2016]. In the coming years multiple approaches for motion management will likely coexist, and the particle therapy centers will have to choose

the best option, based upon their technical characteristics, their mix of indications, their clinical approach, etc.

4.2 Dosimetric reproducibility of planned target coverage

Paper 1 and ***paper 2*** present the first investigations on target coverage reproducibility in repeated applications of HFJV for tumor fixation in the novel context of scanned beam particle irradiation. In the datasets used for this study, lung tumors were proven to be static, and thus effects of intrafractional motion such as interplay effects could be ignored. The results show that this procedure is reproducible and that satisfactory tumor coverage is achieved in most cases. As expected, larger anatomical differences correlate significantly with decrease in the coverage indexes. Anatomical variations e.g. due to patient positioning, which may have no significant impact on high-precision photon dose distributions, can cause large mis-dosages in a particle therapy treatment. Selected patients in this study would have necessitated actions to correct for such anatomical deviations before particle irradiation. Mis-dosage is more pronounced in the case of small PTVs since dosimetric deviations in a static tumor as made possible by HFJV take place preferentially at the target borders. The influence of the target size observed in this study is in agreement with results of similar investigations on proton lung irradiation under breath hold [Dueck 2016].

Treatment planning settings can help to compensate for anatomical deviations, such as the use of an increased number of beams and carefully selected beam directions as shown in ***paper 2***. In general, larger anatomical differences were observed in the ventrolateral direction caused by the arm mobility, and for this reason special care has to be taken when choosing this direction for irradiation of the chest. This is especially important in facilities with fixed oblique beam lines with reduced beam angle options such as MIT. Certain raster scan settings can also contribute to confer the plan dosimetric robustness and in ***(figure 1 paper 2)*** an observation was made indicating a preserved target coverage for carbon ions when larger spot sizes and decreased grid sizes and energy steps were used, which is in line with the findings of other studies [Richter 2014, Brevet 2015]. In contrast, none of the previous plan settings were included in the best multivariate linear model, but the choice made on the contour extension, a planning parameter which is rarely specified in published planning studies for scanned beam particle therapy of the kind of the present study, was found to have a significant role in plan conformity and homogeneity, as well as in dosimetric reproducibility. This result suggests that this parameter (when available)

should also be reported when performing dosimetric studies similar to the one at hand. A check for the effect of range uncertainties showed acceptable changes of the delivered GTV coverage in most patients. This suggests that 5 mm isotropic margins might be adequate for the irradiation scenario assumed here, based on tumor fixation.

4.3 Need of intrafractional imaging

One limitation of the present work is that no intrafractional nor post-treatment imaging was available for the patient cohort. Therefore, no information was available on possible intrafractional tumor baseline shift, caused for instance by muscle relaxation during the treatment. Data exist which show that settlement movements occur in the chest during the first seconds of both assisted and unassisted breath hold as well as chest deflation causing tumor movement [Parkes 2016]. Under use of percussion ventilation techniques, tumor movement has been estimated in the range of 2-4 mm or larger from the beginning of the fraction until the end [Péguret 2016]. Research is thus required to determine the size of these effects before determination of the optimal technique-specific PTV margins.

Image guidance is necessary to fully exploit the dosimetric advantages of particle therapy in lung tumors, even more than in high precision photon therapy. However, extensive use of x-ray imaging of moving targets before and during treatment increases the overall patient dose. Low-dose protocols and protocol optimization can reduce the imaging dose to the patient substantially. The total dose received by radiotherapy patients should be assessed, and strategies should be worked out to reduce it if necessary. Little is known about the status of imaging dose in particle therapy centers. Measurements were performed at MIT (Alina Santiago, Urszula Jelen) for a study aiming at determination of the total imaging dose for a patient under employ of different image guidance solutions for photon and particle beam therapy [Steiner 2013]. For the final dose calculation, realistic imaging protocols were assumed, adapted to single fraction or three-fraction treatment under use of HFJV. It was found that OAR doses depended on imaging modality and OAR position and, as an example, that comparison of the imaging dose for hypothetical 3-fraction treatment protocols at the participating centers shows a large span of values with doses to the anterior skin at the isocenter ranging from 323 to 27 mGy, with doses at MIT being 53 mGy.

4.4 Irradiation time reduction through use of new design ripple filters

Gating, breath hold or a combination of these lead to longer irradiation times as does rescanning, alone or in combination with gating. At synchrotron-based facilities the change between isoenergy slices is the most time-consuming part of the pure irradiation and by reducing the number of isoenergy slices required to homogeneously cover a target, a significantly shorter irradiation time can be achieved. A method for this applied in carbon ion therapy treatments at centers like HIT and MIT is the ripple filter [Weber 1999]. A thicker optimized filter design, which can lower the irradiation time even further, is currently under investigation [Ringbæk 2016] and could potentially be used in proton therapy as well. A thicker filter is of particular benefit in the case of moving targets such as in the lung**.** The NSCLC cases presented in ***paper 1*** and ***paper 2*** were among a cohort of patients selected for planning comparisons between ripple filter designs and thicknesses [Ringbæk 2016] and was specially chosen for testing the limits of the performance of the ripple filters for superficially located, small targets as well as for lung tumors. Thicker ripple filters were found to yield comparable results in terms of coverage, dose homogeneity and OAR sparing when compared with the clinically established thinner ripple filter, with a slightly worse conformity.

4.5 Dose-response relationship based on clinical NSCLC data

In this work a question was addressed which is relevant for two different topics in radiotherapy: design and optimization of hypofractionated photon treatments and biological treatment planning for ion therapy. The need of reliable models to estimate biological effects has been pointed out independently in both fields, to describe accurately the treatment outcome under specific fractionation schedules. State-of-the-art modeling procedures for analysis of clinical data were used to compare the fits provided by the generally accepted LQ model and the LQ-L correction for high dose fractions, and to obtain an estimation of the clinical α/β values for NSCLC. Ideally, pooled individual outcome data allow precise metaanalyses [Guckenberger 2013]. Alternatively, review of published clinical data allows collecting long term information from a large number of patients. Such analyses present a series of challenges. These data collections are highly heterogeneous in relation to target volume definition, dose prescription, planning concepts and delivery techniques among other aspects, as explained in detail in the discussion section of ***paper 3***. We tried to apply strict inclusion criteria to the reviewed cohorts to reduce this

heterogeneity. In ***paper 3*** we present the full raw data to allow independent check of our calculations, or to answer further research questions.

The collected dose response data set cover the full range of fractionation schemes, as required for the intended task. As mentioned, the outcome data was fitted to both applied dose at the PTV edge and at the isocenter. That the Spearman's correlations between LC and BED for different α/β values are consistently lower for the doses at the PTV edge may suggest that the isocenter doses are more robust for retrospective modeling of the dose response relationship. Possible reasons for this could be the different margins employed by different institutions and the uncertainties in the dose calculation methods, which in the case of outdated, less accurate dose calculation algorithms for the lung would produce large dose mis-estimation at the PTV edge.

The dose response curves based on conventional fractionation data and with α/β fixed to 10 Gy reproduce well the steepness of the curve around the TCD_{50} value. We obtained a similar curve to the one in [Martel 1999], based on advanced NSCLC data, although displaying a lower TCD_{50} value since early stage tumors require lower curative doses. For the curve fits including the HF data the TCD_{50} values become smaller, and the steepness of the curve lower, similarly to what was observed in a study based on pooled individual outcome data after SBRT treatment [Guckenberger 2013]. The local control at high BED values does not approach 100% and the observed dose-effect for local control in NSCLC is weaker at high BED values due to data dispersion. This might reflect that other factors dominate the dose response relationship at high doses such as target delineation errors or geographic miss.

For the dose response fits based on the LQ-L relationship, we obtained D_t values between 9.8 and 12.4 Gy under the different assumptions: all data sets, only HF data, and for both doses at the isocenter and the PTV edge. Only the value obtained for doses at the isocenter for the full data set was statistically significant, 11 Gy (68%CI: 8.4-16.7). Both LQ and LQ-L fits can model local tumor control after conventionally and HF irradiation, and for BED 10 values of 100–150 Gy in ≥3 fractions, the differences in isoeffects predicted by both models are small and can be neglected. Our findings did not allow us to suggest use of the LQ-L model for an improved fitting compared to the LQ model of local control data in case of hypofractionation. A tentative analysis to establish the optimal α/β ratio in the frame of the LQ model for the full fractionation range did not produce significant estimates, although it showed a trend for α/β values lower than 10 Gy.

Modeling of radiobiological effects is a complex but crucial task for ion beam therapy treatment planning. The LEM requires the input of LQ parameters, namely α and β separate values, although their influence on the RBE is small compared to the α/β ratio [Jäkel 2007]. This fact allows potentially to incorporate α/β values from clinical data, for both tumor and normal tissue reactions [Schardt 2010]. As mentioned in section 1.5, realistic clinical α/β values are necessary for particle therapy planning. A fixed α/β value of 2 Gy derived from normal brain tissue has been used for different tumor entities undergoing treatment with carbon ions at one of the three scanned ion beam facilities in Europe using LEM-based TPS [Krämer 2000]. Certain lung tumors are planned to be treated within a clinical trial at HIT but so far no α/β values have been specified for biological treatment planning [Hauswald 2015].

4.6 Outlook

In-house tools such as for the quantification of the changes in radiological depth can be helpful in treatment planning, for instance to determine anatomically stable irradiation directions. Some functions that are not available in commercial TPS may be desirable for checking the need of adaptive strategies and for patient related quality assurance in a context of particle radiotherapy treatment of moving targets. Together with specific plan optimization approaches, calculation of dedicated margins are the two strategies to achieve plan robustness [Flampouri 2014, Knopf 2016]. Based on the present work, a tool for the calculation of beam specific PTV has been developed to explore the performance of novel margin definitions aiming at improved dosimetric plan robustness towards setup and range uncertainties, under use of HFJV. Small changes in the radiological depth caused by anatomical changes, mispositioning, or uncertainties in the range estimation are enlarged by the low density of lung tissue surrounding the tumor. A follow up project will evaluate different margin concepts for scanned beam particle therapy, applied to the exploration of concepts for dose escalation and reduced side effects for advanced stage NSCLC.

Only one recent publication offers an α/β ratio of 6 Gy for treatment planning for lung tumors in a research context [Wölfelschneider 2015], estimated after comparison with treatment results and biological doses from passive scattering carbon ion experiences in Japan. For the moment, it is not possible to contribute with a good estimate of α/β purely derived from clinical outcomes. A new value should only be used clinically under the certainty that the description of the biological effects of carbon ions will be more accurate.

However, in silico studies on the consequences of different assumptions made on α/β for plan optimization can be useful for hypothesis generation, for instance, for design of new treatment schedules.

5 References

Albertini F, Hug EB and Lomax AJ. Is it necessary to plan with safety margins for actively scanned proton therapy? Phys. Med. Biol. 56 (2011) 4399–4413.

Allen AM, Pawlicki T, Dong L, Fourkal E, Buyyounouski M, Cengel K et al. An Evidence Based Review of Proton Beam Therapy: The report of ASTRO's emerging technology committee. Radiother Oncol 2012; 103:8–11.

Allen Li X, Alber M, Deasy JO, Jackson A, Ken Jee KW, Marks LB, et al. The use and QA of biologically related models for treatment planning: short report of the TG-166 of the Therapy Physics Committee of the AAPM. Med Phys 2012; 39:1386–409.

Astrahan M. Some implications of linear-quadratic-linear radiation dose-response with regard to hypofractionation. Med Phys 2008; 35:4161–72.

Barendsen GW Dose fractionation, dose rate and iso-effect relationships for normal tissue responses. Int J Radiat Oncol Biol Phys 1982; 8:1981–97.

Baumann M, Overgaard J. Bridging the valley of death: The new Radiotherapy & Oncology section "First in man - Translational innovations in radiation oncology". Radiother Oncol. 2016 Feb;118(2):217-9.

Berman AT, James SS, Rengan R. Proton beam therapy for non-small cell lung cancer: Current clinical evidence and future directions. Cancers (Basel) 2015; 7:1178–90.

Bert C, Durante M. Motion in radiotherapy: particle therapy. Phys Med Biol 2011; 56:R113–44.

Bert C, Graeff C, Riboldi M, Nill S, Baroni G, Knopf AC. Advances in 4d treatment planning for scanned particle beam therapy - report of dedicated workshops. Technol Cancer Res Treat 2014; 13:485–95.

Blakely EA, Tobias CA, Ngo FQH, Curtis SB. Physical and cellular radiobiological properties of heavy ions in relation to cancer therapy application. Biological and medical research with accelerated heavy ions at the Bevalac, 1977-1980. Report Lawrence Berkeley Laboratory LBL-11220 1980. Technical report.

Boda-Heggemann J, Knopf AC, Simeonova-Chergou A, Wertz H, Stieler F, Jahnke A, Jahnke L, Fleckenstein J, Vogel L, Arns A, Blessing M, Wenz F, Lohr F. Deep

inspiration breath hold-based radiation therapy: A clinical review. Int J Radiat Oncol Biol Phys 2016; 94:478–92.

Böhlen TT, Brons S, Dosanjh M, Ferrari A, Fossati P, Haberer T, Patera V, Mairani A. Investigating the robustness of ion beam therapy treatment plans to uncertainties in biological treatment parameters. Phys Med Biol 2012; 57:7983–8004.

Bradley JD, Paulus R, Komaki R, Masters G, Blumenschein G, Schild S, et al. Standard-dose versus high-dose conformal radiotherapy with concurrent and consolidation carboplatin plus paclitaxel with or without cetuximab for patients with stage IIIa or IIIb non-small-cell lung cancer (RTOG 0617): a randomised, two-by-two factorial phase 3 study. Lancet Oncol 2015; 16:187–99.

Brevet R, Richter D, Graeff C, Durante M, Bert C. Treatment Parameters Optimization to Compensate for Interfractional Anatomy Variability and Intrafractional Tumor Motion. Front Oncol. 2015 Dec 24;5:291.

Britton KR, Starkschall G, Liu H, Chang JY, Bilton S, Ezhil M, et al. Consequences of anatomic changes and respiratory motion on radiation dose distributions in conformal radiotherapy for locally advanced non-small-cell lung cancer. Int J Radiat Oncol Biol Phys 2009; 73:94–102.

Brown JM, Carlson DJ, Brenner DJ. The tumor radiobiology of SRS and SBRT: are more than the 5 Rs involved? Int J Radiat Oncol Biol Phys 2014; 88:254–62.

Carabe A, Moteabbed M, Depauw N, Schuemann J, Paganetti H. Range uncertainty in proton therapy due to variable biological effectiveness. Phys Med Biol 2012; 57:1159–72.

Casares-Magaz O, Toftegaard J, Muren LP, Kallehauge JF, Bassler N, Poulsen PR, Petersen JBB. A method for selection of beam angles robust to intra-fractional motion in proton therapy of lung cancer. Acta Oncol 2014; 53:1058–63.

Castro J. Heavy ion therapy: Bevalac epoch. Report Lawrence Berkeley Laboratory LBL-35418 1993. Technical report.

Chang JY, Kestin LL, Barriger RB, Chetty IJ, Ginsburg ME, Kumar S, et al. ACR appropriateness criteria for nonsurgical treatment for locally advanced non-small-

cell lung cancer: good performance a status/definitive intent. Oncology (Williston Park) 2014; 28:706–10, 712, 714 passim.

Chang JY, Jabbour SK, De Ruysscher D, Schild SE, Simone CB, Rengan R, et al; International Particle Therapy Co-operative Group Thoracic Subcommittee. Consensus Statement on Proton Therapy in Early-Stage and Locally Advanced Non-Small Cell Lung Cancer. Int J Radiat Oncol Biol Phys. 2016 May 1;95(1):505-16.

Chanrion MA, Sauerwein W, Jelen U, Wittig A, Engenhart-Cabillic R, Beuve M. The influence of the local effect model parameters on the prediction of the tumor control probability for prostate cancer. Phys Med Biol 2014; 59:3019–40.

Chi A, Nguyen NP, Welsh JS, Tse W, Monga M, Oduntan O, et al. Strategies of dose escalation in the treatment of locally advanced non-small cell lung cancer: image guidance and beyond. Front Oncol 2014; 4:156.

Chi A, Wen S, Liao Z, Fowler J, Xu J, Nguyen NP, Welsh JS, Komaki R. What would be the most appropriate a/b ratio in the setting of stereotactic body radiation therapy for early stage non-small cell lung cancer. Biomed Res Int 2013; 2013:391 021.

Combs SE, Debus J. Treatment with heavy charged particles: systematic review of clinical data and current clinical (comparative) trials. Acta Oncol. 2013 Oct;52(7):1272-86.

Combs SE, Djosanjh M, Pötter R, Orrechia R, Haberer T, Durante M, et al. Towards clinical evidence in particle therapy: ENLIGHT, PARTNER, ULICE and beyond. J Radiat Res 2013; 54 Suppl 1:i6–12.

De Ruysscher D, Chang JY. Clinical controversies: proton therapy for thoracic tumors. Semin Radiat Oncol 2013; 23:115–9.

De Ruysscher D, Mark Lodge M, Jones B, Brada M, Munro A, Jefferson T, Pijls-Johannesma M. Charged particles in radiotherapy: a 5-year update of a systematic review. Radiother Oncol 2012; 103:5–7.

Delaney G, Jacob S, Featherstone C, Barton M. The role of radiotherapy in cancer treatment: estimating optimal utilization from a review of evidence-based clinical guidelines. Cancer 2005; 104:1129–37.

Demizu Y, Fujii O, Iwata H, Fuwa N. Carbon ion therapy for early-stage non-small-cell lung cancer. Biomed Res Int 2014; 2014:727 962.

Dueck J, Knopf AC, Lomax A, Albertini F, Persson GF, Josipovic M, et al. Robustness of the voluntary breath-hold approach for the treatment of peripheral lung tumors using hypofractionated pencil beam scanning proton therapy. Int J Radiat Oncol Biol Phys 2016; 95:534–41.

Eberhardt WEE, De Ruysscher D, Weder W, Le Péchoux C, De Leyn P, Hoffmann H, et al. 2nd ESMO consensus conference in lung cancer: locally advanced stage III non-small-cell lung cancer. Ann Oncol 2015; 26:1573–88.

Elsässer T, Kr ämer M, Scholz M. Accuracy of the local effect model for the prediction of biologic effects of carbon ion beams in vitro and in vivo. Int J Radiat Oncol Biol Phys 2008; 71:866–72.

Enghardt W, Debus J, Haberer T, Hasch BG, Hinz R, Jäkel O, et al. The application of pet to quality assurance of heavy-ion tumor therapy. Strahlenther Onkol 1999; 175 Suppl 2:33–6.

Flampouri S, Hoppe BS, Slopsema RL, Li Z. Beam-specific planning volumes for scattered-proton lung radiotherapy. Phys Med Biol 2014; 59:4549–66.

Fowler JF. Development of radiobiology for oncology-a personal view. Phys Med Biol 2006; 51:R263–86.

Friedrich T, Scholz U, Elsässer T, Durante M, Scholz M. Systematic analysis of RBE and related quantities using a database of cell survival experiments with ion beam irradiation. J Radiat Res 2013; 54:494–514.

Friedrich T. Phys med biol. 2013 Oct 7;58(19):6827-49. Sensitivity analysis of the relative biological effectiveness predicted by the local effect model

Fritz P, Kraus HJ, Mühlnickel W, Sassmann V, Hering W, Strauch K. High-frequency jet ventilation for complete target immobilization and reduction of planning target volume in stereotactic high single-dose irradiation of stage I non-small cell lung cancer and lung metastases. Int J Radiat Oncol Biol Phys. 2010 Sep 1;78(1):136-42.

Giovannini G, Böhlen T, Cabal G, Bauer J, Tessonnier T, Frey K, Debus J, Mairani A, Parodi K. Variable RBE in proton therapy: comparison of different model predictions and their influence on clinical-like scenarios. Radiat Oncol 2016; 11:68.

Gray LH, Conger AD, Ebert M, Hornsey S, Scott OC. The concentration of oxygen dissolved in tissues at the time of irradiation as a factor in radiotherapy. Br J Radiol 1953; 26:638–48.

Guckenberger M, Klement RJ, Allgäuer M, Appold S, Dieckmann K, Ernst I et al. Applicability of the linear-quadratic formalism for modeling local tumor control probability in high dose per fraction stereotactic body radiotherapy for early stage non-small cell lung cancer. Radiother Oncol. 2013 Oct;109(1):13-20.

Guckenberger M, Andratschke N, Alheit H, Holy R, Moustakis C, Nestle U, et al. Definition of stereotactic body radiotherapy: principles and practice for the treatment of stage I non-small cell lung cancer. Strahlenther Onkol. 2014 Jan;190(1):26-33

Guerrero M, Li XA. Extending the linear-quadratic model for large fraction doses pertinent to stereotactic radiotherapy. Phys Med Biol 2004; 49:4825–35.

Hall E and Giaccia A. Radiobiology for the Radiologist 6th edition. Lippincott William & Wilkins 2006, Philadelphia.

Hauswald H, Rieken S, Dienemann HC, Thomas M, Kieser M, Debus J et al. Ion therapy within the trimodal management of superior sulcus tumors: the INKA trial. BMC Cancer. 2015 Mar 28;15:192.

Herrmann T, Baumann M, Dörr W. Klinische Strahlenbiologie - kurz und bündig. 4. Edition. 2006. Urban&Fischer, Munich.

IAEA. Relative biological effectiveness in ion beam therapy. International Atomic Energy Agency; 2008. 461. Technical report series.

ICRU, Prescribing, recording and reporting proton-beam therapy. ICRU Report No. 78 . International Commission on Radiation Units and Measurements, Bethesda, MD, 2007.

Jäkel O, Schulz-Ertner D, Debus J. Specifying carbon ion doses for radiotherapy: the Heidelberg pproach. J Radiat Res 2007; 48 Suppl A:A87–95.

Jelen U, Bubula ME, Ammazzalorso F, Engenhart-Cabillic R, Weber U, Wittig A. Dosimetric impact of reduced nozzle-to-isocenter distance in intensity-modulated

proton therapy of intracranial tumors in combined proton-carbon fixed-nozzle treatment facilities. Radiat Oncol 2013; 8:218.

Joiner M, van der Kogel. A Basic Clinical Radiobiology.

Josipovic M, Persson GF, Dueck J, Bangsgaard JP, Westman G, Specht L, et al. Geometric uncertainties in voluntary deep inspiration breath hold radiotherapy for locally advanced lung cancer. Radiother Oncol 2016; 118:510–4.

Karube M, Mori S, Tsuji H, Yamamoto N, Nakajima M, Nakagawa K et al. Carbon-ion pencil beam scanning for thoracic treatment - initiation report and dose metrics evaluation. J Radiat Res. 2016 Sep;57(5):576-581.

Kim JO, Chu KP, Fairchild A, Ghosh S, Butts C, Chu Q, et al. Dose-escalated hypofractionated intensity-modulated radiation therapy with concurrent chemotherapy for inoperable or unresectable non-small cell lung cancer. Am J Clin Oncol 2014.

Kirkpatrick JP, Brenner DJ, Orton CG. Point/counterpoint. the linear-quadratic model is inappropriate to model high dose per fraction effects in radiosurgery. Med Phys 2009; 36:3381–4.

Knopf AC, Hong TS, Lomax A. Scanned proton radiotherapy for mobile targets-the effectiveness of re-scanning in the context of different treatment planning approaches and for different motion characteristics. Phys Med Biol 2011; 56:7257–71.

Knopf AC, Stützer K, Richter C, Rucinski A, da Silva J, Phillips J, et al. Required transition from research to clinical application: Report on the 4D treatment planning workshops 2014 and 2015. Phys Med 2016; 32:874–82.

Koay EJ, Lege D, Mohan R, Komaki R, Cox JD, Chang JY. Adaptive/nonadaptive proton radiation planning and outcomes in a phase II trial for locally advanced non-small cell lung cancer. Int J Radiat Oncol Biol Phys 2012; 84:1093–100.

Kong FMS, Zhao J, Wang J, Faivre-Finn C. Radiation dose effect in locally advanced non-small cell lung cancer. J Thorac Dis 2014; 6:336–47.

Kraft, G. Tumor therapy with heavy charged particles. Prog in Part and Nucl Phy 2000. 45: 473-544.

Krämer M, Scholz M. Treatment planning for heavy-ion radiotherapy: calculation and optimization of biologically effective dose. Phys Med Biol 2000; 45:3319–30.

Krämer M, Jäkel O, Haberer T, Rietzel E, Schardt D, Scholz M, et al. Treatment planning for scanned ion beams. Radiother Oncol 2004; 73 Suppl 2:S80–5.

Krämer M, Scifoni E, Schuy C, Rovituso M, Tinganelli W, Maier A, et al. Helium ions for radiotherapy? physical and biological verifications of a novel treatment modality. Med Phys 2016; 43:1995.

Kummermehr J, Palme B, Galwas K, Sanchez-Brandelik R, Scholz M. Response of a mammary carcinoma in vivo to single dose irradiation with 2cm SOBP carbon ions. GSI Sci Rep 2002. Technical report.

Kwint M, Conijn S, Schaake E, Knegjens J, Rossi M, Remeijer P, et al. Intra thoracic anatomical changes in lung cancer patients during the course of radiotherapy. Radiother Oncol 2014; 113:392–7.

Langen KM, Jones DT. Organ motion and its management. Int J Radiat Oncol Biol Phys 2001; 50:265–78.

Martel MK, Ten Haken RK, Hazuka MB, Kessler ML, Strawderman M, Turrisi AT et al. Estimation of tumor control probability model parameters from 3-D dose distributions of non-small cell lung cancer patients. Lung Cancer. 1999 Apr;24(1):31-7.

Mehta N, King CR, Agazaryan N, Steinberg M, Hua A, Lee P. Stereotactic body radiation therapy and 3-dimensional conformal radiotherapy for stage I non-small cell lung cancer: A pooled analysis of biological equivalent dose and local control. Pract Radiat Oncol 2012. 2(4):288-95.

Mori S, Yamamoto N, Nakajima M, Baba M. Changes in chest wall thickness during four-dimensional CT in particle lung treatment planning. Br J Radiol 2011; 84:e158–60.

Moyers MF, Miller DW, Bush DA, Slater JD. Methodologies and tools for proton beam design for lung tumors. Int J Radiat Oncol Biol Phys 2001; 49:1429–38.

Muren LP, Rossi C, Hug E, Lee A, Glimelius B. Establishing and expanding the indications for proton and particle therapy. Acta Oncol 2013; 52:459–62.

Paganetti H. Relative biological effectiveness (rbe) values for proton beam therapy. variations as a function of biological endpoint, dose, and linear energy transfer. Phys Med Biol 2014; 59:R419–72.

Paganetti H, Niemierko A, Ancukiewicz M, Gerweck LE, Goitein M, Loeffler JS, et al. Relative biological effectiveness (RBE) values for proton beam therapy. Int J Radiat Oncol Biol Phys 2002; 53:407–21.

Palma D, Senan S. Stereotactic radiation therapy: changing treatment paradigms for stage I nonsmall cell lung cancer. Curr Opin Oncol 2011; 23:133–9.

Park PC, Zhu XR, Lee AK, Sahoo N, Melancon AD, Zhang L, et al. A beam-specific planning target volume (PTV) design for proton therapy to account for setup and range uncertainties. Int J Radiat Oncol Biol Phys 2012; 82:e329–36.

Parkes MJ, Green S, Cashmore J, Stevens AM, Clutton-Brock TH, Bel A, Lens E et al. In Regard to Boda-Heggemann et al. Int J Radiat Oncol Biol Phys. 2016 Nov 1;96(3):709-10.

Patel S, Kostaras X, Parliament M, Olivotto IA, Nordal R, Aronyk K, et al. Recommendations for the referral of patients for proton-beam therapy, an Alberta health services report: a model for Canada? Curr Oncol 2014; 21:251–62.

Peeters A, Grutters JPC, Pijls-Johannesma M, Reimoser S, De Ruysscher D, Severens JL, et al. How costly is particle therapy? Cost analysis of external beam radiotherapy with carbon-ions, protons and photons. Radiother Oncol 2010; 95:45–53.

Péguret N, Ozsahin M, Zeverino M, Belmondo B, Durham AD, Lovis A, et al. Apnea-like suppression of respiratory motion: First evaluation in radiotherapy. Radiother Oncol. 2016 Feb;118(2):220-6.

Peschke P, Karger CP, Scholz M, Debus J, Huber PE. Relative biological effectiveness of carbon ions for local tumor control of a radioresistant prostate carcinoma in the rat. Int J Radiat Oncol Biol Phys 2011; 79:239–46.

Pflugfelder D, Wilkens JJ, Oelfke U. Worst case optimization: a method to account for uncertainties in the optimization of intensity modulated proton therapy. Phys Med Biol 2008; 53:1689–700.

PTCOG(a) Particle Therapy Co-Operative Group (2016). Patient Statistics. Accessed June 2016, http://www.ptcog.ch/index.php/patient-statistics.

PTCOG(b) Particle Therapy Co-Operative Group (2016). Facilities in Operation. Accessed June 2016, http://www.ptcog.ch/index.php/facilities-in-operation.

Ramroth J, Cutter DJ, Darby SC, Higgins GS, McGale P, Partridge M, Taylor CW. Dose and Fractionation in Radiation Therapy of Curative Intent for Non-Small Cell Lung Cancer: Meta-Analysis of Randomized Trials. Int J Radiat Oncol Biol Phys. 2016 Jul 25.

Richter D, Graeff C, Jäkel O, Combs SE, Durante M, Bert C. Residual motion mitigation in scanned carbon ion beam therapy of liver tumors using enlarged pencil beam overlap. Radiother Oncol. 2014 Nov;113(2):290-5.

Ringbæk TP, Weber U, **Santiago A**, Simeonov Y, Fritz P, Krämer M, Wittig A, Bassler N, Engenhart-Cabillic R, Zink K. Dosimetric comparisons of carbon ion treatment plans for 1D and 2D ripple filters with variable thicknesses. Phys Med Biol. 2016 Jun 7;61(11):4327-41.

Rodrigues G, Choy H, Bradley J, Rosenzweig KE, Bogart J, Curran WJ, et al. Definitive radiation therapy in locally advanced non-small cell lung cancer: Executive summary of an American Society for Radiation Oncology (ASTRO) evidence-based clinical practice guideline. Pract Radiat Oncol 2015; 5:141–8.

Schardt D, Elsässer T, and Schulz-Ertner D. Heavy-ion tumor therapy: Physical and radiobiological benefits. Rev. Mod. Phys 2010. 82, 383-425.

Scholz M, Kraft G. Track structure and the calculation of biological effects of heavy charged particles. Adv Space Res 1996; 18:5–14.

Scholz M, Kellerer AM, Kraft-Weyrather W, Kraft G. Computation of cell survival in heavy ion beams for therapy. The model and its approximation. Radiat Environ Biophys. 1997 Feb;36(1):59-66.

Scholz M, Matsufuji N and Kanai T. Test of the local effect model using clinical data: tumour control probability for lung tumours after treatment with carbon ion beams. Radiation Protection Dosimetry 2006, Vol. 122, No. 1–4, pp. 478–479.

Schulz-Ertner D, Tsujii H. Particle radiation therapy using proton and heavier ion beams. J Clin Oncol 2007; 25:953–64.

Seco J, Panahandeh HR, Westover K, Adams J, Willers H. Treatment of non-small cell lung cancer patients with proton beam-based stereotactic body radiotherapy: dosimetric comparison with photon plans highlights importance of range uncertainty. Int J Radiat Oncol Biol Phys 2012; 83:354–61.

Seco J, Spadea MF. Imaging in particle therapy: State of the art and future perspective. Acta Oncol 2015; 54:1254–8.

Sørensen BS, Horsman MR, Alsner J, Overgaard J, Durante M, Scholz M, et al. Relative biological effectiveness of carbon ions for tumor control, acute skin damage and late radiation-induced fibrosis in a mouse model. Acta Oncol 2015; 54:1623–30.

Steiner E, Stock M, Kostresevic B, Ableitinger A, Jelen U, Prokesch H, **Santiago A**, et al. Imaging dose assessment for IGRT in particle beam therapy. Radiother Oncol. 2013 Dec;109(3):409-13.

Stuschke M, Pottgen C. Altered fractionation schemes in radiotherapy. Front Radiat Ther Oncol 2010; 42:150–6.

Stuschke M, Kaiser A, Pöttgen C, Lübcke W, Farr J. Potentials of robust intensity modulated scanning proton plans for locally advanced lung cancer in comparison to intensity modulated photon plans. Radiother Oncol. 2012 Jul;104(1):45-51.

Suit H, DeLaney T, Goldberg S, Paganetti H, Clasie B, Gerweck L, et al. Proton vs carbon ion beams in the definitive radiation treatment of cancer patients. Radiother Oncol 2010; 95:3–22.

Takahashi W, Nakajima M, Yamamoto N, Yamashita H, Nakagawa K, Miyamoto T et al. A prospective nonrandomized phase I/II study of carbon ion radiotherapy in a favorable subset of locally advanced non-small cell lung cancer (NSCLC).Cancer. 2015 Apr 15;121(8):1321-7.

Thames HD, Bentzen SM, Turesson I, Overgaard M, Van den Bogaert W. Time-dose factors in radiotherapy: a review of the human data. Radiother Oncol 1990; 19:219–35.

Timmerman R, Heinzerling J, Abdulrahman R, Hak Choy, Meyer JL. Stereotactic body radiotherapy for thoracic cancers: recommendations for patient selection, setup and

therapy. In: IMRT, IGRT, SBRT advances in the treatment planning and delivery of radiotherapy. Basel, Freiburg, Paris: Karger; 2011. p. 406.

Tommasino F, Scifoni E, and Durante M. New Ions for Therapy. International Journal of Particle Therapy: Winter 2016, Vol. 2, No. 3, pp. 428-438.

van Baardwijk A, Bosmans G, Bentzen SM, Boersma L, Dekker A, Wanders R, Wouters BG, Lambin P, De Ruysscher D Radiation dose prescription for non-small-cell lung cancer according to normal tissue dose constraints: an in silico clinical trial. Int J Radiat Oncol Biol Phys 2008; 71:1103–10.

Vansteenkiste J, CrinòL, Dooms C, Douillard JY, Faivre-Finn C, Lim E, et al. 2nd ESMO consensus conference on lung cancer: early-stage non-small-cell lung cancer consensus on diagnosis, treatment and follow-up. Ann Oncol 2014; 25:1462–74.

Wambersie A, Hendry J, Gueulette J, Gahbauer R, Pötter R, Grégoire V. Radiobiological rationale and patient selection for high-LET radiation in cancer therapy. Radiother Oncol 2004; 73 Suppl 2:S1–14.

Wambersie A, Menzel HG, Andreo P, DeLuca PM, Gahbauer R, Hendry JH, et al. Iso-effective dose: a concept for biological weighting of absorbed dose in proton and heavier-ion therapies. Radiat Prot Dosimetry 2011; 143:481–6.

Weber U, Kraft G. Design and construction of a ripple filter for a smoothed depth dose distribution in conformal particle therapy. Phys Med Biol 1999; 44:2765–75.

Weber U, Kraft G. Comparison of carbon ions versus protons. Cancer J 2009; 15:325–32.

Weyrather WK, Kraft G. RBE of carbon ions: experimental data and the strategy of RBE calculation for treatment planning. Radiother Oncol 2004; 73 Suppl 2:S161–9.

Weyrather WK, Ritter S, Scholz M, Kraft G. RBE for carbon track-segment irradiation in cell lines of differing repair capacity. Int J Radiat Biol 1999; 75:1357–64.

Wilkens JJ, Oelfke U. Direct comparison of biologically optimized spread-out bragg peaks for protons and carbon ions. Int J Radiat Oncol Biol Phys 2008; 70:262–6.

Wilson RR. Radiological use of fast protons. Radiology 1946; 47:487–91.

Wink KCJ, Roelofs E, Solberg T, Lin L, Simone CB, Jakobi A, et al. Particle therapy for non-small cell lung tumors: where do we stand? A systematic review of the literature. Front Oncol 2014; 4:292.

WHO (a), World Health Organization (2016). Cancer. Accessed June 2016. http://www.who.int/cancer/en/.

WHO (b), World Health Organization (2016), accessed June 2016. http://www.who.int/mediacentre/news/releases/2003/pr27/en/.

Zacharias T, Dörr W, Enghardt W, Haberer T, Krämer M, Kumpf R, et al. Acute response of pig skin to irradiation with 12C-ions or 200 kV X-rays. Acta Oncol 1997; 36:637–42.

Zhang J, Yang F, Li B, Li H, Liu J, Huang W, et al. Which is the optimal biologically effective dose of stereotactic body radiotherapy for stage I non-small-cell lung cancer? A meta-analysis. Int J Radiat Oncol Biol Phys 2011; 81:e305–16.

6 Articles

6.1 Publication 1

Reproducibility of target coverage in stereotactic spot scanning proton lung irradiation under high frequency jet ventilation

6.2 Publication 2

Changes in the radiological depth correlate with dosimetric deterioration in particle therapy for stage I NSCLC patients under high frequency jet ventilation

6.3 Publication 3

Challenges in radiobiological modeling: can we decide between LQ and LQ-L models based on reviewed clinical NSCLC treatment outcome data?

Radiotherapy and Oncology 109 (2013) 45–50

Contents lists available at ScienceDirect

Radiotherapy and Oncology

journal homepage: www.thegreenjournal.com

Particle beam therapy for lung cancer

Reproducibility of target coverage in stereotactic spot scanning proton lung irradiation under high frequency jet ventilation

Alina Santiago [a,*], Urszula Jelen [a], Filippo Ammazzalorso [a], Rita Engenhart-Cabillic [a], Peter Fritz [b], Werner Mühlnickel [b], Wolfgang Enghardt [c], Michael Baumann [c], Andrea Wittig [a]

[a] University of Marburg, Department of Radiotherapy and Radiation Oncology; and [b] St Marien-Krankenhaus, Department of Radiotherapy, Siegen; [c] Medical Faculty and University Hospital Carl Gustav Carus Technische Universität Dresden, Department of Radiation Oncology and OncoRay, National Center for Radiation Research in Oncology, Germany

ARTICLE INFO

Article history:
Received 1 June 2013
Received in revised form 13 September 2013
Accepted 20 September 2013
Available online 12 October 2013

Keywords:
Non small cell lung cancer
Particle therapy
Proton therapy
SBRT
High frequency jet ventilation
Reproducibility

ABSTRACT

Purpose: To investigate scanned-beam proton dose distribution reproducibility in the lung under high frequency jet ventilation (HFJV).

Materials and methods: For 11 patients (12 lesions), treated with single-fraction photon stereotactic radiosurgery under HFJV, scanned-beam proton plans were prepared with the TRiP98 treatment planning system using 2, 3–4 and 5–7 beams. The planning objective was to deliver at least 95% of the prescription of 33 Gy (RBE) to 98% of the PTV. Plans were subsequently recomputed on localization CT scans. Additionally, for selected cases, the effects of range uncertainties were investigated.

Results: Median GTV $V_{98\%}$ was 98.7% in the original 2-field plans and 93.7% in their recomputation ($p = 0.039$). The respective values were 99.0% and 98.0% ($p = 0.039$) for the 3–4-field plans and 100.0% and 99.6% ($p = 0.125$) for the 5–7-field plans. CT calibration uncertainties of ±3.5% led to a GTV $V_{98\%}$ reduction below 1.5 percentual points in most cases and reaching 3 percentual points for 2-field plans with beam undershoot.

Conclusions: Through jet ventilation, reproducible tumor fixation for proton radiotherapy of lung lesions is achievable, ensuring excellent target coverage in most cases. In few cases, non-optimal patient setup reproducibility induced density changes across beam entrance channels, leading to dosimetric deterioration between planning and delivery.

Stereotactic body radiotherapy (SBRT) is an established alternative to surgery for medically inoperable early stage (T1–2) non small cell lung cancer (NSCLC) and lung metastases, yielding high 5-year local control rates of 70–90% and low toxicity rates with usually less than 5–8% severe toxicity (grade III) [1–2]. SBRT involves highly conformal, single-fraction or hypofractionated treatments using (non-coplanar) multiple-field techniques that aim at delivering an ablative dose to the tumor, while sharp dose gradients enable sparing of surrounding normal structures. Inherent to the technique is high precision of dose delivery even in moving targets.

Application of proton beam therapy, with its accurate dose localization, has the potential to minimize dose to the lungs and organs at risk as demonstrated in numerous dosimetric comparison studies [3–5], even if compared to very advanced photon techniques [6]. Hence, it is expected to reduce side effects, posing as alternative to SBRT, for early but also more advanced inoperable NSCLC cases, where tolerances of normal structures may limit application of a curative photon dose [7]. Recent retrospective series have shown, that high-dose hypofractionated proton therapy for peripherally and centrally located NSCLC achieves excellent outcomes in terms of local tumor control and safety profile [8]. A phase I trial including also advanced disease has recently proven hypofractionated proton radiotherapy to be well tolerated [9].

However, efficacy and tolerability of proton therapy in comparison to current standards is not yet proven in clinical trials [7,10–12]. This is partly due to the limited number of clinical particle therapy facilities, but also due to challenges in the technical implementation of particle therapy in lung tumors, especially management of tumor motion. The risk of target miss due to organ motion and deformation is expected to be greater in particle therapy than in photon therapy due to the finite particle range, which is typically addressed by extended distal and proximal margins. Additionally, the interplay of target motion and beam scanning renders extra complexity to the irradiation of lung tumors [13]. For this reason, a margin-based approach through the definition of an internal target volume (ITV), encompassing the tumor position in all phases of the respiratory cycle, might not be sufficient to ensure adequate and homogeneous target coverage.

* Corresponding author. Address: Department of Radiotherapy and Radiation Oncology, University of Marburg, Baldingerstrasse 1, 35043 Marburg, Germany.
E-mail address: santiago@staff.uni-marburg.de (A. Santiago).

0167-8140/$ - see front matter © 2013 Elsevier Ireland Ltd. All rights reserved.
http://dx.doi.org/10.1016/j.radonc.2013.09.013

Various solutions to counteract motion interplay effects have been proposed, for instance gating, tracking, and re-scanning, and their clinical applicability is under active investigation. In contrary, other approaches, like apnea and high frequency jet ventilation (HFJV), aim at target fixation [13]. HFJV is a modality of mechanical ventilatory support, which utilizes a respiratory rate greater than the normal value (>150 breaths per minute) and very small tidal volumes, thus preventing any movement of the tumor with respiration [14–17]. The interest of target fixation techniques in particle therapy of the lung lies not only in the expected target volume reduction, but also in managing the sensitivity of particle range to density changes in the beam entrance channels. However, if HFJV is to allow a margin-based planning approach for particle irradiation in the lung, it must be reproducible, since this procedure has to be repeated at least twice, i.e., for the planning computed tomography (CT) acquisition and later for the actual irradiation(s).

The goal of the present work was to investigate the reproducibility of the delivered proton dose distribution under HFJV by means of a planning study based on delivery-time localization CT scans from patients who were treated with photon SBRT under HFJV.

Materials and methods

Patient data

Datasets of 11 patients with 12 lesions were selected. All patients were treated for peripheral stage I NSCLC (9 patients) or metastases (2 patients), within an experimental protocol, with single-fraction stereotactic radiosurgery, to up to 33 Gy isocenter dose, under HFJV at the St. Marien-Krankenhaus [15–16]. According to the institutional protocol, patients qualify to receive treatment under HFJV, if the target motion amplitude exceeds 1 cm [15–16]. The HFJV is performed with pulse frequency of 300–400 times a minute, inducing virtually complete standstill of the lung [15–17] (see movie in electronic Supplementary material).

All patients received two CT scans, both under HFJV and immobilized in a vacuum mattress combined with a stereotactic body frame: one as planning CT and the second for target localization verification on the day of irradiation. Localization CT datasets were restricted longitudinally to the slices encompassing the tumor region.

Delineation of relevant structures was performed with the Pinnacle^3 (version 8.0; Philips Radiation Oncology Systems, Best, The Netherlands) treatment planning system on both planning and localization CT. The planning target volume (PTV) was defined by isotropic 3D expansion of the gross tumor volume (GTV) by 5 mm. Median (range) GTV and PTV volumes were 6.7 (1.0–22.9) cm^3 and 24.6 (7.2–71.5) cm^3, respectively. Subsequent to contouring, for each lesion, rigid coregistration of both CT datasets was performed with focus on the tumor region.

Treatment planning

Using the original planning CTs, scanned-beam proton treatment plans were prepared with the TRiP98 treatment planning system (GSI, Darmstadt, Germany) [18]. The total prescription dose was 33 Gy (RBE) and the planning objective was the delivery of at least 95% of such prescription to 98% of the PTV, while, owing to the peripheral localization of all lesions, no normal tissue optimization constraints were deemed necessary. For each patient, three treatment plans were prepared: (a) a plan using two coplanar fields entering the patient ipsilaterally at 0° and 45° in compliance with the fixed nozzles (horizontal and oblique) installed at the Marburg Ion Therapy center (MIT), (b) a plan using 3–4 fields (similarly to [19]) and (c) a plan using 5–7 fields (similarly to [6]), the latter two representing increasing degrees of freedom offered by additional fixed beam lines, patient positioning solutions or a rotating gantry.

Non-coplanar beam setups were excluded because of the limited longitudinal extent of the localization CTs. Plans were optimized for a nozzle-to-treatment-isocenter distance of 60 cm, as available at the MIT center to reduce excess spot size enlargement stemming from the proton beam divergence [20]. Single-field-uniform-dose optimization was used, for its expected lower sensitivity to delivery-time uncertainties in comparison to intensity modulation (IMPT) [21].

The irradiation raster pitch was set to 3 mm, while available spot sizes, at the energies required by the cases under investigation, ranged from 6 to 18 mm full-width-half-maximum (FWHM). Further optimization parameters, expressed in beam's eye view coordinates, were an in-depth spot positioning step of 2 mm and a lateral allowance in placing spots outside the PTV of 1.5 times the spot size.

Successive delivery of the optimized proton plans was simulated by forward-recomputing them on the coregistered localization CT scans.

Additionally, in order to investigate delivery stability in presence of range uncertainties, for the two patients with the least and most deeply seated tumors in the cohort, all plans were recomputed introducing systematic CT calibration errors of ±3.5% [5,22].

Evaluation

The original and recomputed treatment plans were compared in terms of dose distributions and dose–volume histograms (DVH). For a quantitative assessment, different dosimetric parameters were employed: the percentage of the PTV receiving at least 95% of the prescription dose ($V_{95\%}$), and similarly $V_{95\%}$ and $V_{98\%}$ of the GTV. For statistical comparisons a two-sided sign test was performed with a significance level of 0.05 (with Bonferroni correction) using the *R* statistical environment [23].

Results

Dosimetric quality of the optimized plans

The PTV $V_{95\%}$ was >98% for all patients in all plans, without statistically significant differences between planning techniques, and normal tissue dose–volume indexes were below recommended reference values [24] (Table 1). Exceptionally, recommended limits were exceeded for the chest wall in individual cases because of inclusion in the PTV, independently of the planning approach, while its median population value could be reduced through use of more than 2 fields. This in turn resulted in significantly increased involvement of the ipsilateral lung. As only patients with peripheral tumors were included, organs like liver, spine, esophagus and trachea received very low doses (Table 1, structures with median $D_{\text{near-max}} = 0$ not shown), independently of the planning technique.

Qualitative reproducibility assessment

Concerning anatomical reproducibility in the localization CTs, even if patient setup was performed with stereotactic precision, in few patients changes due to repositioning were observed e.g., arm mispositioning or slight body rotations. Tumor position reproducibility was in general very good.

Fig. 1 shows an example of registration results for two patients (a and b), as well as Hounsfield unit (HU) profiles along the central

Table 1
Median (range) dosimetric indexes of PTV and normal tissue for all optimized plans.

Index [%]	2-field plan	3-4-field plan	5-7-field plan
PTV $V_{95\%}$ [%]	99.6 (98.4–99.9)	99.8 (98.5–100.0)	99.9 (98.5–100.0)
Lung ipsilateral (excl. PTV) $V_{5\%}$ [cm^3]	568.4 (230.8–775.5)	767.4 (231.5–1044.0)[a]	908.6 (436.4–1205.0)[a,b]
Lung ipsilateral (excl. PTV) $V_{7\,Gy}$ [cm^3]	286.2 (91.5–409.8)	359.6 (83.0–527.7)	403.4 (124.4–544.3)[a]
Lung ipsilateral (excl. PTV) $V_{20\,Gy}$ [cm^3]	120.7 (28.7–226.6)	120.0 (24.9–242.4)[a]	116.9 (33.7–231.2)[a,b]
Lung ipsilateral (excl. PTV) $V_{95\%}$ [cm^3]	23.7 (3.8–64.2)	17.8 (2.5–61.8)[a]	15.0 (2.5–48.0)[a]
Lung ipsilateral (excl. PTV) D_{mean} [Gy]	3.0 (0.7–4.5)	3.2 (0.7–5.3)	3.7 (1.0–5.8)[a,b]
Heart $D_{near\text{-}max}$ [Gy]	0.0 (0.0–14.7)	0.0 (0.0–7.9)	0.0 (0.0–6.5)
Main bronchus ipsilateral $D_{near\text{-}max}$ [Gy]	2.8 (0.0–29.9)	4.8 (0.0–30.3)	2.6 (0.0–26.3)
Thorax wall $D_{near\text{-}max}$ [Gy]	22.3 (13.2–32.7)	15.8 (9.0–32.7)[a]	12.8 (8.7–32.6)[a,b]
Thorax wall $V_{30\,Gy}$ [cm^3]	0.4 (0.0–23.2)	0.0 (0.0–23.6)	0.0 (0.0–16.8)[a]
Ribs $V_{22\,Gy}$ [cm^3]	2.0 (0.1–15.9)	0.1 (0.0–16.7)[a]	0.0 (0.0–11.8)[a]
Skin $D_{near\text{-}max}$ [Gy]	5.9 (1.8–12.0)	4.2 (2.7–12.9)	2.8 (2.4–6.8)[b]

Abbreviations: PTV, planning target volume; $V_{x\%}$, volume receiving $x\%$ of the prescribed dose, D_{mean}, mean dose, $D_{near\text{-}max}$, maximum dose delivered to 1% of the volume.
[a] Statistically significant differences ($p < 0.05$ with Bonferroni correction) with respect to the 2-field technique.
[b] Statistically significant differences ($p < 0.05$ with Bonferroni correction) with respect to the 3-4-field technique.

axis (averaged across a 3 × 3-voxel perpendicular neighborhood) of each beam used in the 2-field plans. In the upper half, a typical case is shown in which the tumor position as well as the whole anatomy were well reproduced, yielding an excellent conservation of the planned dose distribution on the localization CT dataset (Fig. 2a). In the lower half, a case is shown in which target coverage in the recomputation was compromised. The discrepancies in the anatomy between the planning and the localization images are well visible in the HU profiles, in particular for the oblique beam. The registration visualization of the latter case (Fig. 1b) shows that, although the tumor position was well reproduced between the two CT sets, the anatomy at the entrance of the oblique beam presents differences, including a noticeable thickening of the soft tissue region in the localization image (indicated with a red arrow) that resulted in an underdosage in the distal section of the PTV (Fig. 2b).

These two examples illustrate the general observation of this study, that, through use of jet ventilation, in most of the cases only small changes in conformality and target coverage were observed between planning and simulated delivery, while, in the few cases affected by significant target coverage decrease, this could be correlated with anatomical variations in the beam entrance channels. This is reflected in the dose–volume histograms, presented in Fig. 3.

Target coverage reproducibility

Using a 2-field planning approach, after recomputation, the GTV $V_{95\%}$ remained above 98% in 10 of 12 cases. One of these worst cases is presented in Fig. 1 and commented above in the text. The other was instead one of the two metastatic patients, presenting the smallest tumor volume in the series (PTV volume 7.2 cm^3) adjacent to the thorax wall.

With 2-field plans, the GTV $V_{98\%}$ remained above 95% in 4 of 12 cases, above 90% in 9 and in only 3 cases it reached lower values, down to 84.0%. With 3–4-field plans, the GTV $V_{98\%}$ after recomputation was >95% in 7 of 12 cases, >90% in 11 and in only one case 87.1%. Further improvement was observed with 5–7-field plans, which in 9 of 12 cases maintained, after recomputation, a GTV $V_{98\%} > 98\%$ and in only 3 cases exhibited lower values of 95.0%, 94.0% and 92.8%. Selected target dosimetric indexes for all plans and individual patients are reported in the Supplementary material, Table S1.

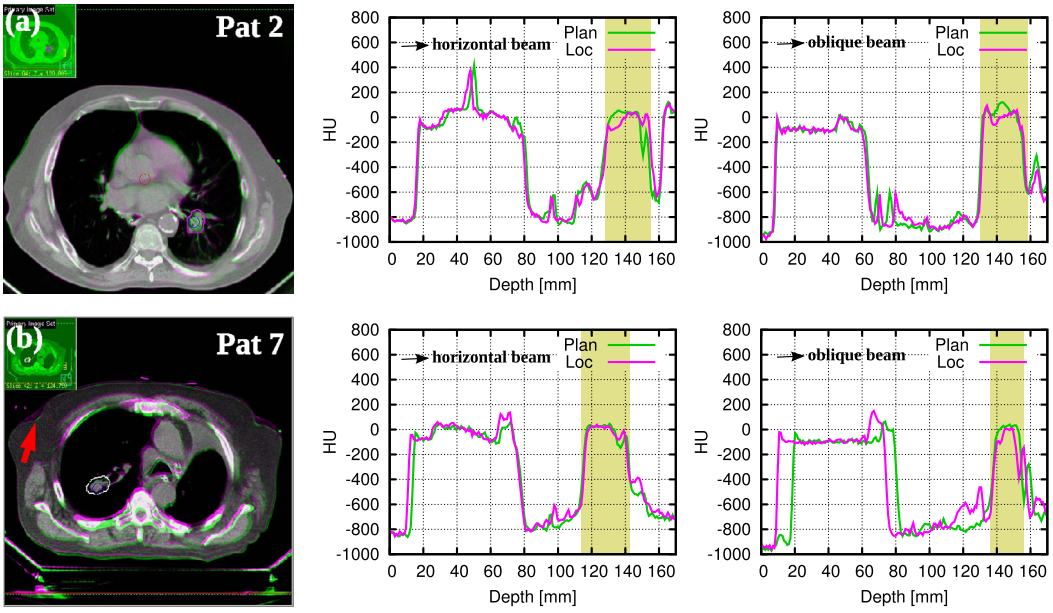

Fig. 1. Examples of coregistered CT data sets of two patients (a and b); green: planning CT, purple: localization CT; and corresponding HU profiles at the central axis of the horizontal and oblique beams (tumor region in yellow).

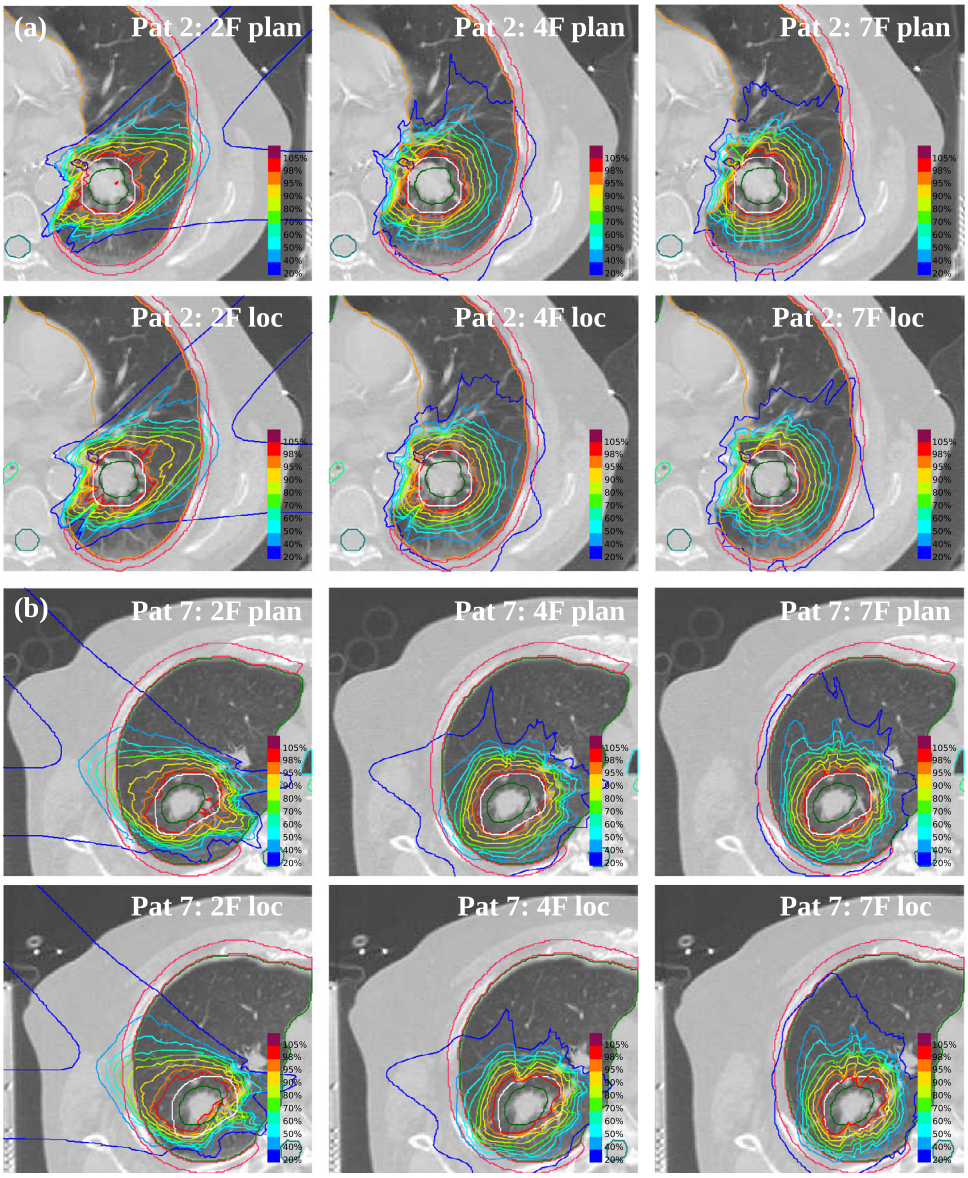

Fig. 2. Central slice of the dose distributions of two patients (a and b), for the optimized plans with 2, 3–4 and 5–7 fields (upper row, left to right) and their recomputation on the localization CTs (lower row).

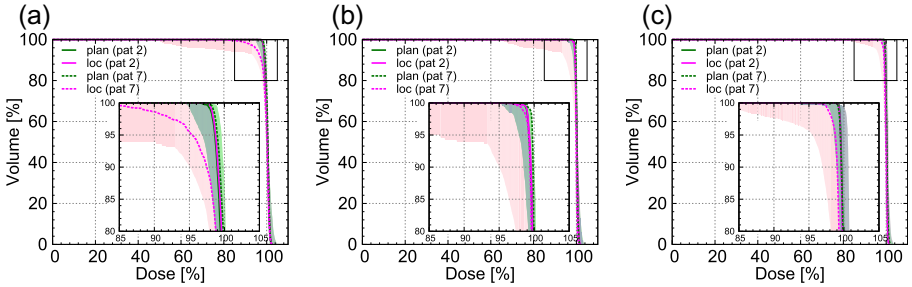

Fig. 3. Dose–volume histograms of the GTV for 2-field plans (a), 3–4 field plans (b), and 5–7 field plans (c). Shaded areas represent the patient cohort and lines the two patients presented in Fig. 2 (green: planning CT, purple: localization CT).

After recomputation, median GTV $V_{95\%}$ was >99.5% for all three plan types, with a statistically significant difference only for the 2-field plans ($p = 0.039$). Larger dosimetric variability between planning approaches could instead be observed through the GTV $V_{98\%}$, with median values of 98.7% in the original 2-field plans and 93.7% in their recomputation ($p = 0.039$) and, respectively, 99.0% and 98.0% ($p = 0.039$) for the 3–4-field plans and 100.0% and 99.6% ($p = 0.125$) for the 5–7-field plans.

The median (range) reduction in GTV $V_{95\%}$ and $V_{98\%}$ between optimized and recomputed plans and the results of statistical com-

Table 2
Median (range) GTV coverage reduction for all optimized and recomputed plans. Reductions with $p < 0.05$ are statistically significant.

Index [%]	2-field plan		3-4-field plan		5-7-field plan	
	Δ [pp]	*p*-Value	Δ [pp]	*p*-Value	Δ [pp]	*p*-Value
GTV $V_{95\%}$	0.1 (−0.1–8.9)	0.039	0.0 (−0.1–6.9)	0.219	0.0 (0.0–2.9)	0.125
GTV $V_{98\%}$	3.9 (−0.6–14.1)	0.039	0.6 (−1.7–12.9)	0.039	0.1 (−0.6–6.5)	0.125

Abbreviations: GTV, gross tumor volume, $V_{x\%}$, volume receiving *x*% of the prescribed dose, Δ, casewise difference between optimized and recomputed plan, pp, percentual point.

parison are reported in Table 2. Notably, the predominance of cases where coverage was preserved can be evinced from the proximity of the medians to the lower range ends, with the higher range ends representing the isolated worst-coverage cases discussed above.

Effects of CT calibration uncertainties

For the patient with the shallowest tumor localization (patient 8), with all beam setups the GTV $V_{95\%}$ remained within 0.5 pp (percentual point) agreement with the results obtained with the nominal CT calibration (Supplementary material, Table S1). With a 3.5% overshoot the GTV $V_{95\%}$ was 99.4–100.0% for the planning CT and 99.7–100.0% for the localization CT, while with a 3.5% undershoot it was 99.3–100.0% and 99.0–100.0%, respectively. The corresponding changes in GTV $V_{98\%}$ were below 1.5 pp.

For the patient with the most deeply seated target (patient 2), the GTV $V_{95\%}$ in presence of beam overshoot was 100.0% for all beam configurations, on both the planning and localization CT. In the case of simulated beam undershoot the $V_{95\%}$ was 99.6–100.0% on the planning CT and 99.9–100.0% on the localization CT, i.e., within 0.5 pp agreement with the values obtained with the nominal CT calibration (Supplementary material, Table S1). The corresponding changes in GTV $V_{98\%}$ were below 1.5 pp for all beam setups, except for the case of 2-field plans recomputed with beam undershoot, where $V_{98\%}$ was reduced by up to 3 pp (both in the planning and localization).

Discussion

The present work is the first planning study attempting at quantifying target coverage reproducibility in repeated applications of HFJV for tumor fixation in scanned-beam proton irradiation. The results demonstrate adequate tumor fixation and anatomical reproducibility, ensuring excellent target coverage in most of the cases.

To date, most clinical applications of lung particle therapy are based on passive scattering techniques, in which the complete target volume is irradiated nearly simultaneously and interplay effects with tumor motion do not occur [e.g., 8]. Consequently, tumor motion can be targeted by ITV-based approaches, possibly in combination with gating or breath-hold to reduce the ITV span and/or with field-specific safety margins designed to compensate the range uncertainties inherent to anatomical changes. Recently, a considerable effort has been invested by several groups into enabling treatment of moving targets, like lung tumors, also with scanned beams [13], exploiting their advantages (e.g., improved conformity, lack of patient-specific hardware etc.), also in consideration of centers that are not equipped with passive beam delivery systems. Most treatment delivery strategies to deal with tumor motion are still in the preclinical phase [13] and their implementation is often technically challenging.

So far, only one center has reported on the use of apnea for tumor fixation during irradiation with scanned-beam protons, with a reproducibility of <2 mm [25]. To our best knowledge, no data on the actual target coverage have been published.

HFJV can prevent any movement of thoracic structures with respiration and has thus been used for surgical procedures on the respiratory tract [14], hepatic and renal radiofrequency ablation [26] as well as stereotactic photon radiosurgery of lung and liver lesions [15,27–28]. The technique is thought to reduce ventilator-associated lung injury [29] and is feasible in patients with impaired lung function, who are unable to cooperate in procedures like coached gating or breath-hold techniques [16]. Due to reliable tumor fixation [16], without prolongation of the irradiation time, HFJV offers unique advantages for irradiation of lung lesions with scanned particle beams. The technique is however invasive and the procedure therefore restricted to single-fraction or oligofractionated treatments.

Our study demonstrates good reproducibility of the anatomical and geometrical tumor position between repeated HFJV procedures, enabling excellent GTV coverage in the great majority of cases, with $V_{95\%}$ above 98%, even for plans employing two fields only. However, in the remaining cases, although the original tumor position could be reproduced in the repeated jet ventilation procedure, changes in the patient setup occurred (repositioning errors). Such errors, small enough to be acceptable for photon radiosurgery, significantly affected the resulting dose distributions for scanned proton treatments. It should be emphasized, that setup errors are inherent to patient positioning and independent of the method used for motion management, however their consequences on proton treatments underline the need for case-by-case verification prior to each fraction, to ensure strict anatomical correspondence of the planned beam channels at treatment time (Fig. 1). Additionally, our results demonstrate that the averaging effect of multiple beams reduces the negative dosimetric effects of range uncertainties, introduced e.g., by anatomical variations (Fig. 2, Table 2), although this may come at the cost of a larger lung volume receiving low doses (Table 1).

With respect to the clinical planning and evaluation approach, the good reproducibility of the tumor position supports a margin-based concept for PTV definition, which should however be detailed with further studies aiming at establishing optimal planning parameters and clinical decision guidelines, specific to application of jet ventilation in particle therapy. For a safe implementation of high frequency jet ventilation in particle therapy, application of robust planning strategies is warranted [30].

Conclusions

Jet ventilation appears to be a feasible and reliable technique for tumor fixation in scanned proton irradiation of lung lesions, with the presented results demonstrating general anatomical and geometrical tumor position reproducibility, sufficient to ensure excellent target coverage at delivery. Small changes in patient setup can lead to dose deterioration, independently of the motion management technique employed, thus confirming the requirement of accurate case-by-case verification prior to irradiation with high-precision particle therapy, to ensure strict anatomical correspondence of the planned beam channels at treatment time.

Conflict of interest statement

No conflict of interest for any of the authors.

Acknowledgements

Funding from the Anneliese Pohl-Stiftung is acknowledged. The authors thank to Dr. Michael Krämer for enabling TRiP98 calculations, Dr. Gheorghe Iancu for providing proton base data, Bernd Nolte-Schröter for collecting patient data, Marie-Anne Chanrion for support with graphics.

Appendix A. Supplementary data

Supplementary data associated with this article can be found, in the online version, at http://dx.doi.org/10.1016/j.radonc.2013.09.013.

References

[1] Palma D, Senan S. Stereotactic radiation therapy: changing treatment paradigms for stage I non small cell lung cancer. Curr Opin Oncol 2011;23:133–9.
[2] Guckenberger M, Allgäuer M, Appold S, et al. Patterns-of-care and outcome analysis of stereotactic body radiotherapy for stage I non-small cell lung cancer in Germany and Austria between 1998 and 2011. J Thoracic Oncol 2013;8:1050–8.
[3] Georg D, Hillbrand M, Stock M, Dieckmann K, Pötter R. Can protons improve SBRT for lung lesions? Dosimetric considerations. Radiother Oncol 2008;88:368–75.
[4] Hoppe BS, Huh S, Flampouri S, et al. Double-scattered proton-based stereotactic body radiotherapy for stage I lung cancer: a dosimetric comparison with photon-based stereotactic body radiotherapy. Radiother Oncol 2010;97:425–6.
[5] Stuschke M, Kaiser A, Pöttgen Ch, Lübcke W, Farr J. Potentials of robust intensity modulated scanning proton plans for locally advanced lung cancer in comparison to intensity modulated photon plans. Radiother Oncol 2012;104:45–51.
[6] Seco J, Gu G, Marcelos T, Kooy H, Willers H. Proton arc reduces range uncertainty effects and improves conformality compared with photon volumetric modulated arc therapy in stereotactic body radiation therapy for non-small cell lung cancer. Int J Radiat Oncol Biol Phys 2013;87:188–94.
[7] Oshiro Y, Sakurai H. The use of proton-beam therapy in the treatment of non-small-cell lung cancer. Expert Rev Med Devices 2013;10:239–45.
[8] Bush DA, Slater JD, Shin BB, Cheek G, Miller DW, Slater JM. Hypofractionated proton beam radiotherapy for stage I lung cancer. Chest 2004;126:1198–203.
[9] Gomez DR, Gillin M, Liao Z, et al. Phase 1 study of dose escalation in hypofractionated proton beam therapy for non-small cell lung cancer. Int J Radiat Oncol Biol Phys 2013;86:665–70.
[10] Pijls-Johannesma M, Grutters JP, Verhaegen F, Lambin P, De Ruysscher D. Do we have enough evidence to implement particle therapy as standard treatment in lung cancer? A systematic literature review. Oncologist 2010;15:93–103.
[11] Grutters JP, Kessels AG, Pijls-Johannesma M, De Ruysscher D, Joore MA, Lambin P. Comparison of the effectiveness of radiotherapy with photons, protons and carbon-ions for non-small cell lung cancer: a meta-analysis. Radiother Oncol 2010;95:32–40.
[12] Allen AM, Pawlicki T, Dong L, et al. An evidence based review of proton beam therapy: the report of ASTRO's emerging technology committee. Radiother Oncol 2012;103:8–11.
[13] Bert C, Durante M. Motion in radiotherapy: particle therapy. Phys Med Biol 2011;56:R113–144.
[14] Bohn D. The history of high-frequency ventilation. Respir Care Clin N Am 2001;7:535–48.
[15] Fritz P, Kraus HJ, Mühlnickel W, Sassmann V, Hering W, Strauch K. High-frequency jet ventilation for complete target immobilization and reduction of planning target volume in stereotactic high single-dose irradiation of stage I non-small cell lung cancer and lung metastases. Int J Radiat Oncol Biol Phys 2010;78:136–42.
[16] Fritz P, Kraus HJ, Blaschke T, et al. Stereotactic, high single-dose irradiation of stage I non-small cell lung cancer (NSCLC) using four-dimensional CT scans for treatment planning. Lung Cancer 2008;60:193–9.
[17] Hof H, Herfarth KK, Münter M, et al. Stereotactic single-dose radiotherapy of stage I non-small-cell lung cancer (NSCLC). Int J Radiat Oncol Biol Phys 2003;56:335–41.
[18] Krämer M, Jäkel O, Haberer T, Kraft G, Schardt D, Weber U. Treatment planning for heavy-ion radiotherapy: physical beam model and dose optimization. Phys Med Biol 2000;45:3299–317.
[19] Seco J, Panahandeh HR, Westover K, Adams J, Willers H. Treatment of non-small cell lung cancer patients with proton beam-based stereotactic body radiotherapy: dosimetric comparison with photon plans highlights importance of range uncertainty. Int J Radiat Oncol Biol Phys 2012;83:354–61.
[20] Jelen U, Bubula ME, Ammazzalorso F, Engenhart-Cabillic R, Weber U, Wittig A. Dosimetric impact of reduced nozzle-to-isocenter distance in intensity-modulated proton therapy of intracranial tumors in combined proton-carbon fixed-nozzle treatment facilities. Radiat Oncol 2013;8:218.
[21] Lomax AJ. Intensity modulated proton therapy and its sensitivity to treatment uncertainties 2: the potential effects of inter-fraction and inter-field motions. Phys Med Biol 2008;53:1043–56.
[22] Moyers MF, Miller DW, Bush DA, Slater JD. Methodologies and tools for proton beam design for lung tumors. Int J Radiat Oncol Biol Phys 2001;5:1429–38.
[23] R Core Team, R: A language and environment for statistical computing, 2012. http://www.R-project.org.
[24] Timmerman R, Heinzerling J, Abdulrahman R, Hak Choy, Meyer JL. Stereotactic body radiotherapy for thoracic cancers: recommendations for patient selection, setup and therapy. In: IMRT, IGRT, SBRT advances in the treatment planning and delivery of radiotherapy. Basel, Freiburg, Paris: Karger; 2011. p. 406.
[25] Herbst M. First clinical experience at the Rinecker Proton Therapy Center, Munich. In: Abstract book of the 48th congress of the particle therapy co-operative group (PTCOG) 2009; FC93.
[26] Abderhalden S, Biro P, Hechelhammer L, Pfiffner R, Pfammatter T. CT-guided navigation of percutaneous hepatic and renal radiofrequency ablation under high-frequency jet ventilation: feasibility study. J Vasc Interv Radiol 2011;22:1275–8.
[27] Fritz P, Kraus HJ, Dölken W, Mühlnickel W, Müller-Nolte F, Hering W. Technical note: gold marker implants and high-frequency jet ventilation for stereotactic, single-dose irradiation of liver tumors. Technol Cancer Res Treat 2006;5:9–14.
[28] Wahlers B, Debus J, Dröge S, Brendle B, Freitag L. High-dose, stereotactic, one-time radiotherapy with curative intent for peripheral lung cancer. Pneumologie 2000;54:486–8.
[29] Krishnan JA, Brower RG. High-frequency ventilation for acute lung injury and ARDS. Chest 2000;118:795–807.
[30] Ammazzalorso F, Jelen U, Krämer M, Straßmann G, Engenhart-Cabillic R. Validation of a homogeneity index for the optimal selection of robust beam configurations in heavy ion radiotherapy planning. Radiother Oncol 2009;92:S109.

Supplementary Material, Table S1. Individual GTV coverage indexes for all optimized and recomputed plans.

Index / CT dataset	Pat. 1	Pat. 2	Pat. 3	Pat. 4	Pat. 5	Pat. 6	Pat. 7	Pat. 8	Pat. 9	Pat. 10a	Pat. 10b	Pat. 11	$N_{x\%}$
2 beam plans													
GTV $V_{95\%}$ [%]													
Plan	100.0	100.0	99.9	99.9	100.0	100.0	100.0	99.3	100.0	100.0	100.0	100.0	12
Localization	99.3	100.0	99.8	100.0	100.0	99.1	95.5	99.2	100.0	91.1	98.5	99.9	10
GTV $V_{98\%}$ [%]													
Plan	100.0	98.9	97.0	97.9	98.4	99.1	99.7	88.1	99.7	98.1	99.7	96.0	11
Localization	94.2	99.5	94.0	98.5	97.1	90.7	87.8	88.0	97.7	84.0	93.4	91.2	4
3-4 beam plans													
GTV $V_{95\%}$ [%]													
Plan	100.0	100.0	100.0	100.0	100.0	100.0	100.0	100.0	100.0	100.0	100.0	99.8	12
Localization	99.9	100.0	99.4	100.0	100.0	99.0	100.0	100.0	100.0	93.1	99.1	99.9	11
GTV $V_{98\%}$ [%]													
Plan	98.6	100.0	96.0	99.1	99.9	98.9	100.0	94.3	99.9	100.0	95.2	97.7	11
Localization	98.1	99.8	94.2	99.5	99.5	90.7	99.4	94.2	97.8	87.1	90.8	99.4	7
5-7 beam plans													
GTV $V_{95\%}$ [%]													
Plan	100.0	100.0	100.0	100.0	100.0	99.8	100.0	100.0	100.0	100.0	100.0	100.0	12
Localization	100.0	100.0	97.3	100.0	100.0	98.0	100.0	100.0	100.0	100.0	97.1	99.9	10
GTV $V_{98\%}$ [%]													
Plan	100.0	100.0	99.3	99.7	100.0	99.5	100.0	100.0	100.0	100.0	99.3	98.9	12
Localization	99.6	100.0	95.0	99.6	100.0	94.0	98.3	100.0	100.0	100.0	92.8	99.5	10

Abbreviations: GTV – gross tumor volume, $V_{x\%}$ – volume receiving x% of the prescribed dose, $N_{x\%}$ – number of plans that reached a value of the respective dosimetric index: $V_{98\%} \geq 95\%$ and $V_{95\%} \geq 98\%$.

Acta Oncologica, 2015; 54: 1631–1637

Taylor & Francis
Taylor & Francis Group

ORIGINAL ARTICLE

Changes in the radiological depth correlate with dosimetric deterioration in particle therapy for stage I NSCLC patients under high frequency jet ventilation

ALINA SANTIAGO[1], PETER FRITZ[2], WERNER MÜHLNICKEL[2], RITA ENGENHART-CABILLIC[1] & ANDREA WITTIG[1]

[1]*Philipps-University Marburg and University Hospital Giessen and Marburg, Department of Radiotherapy and Radiation Oncology, Marburg, Germany and* [2]*St Marien-Krankenhaus, Department of Radiotherapy, Siegen, Germany*

ABSTRACT

Background. Particle dose distributions are highly sensitive to anatomy changes in the beam path, which may lead to substantial dosimetric deviations. Robust planning and dedicated image guidance together with strategies for online decision making to counteract dosimetric deterioration are thus mandatory. We aimed to develop methods to quantify anatomical discrepancies as depicted by repeated computed tomography (CT) imaging and to test whether they can predict deviations in target coverage.

Material and methods. Dedicated software tools allowed for voxel-based calculations of changes in the water equivalent path length (WEPL) in beam directions. We prepared proton and carbon ion plans with different coplanar beam angle settings on a series of lung cancer patients, for which planning and localization CT scans under high frequency jet ventilation (HFJV) for tumor fixation were performed. We investigated the reproducibility of target coverage between the optimized and recalculated treatment plans. We then studied how different raster scan and planning settings influence the robustness. Finally, we carried out a systematic analysis of the variations in the WEPL along different coplanar beam angles to find beam directions, which could minimize such variations.

Results. The Spearman's correlations for the GTV ΔV_{95} and ΔV_{98} with the ΔWEPL for the proton plans with a 0° and −45° two-field configuration were 0.701 ($p = 0.02$) and 0.719 ($p = 0.08$), respectively. For beam configurations 0° and −90°, or 0° and +45°, with lower ΔWEPL, the correlations were no significant. The same trends were observed for the carbon ion plans. Increased beam spot overlap reduced dosimetric deterioration in case of large ΔWEPL.

Conclusion. Software tools for fast online analysis of WEPL changes might help supporting clinical decision making of image guidance. Raster scan and treatment planning settings can help to compensate for anatomical deviations.

Proton and carbon ion therapy, due to the localized dose deposition of charged particles, can decrease the dose to organs at risk as demonstrated in planning comparison studies [1–3]. However, their finite range renders particles more sensitive to changes in the radiological depth in the beam entrance channels. These changes originate from interfractional tumor movement and other anatomical deviations, such as residual positioning errors, tumor shrinkage during the radiotherapy course or fluctuations in patient weight [4]. Such effects can cause clinically relevant alterations in the particle dose distribution [5–8].

Respiratory movement poses a challenge to the application of particle therapy in the lung. Anatomical changes caused by respiration have been related to dosimetric fluctuations inside the target [8,9]. In scattered beam particle therapy, target coverage is typically ensured by extended lateral as well as distal and proximal margins [10] and dedicated internal target volume (ITV) concepts [5]. In scanned beam particle therapy, additional interplay between target motion and beam scanning exists. Therefore, a margin-based approach might not be sufficient to assure both planned target coverage and homogeneity.

Correspondence: A. Santiago, Philipps-University Marburg, Germany, Department of Radiotherapy and Radiation Oncology, University Hospital Giessen and Marburg, Baldingerstrasse, 35043 Marburg, Germany. Tel: + 49 6421 5868161. E-mail: santiago@staff.uni-marburg.de

(Received 23 May 2015; accepted 25 June 2015)

ISSN 0284-186X print/ISSN 1651-226X online © 2015 Informa Healthcare
DOI: 10.3109/0284186X.2015.1067716

Specific means to counteract motion interplay effects have been developed such as gating, tracking, and re-scanning [5]. Clinical applicability of such methods is currently under investigation. Alternatively, tumor fixation approaches might have a role in particle therapy for reduction of target motion as well as tissue density changes in the beam path [5]. High frequency jet ventilation (HFJV) is a modality of mechanical ventilatory support, which utilizes a high respiratory rate and very small tidal volumes, preventing any movement of the tumor with respiration [11]. Due to its invasive nature the method is limited to few dose applications.

In previous work we have investigated the reproducibility of the delivered proton dose for early stage non-small cell lung cancer (NSCLC) patients treated with photon radiosurgery under HFJV [12]. We have proven reproducible tumor fixation through HFJV, warranting excellent target coverage in the majority of investigated cases. However, for few tumors unacceptable dosimetric deviations were observed, illustrating the need for imaging prior to each dose delivery with dedicated protocols, together with the development of intervention thresholds based on the potential impact of anatomical discrepancies on the dose distribution [12].

Current strategies for image guidance in particle therapy have been derived from photon techniques and usually rely on anatomical landmarks or fiducial markers to achieve geometrical tumor repositioning. The purpose of this study was therefore, to develop methods to quantify changes in tissue density and thickness in the beam entrance channels between planning and irradiation time. We analyzed such changes and checked their correlation with loss of target coverage in proton and carbon ion treatment plans. We aimed to investigate, how beam angles and different raster scan and planning settings influence plan robustness. A systematic study of the variations in water equivalent path length (WEPL) along different coplanar beam angles aimed to find beam directions which minimize such variations.

Material and methods

Patient data

We used datasets of a previously published cohort including 12 lung lesions [11,12]. Patients received one planning and one localization three-dimensional (3D) computed tomography (CT) scans, both performed under HFJV. Target volumes and organs at risk were delineated with the Pinnacle^3 treatment planning system (TPS, version 8.0; Philips Radiation Oncology Systems, Best, The Netherlands) on both CT datasets for each patient. The planning target volume (PTV) was defined as the 5-mm isotropic expansion of the gross tumor volume (GTV). Automatic rigid coregistration of both CT datasets with three degrees of freedom was also performed with the Pinnacle^3 system with a cross-correlation method.

Treatment planning

Scanned-beam proton and carbon ion treatment plans, optimized on the planning CT datasets, were prepared for each patient with the TRiP98 TPS (GSI Helmholzzentrum für Schwerionenforschung, Darmstadt, Germany) [13–15]. Total prescribed dose was 33 Gy (absorbed dose). No optimization constraints were considered necessary due to the peripheral localization of all lesions. The angle convention in TRiP98 was used, in which the horizontal direction is represented by 0°, and the ventral and dorsal directions by -90° and 90°, respectively.

Proton plans had been previously calculated with two ipsilateral fields at 0° and −45° (field configuration 2FA) [12]. Additional two-field proton plans with different raster scan settings and with beam setups 0° plus −90° (2FB), and 0° plus 45° (2FC) were calculated for this study. We applied the following standard settings for the proton plans with beam setups 2FB and 2FC: 3 mm grid spacing, 2 mm energy step, and 1.5 planning contour extension, relative to the beam spot full width at half maximum (FWHM). Carbon ion plans were prepared with each of the three two-field coplanar setups and, for the setup 2FA, with different raster scan settings.

Spot grid spacing was set to 3 mm for the proton plans and 2 mm for the carbon ion plans. Energy steps of 2 and 3 mm were tested. For carbon ions, a 3 mm ripple filter was used to spread the pristine Bragg peak to an in-depth width of 3 mm [16]. A freedom was given to the TPS for placing spots laterally outside the PTV, the so-called virtual contour extension, in order to account for the dose fall-off at the lateral edges of the target. This parameter is implemented in TRiP98 in order to avoid dose hot spots on the PTV edges. Contour extension values were fixed to 0.9, 1.2, 1.5, or 1.8, relative to FWHM. A summary of the raster scan and planning settings used for the proton and carbon ion plans are presented in Tables I and II, respectively.

Single-field uniform dose (SFUD) optimization was used with a plain gradient optimization algorithm. For the proton planning we used realistic baseline data for a synchrotron-based facility with a reduced nozzle-to-isocenter distance to counteract spot size enlargement caused by the proton beam divergence [17]. Actual plan delivery was simulated through plan recalculations on the coregistered localization CT scans. The behavior of the coverage preservation was analyzed for all created plans based on recomputations on the localization CT.

Table I. Summary of planning settings, median (range) dosimetric indexes for the proton plans, and median (range) values of the calculated ΔWEPL plan in mm.

Plan no.	Plan settings	V_{95} PTV (%)	PTV V_{95} ≥ 98%	ΔV_{95} GTV (%)	ΔV_{98} GTV (%)	ΔWEPLplan (mm)
Hv5	2FA, 8, 3–3, 2, 0.9	91.9 (89.2–93.5)	0/12	3.8 (−0.7–20.7)	7.6 (−1.4–29)	2FA: 2.6 (1.1–4.6)
Hv4	2FA, 8, 3–3, 2, 1.2	97.9 (96.4–99.1)	6/12	1.6 (−0.7–12.9)	5.4 (−0.6–21)	2FA
Hv7	2FA, 8, 3–3, 2, 1.8	99.9 (99.1–100)	12/12	0.1 (0–6.6)	1.4 (−0.3–10.3)	2FA
Hv6	2FA, 8, 3–3, 3, 1.5	97.1 (85.4–99.6)	6/12	0.9 (−0.3–9.7)	3.8 (−1.3–23.2)	2FA
Hv2	2FB, 8, 3–3, 2, 1.5	99.3 (98.2–99.9)	12/12	0 (−0.3–3.5)	1 (−0.8–13.2)	2FB: 2.2 (1.4–4.7)
Hv3	2FC, 8, 3–3, 2, 1.5	99.5 (98.6–99.9)	12/12	0 (−0.6–0.3)	1.1 (−0.7–2.8)	2FC: 2.1 (1.4–3.1)

Plan settings include in this order: number of fields and angles: 2FA, 0° and −45°; 2FB, 0° and −90°; 2FC, 0° and 45°; beam spot size at FWHM at the isocenter (mm); spot spacing in x-y directions (mm); energy spacing (mm), planning contour extension in relative units to the beam spot FWHM.

Image analysis (WEPL)

Hounsfield units (HU) of the planning and localization CT scans were converted to relative stopping power in water according to the default look-up table in TRiP98. The voxel-based differences in the WEPL along each beam path were calculated on the co-registered datasets. Statistical measures inside the PTV contour of the planning CT were calculated, namely, the average value of the WEPL and the mean absolute value of the local differences in the WEPL, referred to as ΔWEPL. More details of the WEPL calculation can be found in the Supplementary Materials (available online at http://informahealthcare.com/doi/abs/10.3109/0284186X.2015.1067716). The program dcm2trip was used to convert all patient DICOM datasets to the TRiP98 format [18]. DVH and selected dosimetric indexes were extracted with the tool trip2png [19]. Image analysis (coregistration and range calculations), data manipulation, statistical analysis and graphing were done with the software package R, version 2.15.0 [20] and Python 2.7.3 [21].

Plan evaluation

Optimized plans were considered clinically acceptable if the percentage of the PTV receiving at least 95% of the prescribed dose (V_{95}) was 98% or more. The original and recomputed treatment plans were compared using dose distributions and dose-volume histograms (DVH). Coverage was evaluated with the V_{95} for the PTV in the optimized plans, as well as with the V_{95} and V_{98} for the GTV in both plans and recomputations. The conformity index (CI) at the 95% isodose level as defined by Paddick et al. [22] was calculated for the PTV. The homogeneity index (HI) calculated as (D2%–D98%) was assessed for both the PTV and the GTV in the optimized plans as well as for the GTV in the recomputations.

Table II. Summary of planning settings and median (range) dosimetric indexes for the carbon ion plans.

Plan no.	Plan settings	V_{95} PTV (%)	PTV V_{95} ≥ 98%	ΔV_{95} GTV (%)	ΔV_{98} GTV (%)
C12v16	2FA, 5, 2–2, 2, 1.2	99.9 (98.9–100)	0/12	0.3 (0.0–7.4)	1.5 (0–12)
C12v7	2FA, 5, 2–2, 3, 0.9	98.4 (95.9–99.4)	9/12	2.9 (0–14.6)	9.0 (0–27.2)
C12v8	2FA, 5, 2–2, 3, 1.2	99.6 (97.8–99.9)	11/12	0.6 (0–8.4)	2.8 (0–16)
C12v9	2FA, 5, 2–2, 3, 1.5	99.8 (98.2–99.9)	12/12	0.4 (0–6.5)	1.0 (0–14.1)
C12v4	2FA, 6, 2–2, 2, 0.9	99.3 (97.6–99.8)	10/12	1.8 (0–10.6)	6.4 (0–21.4)
C12v5	2FA, 6, 2–2, 2, 1.2	99.8 (98.9–100)	12/12	0.3 (0–5.9)	1.0 (0–9.9)
C12v6	2FA, 6, 2–2, 2, 1.5	99.9 (99.2–100)	12/12	0.1 (0–6.3)	0.4 (0–5.9)
C12v0	2FA, 6, 2–2, 3, 0.6	89.9 (84.8–95.6)	0/12	9.0 (0–30.3)	12.6 (0.1–39.7)
C12v1	2FA, 6, 2–2, 3, 0.9	98.2 (95.5–99.4)	7/12	2.8 (0–11.8)	7.6 (−0.2–22.3)
C12v2	2FA, 6, 2–2, 3, 1.2	99.7 (98.1–99.9)	12/12	0.5 (0–7.2)	2.0 (0–15.7)
C12v3	2FA, 6, 2–2, 3, 1.5	99.9 (98.4–100)	12/12	0.2 (0–5.7)	0.7 (0–11.6)
C12v13	2FA, 8, 2–2, 2, 0.9	99.7 (98.6–99.9)	12/12	1.3 (0–9.6)	5.9 (0–19.5)
C12v14	2FA, 8, 2–2, 2, 1.2	99.9 (99.1–100)	12/12	0.2 (0–6.6)	0.5 (0–7)
C12v15	2FA, 8, 2–2, 2, 1.5	99.9 (99.3–100)	12/12	0 (0–6)	0.4 (0–5.6)
C12v10	2FA, 8, 2–2, 3, 0.9	99.1 (97.5–99.7)	11/12	1.6 (0–10.6)	7.2 (0–23.4)
C12v11	2FA, 8, 2–2, 3, 1.2	99.8 (98.4–99.9)	12/12	0.3 (0–5.8)	1.4 (0–14.4)
C12v17	2FB, 8, 2–2, 2, 1.2	99.9 (99.1–100)	12/12	0.0 (0.0–1.9)	0.0 (0.0–5.9)
C12v18	2FC, 8, 2–2, 2, 1.2	99.9 (99.2–100)	12/12	0.0 (0.0–0.6)	0.2 (0.0–2.19)

Plan settings include in this order: number of fields and angles: 2FA, 0° and −45°; 2FB, 0° and −90°; 2FC, 0° and 45°; beam spot size at FWHM (mm); spot spacing (mm); energy spacing (mm), planning contour extension in relative units to the beam spot FWHM.

Results

Dosimetric quality of the optimized plans

Proton plan versions with energy step of 2 mm and planning contour extension of at least 1.5, i.e. Hv2, Hv3, and Hv7, fulfilled the PTV coverage objective (i.e. PTV V_{95} of at least 98%) in all cases (Table I). However, Hv7 was considered to have an excess contour extension of 1.8 and these plans were excluded from the analysis. For the plan versions with contour extensions of 0.9 and 1.2 (Hv5 and Hv4), or 1.5 with an energy step of 3 mm (Hv6), the PTV V_{95} remained below the acceptance objective for 12/12, 6/12 and 6/12 cases, respectively, and therefore these versions were also discarded. The analysis was restricted to proton plans with 8 mm spot nominal FWHM, 3 mm grid size and energy step of 2 mm, differing only in the beam configuration: Hv2, and Hv3. Changes in the field configuration alone resulted in small changes in conformity (Supplementary Table I, available online at http://informahealthcare.com/doi/abs/10.3109/0284186X.2015.1067716).

From 18 carbon ion plan versions with different raster scan and planning settings, 11 fulfilled the clinical acceptance criteria and were included in the analysis. Excess contour extensions of 1.5 were discarded. PTV V_{95} values for the 11 of 18 clinically accepted plan versions are displayed in Figure 1. Versions C12v4 and C12v10, with the smallest tested contour extension of 0.9 (FWHM) provided a PTV V_{95} $<98\%$ and $>97.5\%$ in 2/12 and 1/12 patients, respectively, which was considered clinically acceptable. Tables I and II present a summary of the dosimetric coverage indexes for proton and carbon ion plans, respectively. All values of the homogeneity and conformity indexes for the proton as well as the carbon ion plans are listed in the Supplementary Tables I and II (available online at http://informahealthcare.com/doi/abs/10.3109/0284186X.2015.1067716).

Influence of different raster scan settings for carbon ion plans

Qualitative comparison of all clinically approved carbon ion plan versions indicated that a larger contour extension led to better coverage preservation in presence of anatomical differences (Figure 1). Attending at the raster scan settings, an enhanced beam spot overlap contributed as well to this effect: use of larger spot sizes (8 and 6 mm), as well as the lower values of grid size (2 mm) and energy step (2 mm) led to improved GTV ΔV_{95}.

A multivariate analysis of the influences of the different parameters on the dosimetric coverage loss for the subset of approved carbon ion plans showed that the best linear model explaining the fluctuations in the CTV ΔV_{95} was given by ΔWEPL, the PTV volume and the contour extension (R^2 of 0.58, $p<0.05$). ΔWEPL was the strongest predictor in this model (this parameter yielded R^2 of 0.40, $p<0.05$, in a univariate analysis). More details on the models

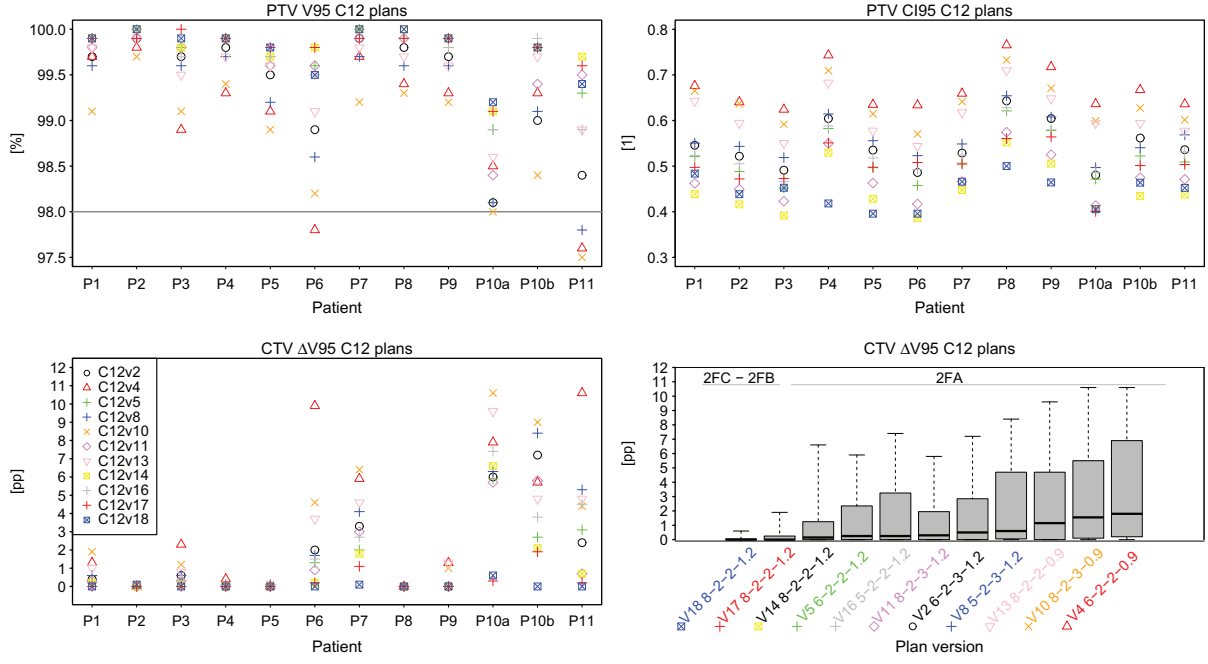

Figure 1. PTV V_{95} and CI_{95} for all prepared carbon ion plans (upper row), and GTV ΔV_{95} for each patient and each plan version with different planning and raster scan settings, as well as boxplots (median, 1st and 3rd quartiles, and range) for each plan version (lower row).

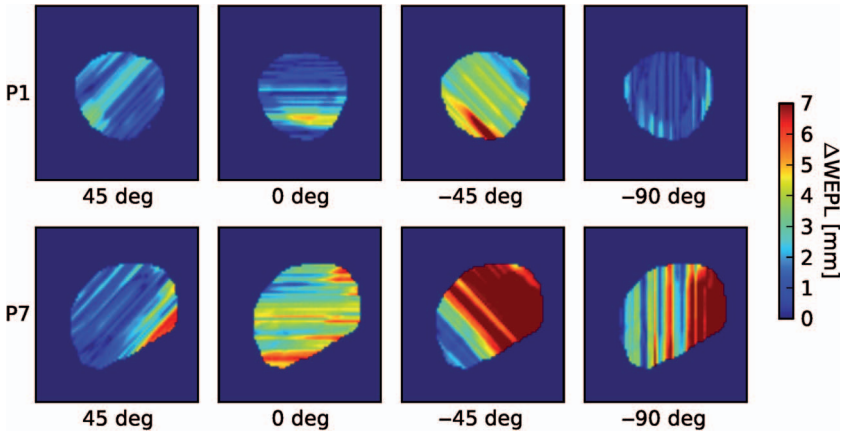

Figure 2. ΔWEPL values in the isocenter PTV slice of two selected patient cases for four different field directions.

can be found in the Supplementary Table IV (available online at http://informahealthcare.com/doi/abs/10.3109/0284186X.2015.1067716).

There are large differences in the behavior of GTV ΔV_{95} depending on the specific patient. An analysis done for the subset of plans with identical beam directions (2FA) showed a significant correlation of the maximum GTV ΔV_{95} value across approved plan versions with the ΔWEPL, with Spearman's r of 0.66, $p = 0.02$, (see Figure 1, bottom left).

Variations in the ΔWEPL with beam angle

Due to the short extent of the localization CT in craniocaudal direction, this study was restricted to coplanar beam directions without couch rotation. The mean ΔWEPL values of the PTV in this patient cohort ranged from 25 to 88 mm in the lateral direction, and from 22 to 100 mm at −45°. Concerning the variability among patients, the lowest ΔWEPL averaged among all angles corresponds to Patient 1 with 1.5 ± 0.6 mm (mean with standard deviation), in opposition to Patient 10a, who shows a maximum averaged ΔWEPL of 3.6 ± 3.9 mm. For six patients the ΔWEPL reached values larger than 5 mm in specific beam directions. These high values concentrated for three patients at angles around the ventrolateral direction (−45°). Two of these specific patients presented considerable anatomical changes between the planning and localization CT in the beam entrance path. Therefore, the ΔWEPL reached extreme values of up to 10 and 19 mm. These changes were visually detectable in the CT co-registration. In the context of a particle therapy treatment, the necessity of set up corrections would have been evident without need of further image analysis. Nevertheless, we did not exclude these cases from the study as they helped us to test the WEPL calculation method. Examples of ΔWEPL values along selected beam directions are shown for two cases in Figure 2. The results of systematic calculations of ΔWEPL for each patient for beam directions entering the patient ipsilaterally between dorsal and ventral in 3°-steps are displayed in Figure 3.

Influence of the different beam angles in dose deterioration

Total ΔWEPL values for each plan were calculated as the averaged ΔWEPL for each beam direction. The Spearman's correlations for the ΔV_{95} and ΔV_{98} with the ΔWEPL for the proton plans with 2FA beam configuration were 0.701 ($p = 0.02$), and 0.719, ($p = 0.08$), respectively. Two patients presented extremely high GTV ΔV_{95} values motivated by WEPL discrepancies in the PTV of up to 4.6 mm. In these two cases, the beam setup 2FB reduced the GTV ΔV_{95}% values to 1.3 and 0.0 pp, respectively. Better anatomical correspondence between planning and localization CT scans for the 2FB setup was also reflected in lower averaged ΔWEPL differences of 3.3 and 1.5 mm, respectively. The GTV ΔV_{95} and ΔV_{98} in median (range) was 0.0 (−0.3–3.5), and 1.0 (−0.8–13.2), respectively. The correlation between

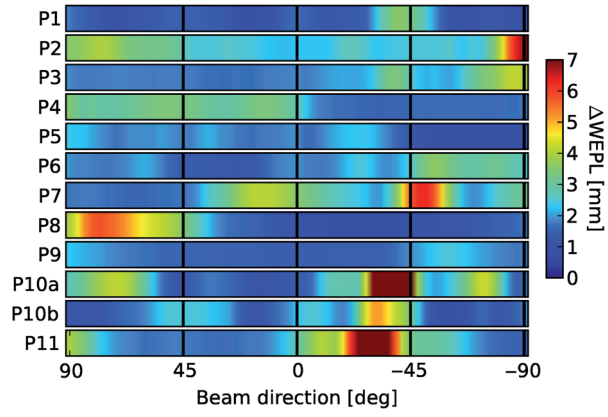

Figure 3. ΔWEPL values for each case of the cohort as a function of changing ipsilateral field directions between dorsal (90°) and ventral (−90°).

ΔV_{95} and ΔWEPL was not significant. New two-field plans were created with beam setup 2FC, i.e. with 0° and 45° beam directions. This beam setup showed generally low ΔWEPL values for all patients. This set of plans yielded median (range) ΔV_{95} and ΔV_{98} of 0 (−0.6–0.3) and 1.1 (−0.7–2.8) pp, respectively. Again, no significant correlation was found between ΔV_{95} nor ΔV_{98} and ΔWEPL (see Figure 4). The same trends were seen for the carbon ion plans, i.e. significant Spearman's correlations between ΔV_{95} and ΔV_{98} and average plan ΔWEPL for the 2FA beam setup of 0.85 and 0.81, respectively, and no significant correlation for the 2FB and 2FC beam configurations.

Discussion

We implemented a method to quantify differences in the water equivalent path length (WEPL). A similar method based on calculation of WEPL changes have been used before by Mori et al. to quantify both intra- and interfractional range variations in the chest wall thickness [8]. Casares et al. carried out an investigation to identify robust angles which minimize scanned-proton therapy dosimetric changes in the ITV within the breathing cycle, based on 4DCT images and under the hypothesis that no motion management strategy is applied [9]. We tested our WEPL calculation method on a cohort of patients with lung lesions which were strictly immobilized using HFJV, and therefore effects of intrafractional motion (especially respiration) could be ignored. Treatment delivered in only one fraction also ruled out anatomical changes which typically occur during the course of fractionated irradiation treatments, such as weight loss. This enabled quantifying anatomical reproducibility in a static situation.

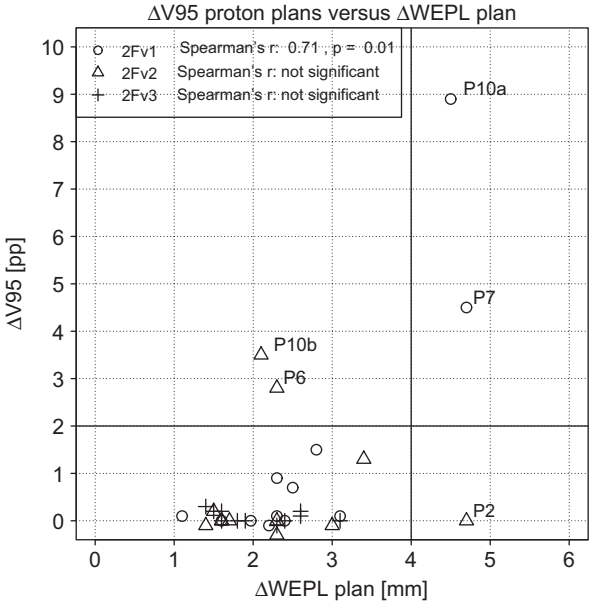

Figure 4. Spearman's r correlation values between GTV ΔV_{95} and ΔWEPL for the proton plans with beam setup 2FA (circles), 2FB (triangles), and 2FC (crosses).

Even under such conditions, this study proved that large anatomical differences can occur. Large variations in the radiological depth significantly correlated with decrease in the coverage indexes. The selected patient cohort was treated with photon radiosurgery. Anatomical variations with little impact on photon dose distributions can cause large mis-dosages in a particle therapy scenario. In at least two patients, actions would have been required to correct for anatomical deviations in case of particle irradiation.

In the case of patient 2, good coverage was observed in the recomputations for all field configurations, although the corresponding ΔWEPL values were as large as 4.7 mm for a beam from the ventral direction. A visual comparison of the two CT images suggested that for this patient, the WEPL differences might arise from small-scale tissue differences within the PTV. These tissue differences could have compensated each other, resulting in good PTV coverage. Possibly, more sophisticated image analysis tools are required to quantify these effects.

In general in the ventrolateral direction larger anatomical differences can occur due to the arm mobility, and for this reason special care has to be taken when choosing this direction for irradiations of the chest. This needs to be taken into account in facilities with fixed oblique beamlines and consequently, reduced beam angle options. Planning settings such as contour extension and raster scan settings, such as beam spot and grid size and energy step, can affect dosimetric robustness, and increased beam spot overlap was found to help preserve target coverage. These results are consistent with previous results from Richter et al. which showed better plan robustness to residual motion if larger spot sizes are used, for the case of liver irradiation [23].

The multivariate analysis showed that ΔWEPL alone can only explain a small fraction of the coverage loss. The PTV size plays a role since dosimetric deviations in a static tumor situation as is the case of our study, take place preferentially at the target borders. The contour extension is a planning parameter, which is seldom mentioned or specified in the published planning studies for particles, and in the present study it was found to have a significant role in plan conformity and homogeneity, as well as in dosimetric reproducibility.

The goal of a tool for automatic analysis, however, is not to detect clinically evident misalignments or anatomical changes, but subtler changes undetectable with visual inspection. This study showed that analysis of WEPL changes alone is possibly not

enough to detect such changes, as other factors influence the dose distribution and therefore, more complex models would be required to support clinical decision making, which could include WEPL and planning information, and possibly other factors including geometrical tumor position. A pragmatic approach would be to correct first for the geometric tumor position and in a second step check if the anatomical changes in the beam paths are below a certain threshold, which would depend, for example on the planning technique, or the PTV margins in case of treatment under HFJV.

Acknowledgments

Funding by the Anneliese Pohl-Stiftung is acknowledged. The authors thank Dr. Michael Krämer for enabling TRiP98 calculations, Dr. Gheorghe Iancu for providing proton baseline data, and Filippo Ammazzalorso for providing software for DICOM conversion and RT plan analysis. The authors thank as well Toke Printz Ringbaek for his careful manuscript proofreading and support with graphing.

Declaration of interest: The authors report no conflicts of interest. The authors alone are responsible for the content and writing of the paper.

References

[1] Georg D, Hillbrand M, Stock M, Dieckmann K, Pötter R. Can protons improve SBRT for lung lesions? Dosimetric considerations. Radiother Oncol 2008;88:368–75.

[2] Hoppe BS, Huh S, Flampouri S, Nichols RC, Oliver KR, Morris CG, et al. Double-scattered proton-based stereotactic body radiotherapy for stage I lung cancer: A dosimetric comparison with photon-based stereotactic body radiotherapy. Radiother Oncol 2010;97:425–30.

[3] Stuschke M, Kaiser A, Pöttgen C, Lübcke W, Farr J. Potentials of robust intensity modulated scanning proton plans for locally advanced lung cancer in comparison to intensity modulated photon plans. Radiother Oncol 2012; 104:45–51.

[4] Britton KR, Starkschall G, Tucker SL, Pan T, Nelson C, Chang JY, et al. Assessment of gross tumor volume regression and motion changes during radiotherapy for non-small-cell lung cancer as measured by four-dimensional computed tomography. Int J Radiat Oncol Biol Phys 2007;68:1036–46.

[5] Bert C, Durante M. Motion in radiotherapy: Particle therapy. Phys Med Biol 2011;56:R113–44.

[6] Trofimov A, Nguyen PL, Efstathiou JA, Wang Y, Lu HM, Engelsman M, et al. Interfractional variations in the setup of pelvic bony anatomy and soft tissue, and their implications on the delivery of proton therapy for localized prostate cancer. Int J Radiat Oncol Biol Phys 2011;80:928–37.

[7] Engelsman M, Kooy HM. Target volume dose considerations in proton beam treatment planning for lung tumors. Med Phys 2005;32:3549–57.

Supplementary material available online

Supplementary materials, Supplementary Figure 1 and Tables I–V to be found online at http://informahealthcare.com/doi/abs/10.3109/0284186X.2015.1067716.

[8] Mori S, Dong L, Starkschall G, Mohan R, Chen GT. A serial 4DCT study to quantify range variations in charged particle radiotherapy of thoracic cancers. J Radiat Res 2014;55: 309–19.

[9] Casares-Magaz O, Toftegaard J, Muren LP, Kallehauge JF, Bassler N, Poulsen PR, et al. A method for selection of beam angles robust to intra-fractional motion in proton therapy of lung cancer. Acta Oncol 2014;53:1058–63.

[10] Seco J, Panahandeh HR, Westover K, Adams J, Willers H. Treatment of non-small cell lung cancer patients with proton beam-based stereotactic body radiotherapy: Dosimetric comparison with photon plans highlights importance of range uncertainty. Int J Radiat Oncol Biol Phys 2012;83:354–61.

[11] Fritz P, Kraus HJ, Mühlnickel W, Sassmann V, Hering W, Strauch K. High-frequency jet ventilation for complete target immobilization and reduction of planning target volume in stereotactic high single-dose irradiation of stage I non-small cell lung cancer and lung metastases. Int J Radiat Oncol Biol Phys 2010;78:136–42.

[12] Santiago A, Jelen U, Ammazzalorso F, Engenhart-Cabillic R, Fritz P, Mühlnickel W, et al. Reproducibility of target coverage in stereotactic spot scanning proton lung irradiation under high frequency jet ventilation. Radiother Oncol 2013;109:45–50.

[13] Krämer M, Scholz M. Treatment planning for heavy-ion radiotherapy: Calculation and optimization of biologically effective dose. Phys Med Biol 2000;45:3319–30.

[14] Krämer M, Jäkel O, Haberer T, Kraft G, Schardt D, Weber U. Treatment planning for heavy-ion radiotherapy: Physical beam model and dose optimization. Phys Med Biol 2000; 45:3299–317.

[15] Kraemer M, Durante M. Ion beam transport calculations and treatment plans in particle therapy. Eur Phys J D 2010;60:195–202.

[16] Weber U, Kraft G. Design and construction of a ripple filter for a smoothed depth dose distribution in conformal particle therapy. Phys Med Biol 1999;44:2765–75.

[17] Jelen U, Bubula M, Ammazzalorso F, Engenhart-Cabilic R, Weber U, Wittig A. Dosimetric impact of reduced nozzle-to-isocenter distance in intensity-modulated proton therapy of intracranial tumors in combined proton-carbon fixed-nozzle treatment facilities. Radiat Oncol 2013;8:218.

[18] Krämer M. TRiP98 Online Manual. 2009. Available from: http://bio.gsi.de/DOCS/TRiP98/DOCS/dcm2trip.html [cited 24 June 2015].

[19] Ammazzalorso F, Chanrion MA, Graef S, Jelen U. A free software display and analysis tool for photon and particle radiotherapy dose distributions [abstract]. Proceedings to the 52nd Annual Meeting for the Particle Therapy Cooperative Group (PTCOG). Int J Particle Ther 2014;1:312–3.

[20] R Development Core Team (2008). R: A language and environment for statistical computing. R Foundation for Statistical Computing, Vienna, Austria. Available from: http://www.R-project.org [cited 24 June 2015].

[21] Python Software Foundation. Python Language Reference, version 2.7. Available from: http://www.python.org [cited 24 June 2015].

[22] Paddick I. A simple scoring ratio to index the conformity of radiosurgical treatment plans. J Neurosurg 2000;93(Suppl 3):219–22.

[23] Richter D, Graeff C, Jäkel O, Combs SE, Durante M, Bert C. Residual motion mitigation in scanned carbon ion beam therapy of liver tumors using enlarged pencil beam overlap. Radiother Oncol 2014;113:290–5.

Supplementary material for Santiago A. et al. Changes in the radiological depth correlate with dosimetric deterioration in particle therapy for stage I NSCLC patients under high frequency jet ventilation. Acta Oncol 2015; doi:10.3109/0284186X.2015.1067716.

Supplementary materials

WEPL calculations

1. Both datasets, planning and localization CT scans, were coregistered according to the shift values calculated with Pinnacle[3].

2. To simplify the calculation of the water equivalent path length, the CT images were rotated in order to align the CT voxels with the beam direction.

3. The Hounsfield units (HU) of the planning and localization CT scans were converted to relative stopping powers in water according to the default look-up table built in TRiP98, which was also used for the planning.

4. The voxel-based differences between the relative stopping powers of both CT datasets were calculated and converted to mm, scaling with the voxel size. Absolute values of the differences calculated this way were extracted.

5. A PTV binary mask (created with the tool trip2png [19]) was overlaid to visualize the absolute value of the local WEPL differences inside the PTV region. Examples of these WEPL difference maps are displayed in Fig. 2.

6. For the correlation of the variations in PTV V95% between planning and dose recomputation, the mean values of the absolute values of the local WEPL differences inside the PTV region were calculated.

Homogeneity and Conformity of the proton and carbon ion plans

All values of the homogeneity and conformity for the proton as well as the carbon ion plans are listed in Table I. Changes of the field configuration alone (i.e. a beam at 0° together with second beam at 45°, 90° and -45° respectively) resulted in small CI and HI changes only. A decrease in CI_{95} and CI_{98} was seen for increasing values of the lateral virtual contour extension, since more dose is allowed outside the PTV. At the same time an increase in V95% was seen for larger values of contour extension, illustrating that a better coverage typically involves compromises in the conformity. Since the peripheral, early stage tumors presented in this study have no critical normal tissue structures in the vicinity of the PTV, with exception of the chest wall and ribs partly encompassed by the PTV in tumors close to these structures, decreases in CI indexes due to large contour extension values had a lower priority in this study, in comparison to a satisfactory PTV coverage. HI values generally decrease with a larger value of the contour extension as well as plans with a larger number of fields. Larger contour extension values lowered the risk of underdosage at the PTV border while a larger number of fields had the potential to flatten the dose distribution and lower the inhomogeneity due to the increased pencil beam overlap within the PTV. Using energy step sizes of 3 mm yielded slightly worsened conformity values, lower coverage and an increase in the HI by a factor of almost 2 for both proton and carbon ion plans. This fact shows that the homogeneity and coverage within the target both depend more markedly on the energy step size, while the conformity of the plans is less dependent on this parameter. The larger the energy step size, the more dose will be given outside of the PTV at the proximal and distal edges, where the actual extent of excess dose will depend on the location of the PTV and the available energy steps from the accelerator.

Supplementary Table I. Summary of planning settings, and median (range) dosimetric indexes for the previously published proton plans in Santiago et al, presented here in order to compare with the dosimetric summary in Table I.

Plan Nr	Plan settings	V_{95} PTV [%]	ΔV_{95} GTV [%]	ΔV_{98} GTV [%]
Hv1*	2FA, 8, 3-3, 2, 1.5	99.6 (98.4-99.9)	0.1 (-0.1-8.9)	3.9 (-0.6-14.1)

* From Santiago et al.

Supplementary Table II. Summary of CI and HI indexes for the proton plans, median [range].

Plan Nr	Plan settings	CI95 PTV [%]	HI PTVplan [%]	HI GTVplan [%]	HI GTVloc [%]
Hv5	2FA, 8, 3-3, 2, 0.9	0.69 (0.57-0.73)	15.2 (13.8-18.4)	12.0(8.8-14.0)	15.2 (9.0-49.2)
Hv4	2FA, 8, 3-3, 2, 1.2	0.60 (0.44-0.64)	8.3 (6.7-10.3)	6.2 (4.7-9.4)	8.9 (5.0-49.4)
Hv1*	2FA, 8, 3-3, 2, 1.5	0.49 (0.29-0.51)	5.0 (3.4-8.6)	3.6 (2.1-8.5)	5.6 (3.4-49.2)
Hv7	2FA, 8, 3-3, 2, 1.8	0.33 (0.19-0.39)	3.5 (1.8-7.9)	3.1 (1.0-8.0)	4.0 (1.6-48.6)
Hv6	2FA, 8, 3-3, 3, 1.5	0.44 (0.30-0.52)	10.2 (5.6-17.7)	8.8 (2.9-16.6)	11.9 (5.9-50.8)
Hv2	2FB, 8, 3-3, 2, 1.5	0.46 (0.34-0.54)	5.8 (3.2-8.5)	4.6 (1.9-7.3)	5.4 (2.6-9.0)
Hv3	2FC, 8, 3-3, 2, 1.5	0.43 (0.30-0.54)	4.8 (2.9-9.3)	3.5 (1.8-8.6)	4.0 (1.8-8.6)

* From Santiago et al.

Supplementary Table III. Summary of CI and HI indexes for the carbon ion plans, median [range].

Plan Nr	Plan settings	CI95 PTV [%]	HI PTVplan [%]	HI GTVplan [%]	HI GTVloc [%]
C12v16	2FA, 5, 2-2, 2, 1.2	0.52(0.47-0.63)	2.2 (1.2-4.8)	1.3 (0.7-2.7)	2.3 (0.7-43.4)
C12v7	2FA, 5, 2-2, 3, 0.9	0.69(0.62-0.77)	7.2 (4.0-14.8)	2.7 (1.7-13.2)	8.2 (1.7-44.4)
C12v8	2FA, 5, 2-2, 3, 1.2	0.55(0.50-0.65)	3.9 (2.1-9.3)	2.1 (1.3-13.0)	3.6 (1.2-44.9)
C12v9	2FA, 5, 2-2, 3, 1.5	0.48(0.40-0.58)	2.9 (1.7-7.1)	2.0 (1.2-13.0)	2.7 (1.2-44.7)
C12v4	2FA, 6, 2-2, 2, 0.9	0.65(0.62-0.77)	4.7 (2.6-8.9)	2.0 (1.1-3.5)	6.1 (1.1-43.0)
C12v5	2FA, 6, 2-2, 2, 1.2	0.51(0.45-0.62)	1.9 (1.1-3.7)	1.3 (0.7-2.4)	2.0 (0.6-42.9)
C12v6	2FA, 6, 2-2, 2, 1.5	0.39(0.34-0.50)	1.5(0.9-2.5)	1.2 (0.6-2.3)	1.4 (0.6-42.2)
C12v0	2FA, 6, 2-2, 3, 0.6	0.76(0.71-0.84)	20.4 (12.0-32.0)	8.8 (3.6-17.2)	22.0(4.2-45.0)
C12v1	2FA, 6, 2-2, 3, 0.9	0.68(0.64-0.76)	7.7 (4.0-18.3)	3.2 (1.6-13.7)	7.7 (1.6-44.1)
C12v2	2FA, 6, 2-2, 3, 1.2	0.54(0.48-0.64)	3.5 (2.0-6.9)	2.1 (1.2-12.6)	3.3 (1.2-44.1)
C12v3	2FA, 6, 2-2, 3, 1.5	0.42(0.37-0.52)	2.6 (1.5-5.5)	1.9 (1.1-10.1)	2.6 (1.1-43.5)
C12v13	2FA, 8, 2-2, 2, 0.9	0.60(0.54-0.71)	3.8 (2.7-5.7)	2.0 (1.2-4.0)	4.8 (1.2-42.7)
C12v14	2FA, 8, 2-2, 2, 1.2	0.44(0.39-0.55)	1.7 (1.1-2.6)	1.3 (0.7-2.2)	1.7 (0.7-42.2)
C12v15	2FA, 8, 2-2, 2, 1.5	0.32(0.26-0.44)	1.4(0.8-2.0)	1.2(0.6-2.0)	1.4 (0.6-41.6)
C12v10	2FA, 8, 2-2, 3, 0.9	0.63(0.57-0.73)	5.6 (3.9-8.8)	2.8 (1.6-13.6)	6.0 (1.7-43.9)
C12v11	2FA, 8, 2-2, 3, 1.2	0.47(0.41-0.57)	3.0 (1.8-5.5)	2.0 (1-2-9.7)	2.9 (1.2-43.2)
C12v17	2FB, 8, 2-2, 2, 1.2	0.50(0.40-0.56)	1.59 (0.93-2.61)	1.16 (0.59-2.13)	1.30 (0.69-5.87)
C12v18	2FC, 8, 2-2, 2, 1.2	0.45(0.40-0.50)	1.68 (1.06-3.00)	1.01(0.68-2.48)	1.28 (0.71-3.45)

Multivariate analysis of the influence of planning settings in the carbon ion plans

We systematically analyzed the influences of the different scanning beam and planning setting variables on the dosimetric coverage loss for the subset of approved carbon ion plans, i.e. with a PTV V95% of at least 98%, which are visually represented in Fig. 1. Linear models were run for each of the different parameters and the correlations for the univariate models as well as for the two best multivariate models are represented in the following table:

Supplementary Table IV.

Correlation of CTV ΔV95% with:	R^2 ($p < 0.05$)
Patient (0)	0.53
ΔWEPL (1)	0.40
Volume PTV (2)	0.20
Contour extension (3)	0.10
FWHM (4)	n.s.
Energy Step (5)	n.s.
Grid size	NA
Linear model ~ (1) + (2)	0.49
Linear model ~ (1) + (2) + (3)	0.58

Single-beam plan calculations

Dose contributions from each individual field for four selected directions, namely 45°, 0°, -45°, and -90° were calculated separately, four single beams for each patient. Spearman's correlations between CTV V95% and V98% of single beams and ΔWEPL in the respective beam directions were calculated for each patient.

Supplementary Table V. Spearman's correlation between CTV ΔV95 or ΔV98 versus ΔWEPL for the protons and carbon ion plans..

Spearman's R ($p < 0.05$) all patients	Carbon ions	Protons
ΔV95%	0.45	0.45
ΔV98%	0.40	0.47

Dosimetric deterioration of 2F proton plans

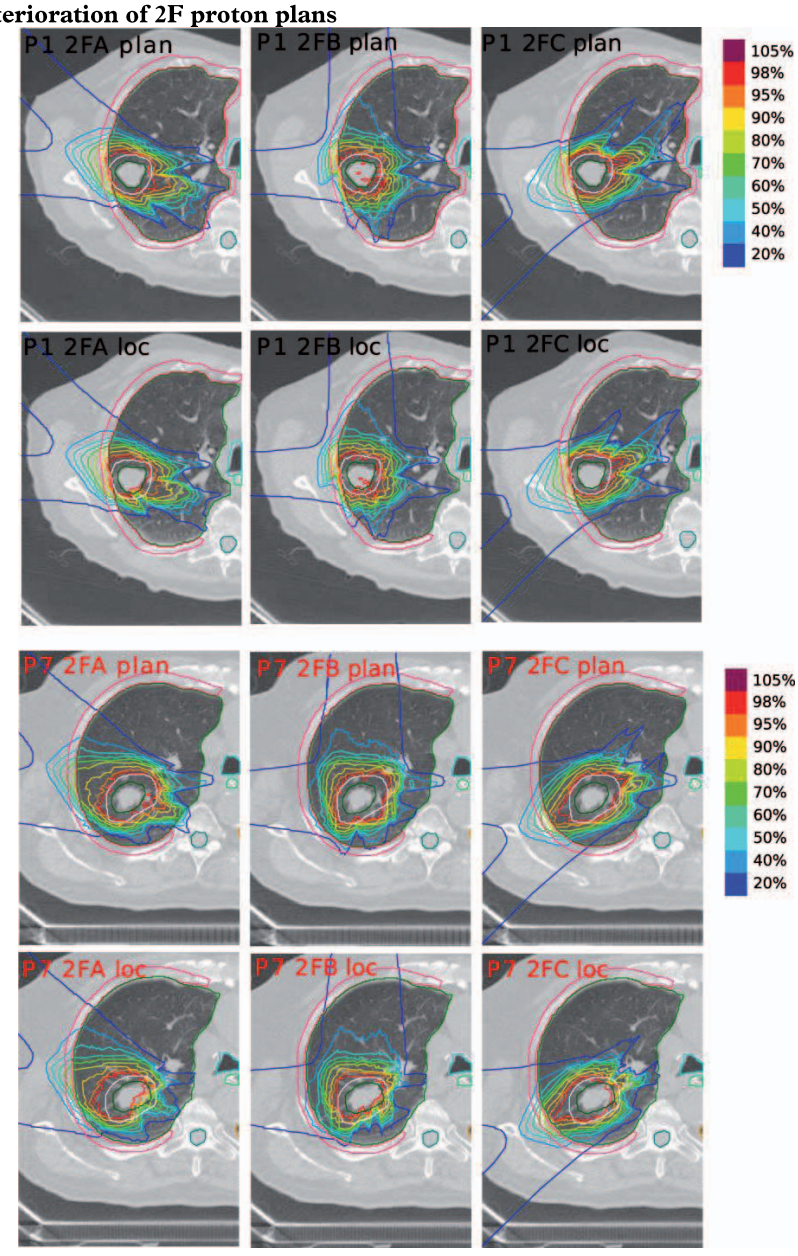

Supplementary Fig. 1. Isodose lines for proton plans calculated on the planning CT and localization CT respectively for two selected patient cases and the three selected beam angle configurations presented in Table I. The 2FA plans have been published before in [12] but are plotted here as well for the convenience of the readers. The corresponding WEPL changes to the beams directions in these plans are represented in Fig. 2.

Santiago et al. Radiation Oncology (2016) 11:67
DOI 10.1186/s13014-016-0643-5

Radiation Oncology

RESEARCH Open Access

Challenges in radiobiological modeling: can we decide between LQ and LQ-L models based on reviewed clinical NSCLC treatment outcome data?

Alina Santiago[1*], Steffen Barczyk[1,2], Urszula Jelen[1,3], Rita Engenhart-Cabillic[1] and Andrea Wittig[1]

Abstract

Aim: To study the dose-response of stage I non-small-cell lung cancer (NSCLC) in terms of long-term local tumor control (LC) after conventional and hypofractionated photon radiotherapy, modeled with the linear-quadratic (LQ) and linear-quadratic-linear (LQ-L) approaches and to estimate the clinical α/β ratio within the LQ frame.

Material and methods: We identified studies of curative radiotherapy as single treatment through MedLine search reporting 3-year LC as primary outcome of interest. Logistic models coupled with the biologically effective dose (BED) at isocenter and PTV edge according to both the LQ and LQ-L models with α/β = 10 Gy were fitted. Additionally, α/β was estimated from direct LQ fits.

Results: Thirty one studies were included reporting outcome of 2319 patients. The LQ-L fit yielded a significant value of 11.0 ± 5.2 Gy for the dose threshold (D_t) for BED_{10} at the isocenter. The LQ and LQ-L fits did not differ substantially. Concerning the estimation of α/β, the value obtained from the direct LQ fit for the complete fractionation range was 3.9 [68 % CI: 2.2–9.0] Gy ($p > 0.05$).

Conclusion: Both LQ and LQ-L fits can model local tumor control after conventionally and hypofractionated irradiation and are robust methods for predicting clinical effects. The observed dose-effect for local control in NSCLC is weaker at high doses due to data dispersion. For BED_{10} values of 100–150 Gy in ≥3 fractions, the differences in isoeffects predicted by both models can be neglected.

Keywords: Non-small cell lung cancer, Dose-response modeling, Biologically effective dose, Linear-quadratic model, Alpha-beta ratio

Introduction

The linear-quadratic (LQ) model was developed to describe experimental survival curves of both normal and tumor cells after irradiation. The LQ model fits the cell surviving fraction through a second-order polynomial on the dose per fraction, with coefficients α and β. The ratio between both coefficients describes the repair capacity of the cells and thus sensitivity to fractionation [1, 2].

The LQ model provides an accurate description of fractionation effects at doses between 1 and 8–10 Gy per fraction [3]. Essentially, this formalism enables iso-effect calculations in current clinical practice, defining the relationships between the biological irradiation effect and key parameters such as dose per fraction, total number of fractions and treatment time. Advancements in this model led to the two most extended, complementary approaches for isoeffect calculation: the biologically effective dose (BED) and the equivalent dose in 2 Gy per fraction (EQD2) [4].

Current treatment of choice for stage I non-small cell lung cancer (NSCLC) is surgical tumor extraction. Since it became technically feasible, radiotherapy has been

* Correspondence: santiago@staff.uni-marburg.de
[1]Department of Radiotherapy and Radiation Oncology, University Hospital Giessen and Marburg, Philipps-University Marburg, Baldingerstrasse, Marburg 35043, Germany
Full list of author information is available at the end of the article

used as an alternative treatment method in inoperable cases. Early approaches used 3D-conformal conventionally fractionated techniques, whereas today, stereotactic body radiotherapy (SBRT) allows for highly precise delivery of radiation, thus enabling hypofractionation to deliver ablative radiation doses in 1–5 fractions [5]. Therefore, SBRT evolved to be the current treatment of choice for early-stage NSCLC in medically inoperable patients and in patients who do not consent to surgery. The high precision of dose delivery facilitates normal tissue sparing, even allowing for dose escalation to potentially improve local control. Despite a growing pool of clinical outcome data, the optimal total dose and fractionation scheme to reach the intended biological effects in terms of both local tumor control and side effects are still under debate [6].

Hypofractionation requires reliable isoeffect calculations. Thus, the relevance of the question has been renewed, whether the description of radiobiological effects based on the LQ formalism is appropriate for hypofractionated treatments [7–9].

If no α/β ratio estimation is available for a specific tumor entity, a generic value of 10 Gy is used for BED calculations, although the precision achievable with such a standard α/β ratio is assumed to be lower. Numerous attempts to calculate clinical α/β values have been made, using available clinical outcome data [10]. Such estimations are specially needed if the α/β of a specific tumor entity is suspected to be lower than 10 Gy. In this case a modified fractionation scheme, which reduces tumor cell recovery between fractions, could increase the therapeutic ratio as is the case e.g. in prostate carcinoma or breast cancer.

Many recent studies aim at outcome review and modeling of the dose response relationship of NSCLC [11–15]. However, studies attempting to estimate the α/β ratio for NSCLC are scarce [11, 15, 16]. It is subject of current debate if the improved outcomes of hypofractionated SBRT are a consequence of an α/β ratio lower than 10 Gy, or even lower than the α/β value of the surrounding normal tissue, which could add a radiobiological rationale to the use of hypofractionation. Alternatively, the improvement could be caused by a reduced repopulation in a shorter overall treatment time.

In addition, in particle radiotherapy, a currently emerging field in radiation oncology, radiobiological considerations are of importance. For proton radiotherapy hypofractionated concepts are aimed for partially as motion management strategy [17–20], so that isoeffect calculations are essential. Apart from isoeffect calculations current treatment planning strategies for light ion therapy also require the attribution of radiobiological properties to both tumor and normal tissues. Specifically, in scanned-beam carbon ion therapy, radiosensitivity is characterized through α/β values obtained from photon irradiation experiments in vitro [21] in one of the mathematical models describing the enhanced biological effect in the Bragg peak, the so called local effect model (LEM), which is implemented in commercial treatment planning systems.

In such situation, clinical long time follow up data is the most valid source of data for modeling approaches, which is however inherently limited by inhomogeneity of treatment parameters and treatment techniques evolving over time. We focused our analysis on the comparison of the LQ-L versus the LQ model, since most of the mathematical model corrections to the LQ model proposed need additional input parameters [16, 22–24], which are not available for the specific clinical situation.

Therefore, this work aims at:

1) investigating the dose-response of NSCLC tumor control data from conventionally fractionated (CF) and stereotactic, hypofractionated radiotherapy treatments (HF), based on a review of published long-term outcome results,
2) evaluating the validity of the LQ and LQ-L models for both conventional and SBRT treatments,
3) and obtaining an estimation of the clinical α/β ratio of NSCLC.

Materials and methods

Study design

We identified inclusion criteria, search strategy, outcome measures of interest and indispensable treatment parameters for the study. The analysis keeps standards of the Preferred Reporting Items for Systematic Reviews and Meta-Analyses (PRISMA) statements [25].

Selection criteria

PubMed was searched (July 2015) without restrictions on the publication date. Abstracts of conference proceedings were excluded and language was restricted to English. Repeated publications based on the same cohort were excluded as were outcome reviews in order to avoid duplicity of cohorts. The selection of studies based on the following criteria was made by two independent researchers.

Study cohorts were eligible only if the following criteria were fulfilled:

1) Patients with stage I NSCLC (cT1/2, cN0, cM0) with either central or peripheral tumor location.
2) Treatment with photon radiotherapy with curative intent either 2D or 3D-conformal radiotherapy or SBRT as single modality treatment. Treatment could be delivered with CyberKnife, GammaKnife or linac-based without restrictions on fractionation schemes

(e.g. normofractionated, accelerated, hyper- or hypofractionated schedules, single fraction irradiation), provided complete information on number of fractions, dose per fraction, total absorbed dose and overall treatment time was available.

3) Reported outcome of interest (actuarial 3-year local control estimations according to Kaplan-Meier or other methods, in which death was a censored event) with a median follow-up time in each cohort ≥17 months.
4) From an original study (i.a. prospective randomized controlled trial or prospective or retrospective observational study or case series).
5) The reported cohorts must include at least 25 patients.
6) Patients could be judged to be either operable or inoperable if the clinical decision was made in favor of radiotherapy.
7) A small amount of heterogeneity in reported dose and patient parameters for a given outcome data point was accepted (e.g. a marginal group of patients treated with a deviating radiation scheme, or a small proportion of tumors included in the report of a stage I population with clinical staging other than I).

Data extraction

The main endpoint of this review was local tumor control (LC) at 3 years. If this value was not explicitly provided in the text, it was extracted from the Kaplan-Meier diagrams.

The fractionation concept (dose per fraction, number of fractions and total treatment time), and the planning technique were extracted together with further treatment- and patient-related parameters. The range of variation in reported cohort parameters for each local tumor control data point was qualitatively assessed and highly heterogeneous cohorts were excluded. Reported mean or preferably median dose values were used to describe the outcome of each specific patient cohort. All prescription doses were translated to doses at the isocenter and at PTV edge, calculated according to the information provided in each publication (more details in the Additional file 1). Mathematical modeling was performed with both, doses at the isocenter and at the PTV edge. The treatments were classified to be hypofractionated (HF) if 1–10 fractions were delivered with doses per fraction at the isocenter above 6 Gy. Treatments were classified as conventionally fractionated (CF) with a broader definition than in the clinical convention, based on the validity limits of the LQ model according to our current knowledge, namely treatment delivered in more than 10 fractions with fraction doses at isocenter ranging between 1.2 and 6 Gy.

Data analysis and mathematical models

Model parameters were fitted with nonlinear least square optimization methods and confidence intervals were calculated with likelihood profiling. A logistic relationship between tumor control probability (TCP) and the biological effective dose (BED) was assumed, according to the parameterization described in Okunieff et al. [26] and Bentzen et al. [27]. BED was based on the LQ model, calculated from the number of fractions and the dose at the isocenter, taking into account neither repopulation nor hypoxia, according to Eq. 1:

$$TCP = \frac{exp\left[\left(BED_{LQ} - TCD_{50}\right)/k\right]}{1 + exp\left[\left(BED_{LQ} - TCD_{50}\right)/k\right]}, with\, BED_{LQ} = nd\left(1 + \frac{d}{\alpha/\beta}\right) \tag{1}$$

where TCD_{50} is the dose necessary to obtain a local tumor control of 50 % and k is a parameter with dose units that is used to calculate the normalized slope, γ_{50}. This parameter quantifies the change in the expected TCP when a 1 % change in dose occurs, evaluated at the dose level of the TCD_{50}, and represents the maximal slope of the dose-response relationship. It can be calculated from k and TCD_{50} with the expression [27, 28]:

$$\gamma_{50} = \frac{4k}{TCD_{50}} \tag{2}$$

The same logistic model was implemented with an alternative BED definition, including a transition from linear-quadratic dependence for the cell survival to purely linear beyond a certain dose level, the dose threshold D_t, as described in [22]:

$$BED_{LQ-L} = \begin{cases} nd\left(1 + \frac{d}{\alpha/\beta}\right) & for\, d < D_t, \\ nD_t\left(1 + \frac{D_t}{\alpha/\beta}\right) + n\left(\frac{\alpha + 2\beta D_t}{\alpha}\right)(d - D_t) & for\, d \geq D_t, \end{cases} \tag{3}$$

where n is the number of irradiation fractions, d is the fraction dose, and D_t is the threshold for the fraction dose.

The LQ and LQ-L models were fitted to the joint dataset, and to the CF and HF subsets separately, for BED doses calculated both at the isocenter and the PTV edge. First, the linear-quadratic (LQ) model was applied with α/β fixed to 10 Gy, as it is universally accepted for conventional fractionation. The alternative BED definition derived from the LQ-L model was also applied with α/β equal to 10 Gy, to test if the inclusion of a dose threshold D_t would improve the previous fit. Additionally, a study to tentatively

estimate the α/β ratio from these clinical data was carried out.

In summary, the following fits were calculated:

1) LQ model with α/β ratio fixed to 10 Gy on the full dataset, and on the HF and CF datasets separately.
2) LQ-L model with α/β ratio fixed to 10 Gy on the full and on the HF datasets.
3) LQ model with free γ_{50}, TCD_{50} and α/β ratio on the full and the CF datasets.

Finally, in order to compare with the results of the recent analysis of Chi et al. [15] the Spearman's correlation between 3-year LC and BED calculated with different fixed α/β ratios was also investigated on the full and on the HF datasets.

The quality of the fits was assessed with checks of the residuals for normality. Models were ranked according to the Akaike Information Criterion (AIC), and for the LQ and LQ-L, being nested models, maximum likelihood ratio tests were made. All fitted and calculated values are reported together with their 68 % confidence intervals (CI), whenever possible. Statistical significance was assumed for p values < 0.05. Data handling, statistical analysis, model fitting and graphing were done with the software package R, version 2.15.0 [29].

Results

Selected patient cohorts and description of the studies

In total, 31 studies were identified, which fulfilled the selection criteria, Of those, 8 studies report outcomes after conventionally fractionated treatments of a total of 344 patients [30–37] and 23 studies including 1975 patients reporting on hypofractionated irradiations [38–60]. A total of 34 local control - schedule data points, with doses per fraction ranging from 30 to 1.2 Gy, applied in 1–58 fractions, were collected (see Tables 1 and 2, and Additional file 1 for details of the publication search).

Of all reported tumors, 63.6 % were confirmed to be stage T1, 36.4 % T2 (Table 3). A total of 68.1 % of tumors were histologically confirmed: 45.8 % adenocarcinomas, 34.1 % squamous cell carcinomas, 6.2 % other histologies and 13.9 % carcinoma not otherwise specified (NOS). Of the patients treated with conventional fractionation 86.3% were confirmed medically inoperable, versus 55.2 % of all patients treated with hypofractionated schedules. Median of the reported median ages [age range] was comparable between both groups, namely 72 [range: 35–90] and 75 [range: 29–94] years in the CF and HF groups respectively. Patients, who received conventionally fractionated RT were treated in the time period from 1976 to 2010, whereas patients treated with hypofractionated regimes were irradiated in the time period from 1996 to 2012. In the CF cohort only in one study PET-CT was performed for staging in 6 out of 31 patients (Bogart et al. [36]), whereas for many of the HF cohorts PET was a routine procedure; for many of the most recent studies PET-staging was even an inclusion criterion in the retrospective series.

In the 8 series of the CF group, generally a margin of 1–1.5 cm was added around the gross tumor volume (GTV), which was in some cases estimated from port films if no planning computer tomography (CT) scan was available. In the HF series, most frequently no GTV-to-CTV (clinical target volume) margins were added, except in 5 out of 23 series. Internal target volume (ITV) concepts were applied in 13/23 studies, based

Table 1 Characteristics of included studies with conventionally fractionated treatment regimes. Studies published between 1993 and 2015

No.	Reference	No. pats.	No. of pats. with stage T1 - T2	Fractionation regime			BED_{10}@ isoc [Gy]	BED_{10}@ PTV edge [Gy]	Dose calculation algorithm	3y-LC [%]	Follow-up Median (range) [m]
				D [Gy]	d [Gy]	T [d]					
1	Kaskowitz 1993 [30]	53	20–33	63 (40–80)	conventional	ns	74.3	69.6	ns	51	ns
2	Jeremic 1997 [31]	49	25–24	69.6	1.2 (2× day)	40	78.0	70.8	ns	55	ns
3	Hayakawa 1999 [32]	36	7–29	60–81	2	48	80.4	75.7	no dens corr	72	(36–216)
4	Cheung 2002 [33]	33	18–15	48	4	21	67.2	62.9	dens corr	63	23
5	Langendijk 2002 [34]	46	26–20	70	2	49	84.0	79.1	dens corr	50	36
6	Bradley 2003 [35]	56	31–25	60–84	1.8–2	42–56	83.7	78.6	no dens corr	63	20 (6–72)
7	Bogart 2005	31	19–12	70	2.3–3.7	39	87.5	83.3	ns	83	29
8	Zehentmayr 2015 [36]	40	19 (Ia)–21 (Ib)	79.2 (73.8–90)	1.8 (2× day)	30–42	93.5	87.5	ns	91	28.5 (2–108)
	Median	43		69.8	2.0	44	82.0	77.2		63	28.5 (2–216)

BED_{10} biologically effective dose with α/β = 10 Gy, *PTV* planning target volume, *D* total dose, *d* dose per fraction, *T* total treatment time, *LC* local control, *ns* not specified

Table 2 Characteristics of included studies with hypofractionated treatment regimes. Studies published between 2003 and 2015

No.	Reference	No. pats.	No. of pats. with stage T1 - T2	Fractionation regime			BED_{10} @isoc [Gy]	BED_{10} @PTV edge [Gy]	Dose calculation algorithm	3y-LC [%]	Follow-up median (range) [m]
				D [Gy]	d [Gy]	T [d]					
9	Onimaru 2003 [38]	25	17–8	48/60	6/7.5	14	76.8	56.8	dens inhom corr	55	18 (2–44)
10	Xia 2006 [39]	25	ns	50	5	[14]	200	75	GammaKnife, ns	96	27 (24–54)
11	Fritz 2008 [40]	40	22–18	30	30	1	120	81.6	modified Batho	81	20 (6–62)
12	Onimaru 2008 [41]	41	13–28	40/48	10/12	5	105.6	75.3	ns	57	27 (9–62)
13	Baumann 2009 [42]	57	40–17	45	15	5 (4–15)	211.2	112.5	PB, dens inhom corr	92	35 (4–47)
14	Brown 2009 [43]	31	20–11	60–67.5	3–5	5	347.5	180.0	ns	86	28 (24–53)
15	Fakiris 2009 [44]	70	34–36	60/66	20/22	5	309.4	211.2	no dens inhom corr	88	50 (1–65)
16	Kopek 2009 [45]	88	51–36	45/67.5	15/22.5	5–8	112.5	60.9	Helax-TMS/ Eclipse, ns	89	44 (2–97)
17	Stephans 2009 [46]	56	42–14	50	10	11 (8–14)	168	100.0	dens inhom corr	97	20 (2–48)
18	Baba 2010 [47]	124	87–37	48/52	12/13	11	105.6/119.6	75.3/84.9	PB convol with Batho	80	26 (7–66) (living pats)
19	Crabtree 2010 [48]	76	57–19	54	18	8–14	219.4	151.2	Trilogy, ns	89	19
20	Timmerman 2010 [49]	55	44–11	54	18	14	286.4	151.2	dens inhom corr	98	34 (5–50)
21	Videtic 2010 [50]	26	22–6	50	10	5	112.3	100	dens inhom corr	94	31 (10–51)
22	Andratschke 2011 [51]	92	31–61	24/45	3/5	5–12	192.2	84.4	dens inhom corr	83	21 (3–87)
23	Hamamoto 2012 [52]	128	101–27	48/60	9.2–14	4–10	105.6	89.9	PB, no dens inhom corr	85	18 (1–60)
24	Lagerwaard 2012 [53]	177	106–71	60	12 20 7.5	14	187.5	132.0	Brainlab, ns	93	32
	Shibamoto 2012 [54]							75.3	PB convo, Batho	83	36
25a	Shibamoto, d2	124	124 T1	48	12	9–21	105.6	75.3		86	
25b	Shibamoto, d3	52	52 T2	52	13	9–21	119.6	84.9		73	
	Shirata 2012 [55]		63–18					89.9	PB convolution Batho	89	30 (0.3–79)
26a	Shirata, d1	45		48	12		105.6	89.9		100	
26b	Shirata, d2	29		60	7.5		105	91.4		82	
	Takeda 2012 [56]								XiO/CMS, CS		
27a	Takeda, d1	27	10–17	40	8	5	100	72.0		72	21 (6–64)
27b	Takeda, d2	138	91–47	50	10	5	140.6	100.0		87	21 (6–64)
28	Inoue 2013 [57]	109	79–30	45/48	15/12	4–7	105.6	75.3	dens inhom corr	81	25 (4–72)
29	Takeda 2013 [58]	109	67–42	40/50	8/10	5	140.6	100	convolution-superposition	84.4	24 (3–65)
30	Hamaji 2015 [59]	104	75–29	48	12	5	105.6	75.3	PB convol, Batho	76.7	43 (6–115)
31	Rwigema [60]	46	-	54	18	5	234.5	151.2	MC	95.5	16.8 (0.6–38.9)
	Median	57		56.0	12.5	7	119.8	89.9		86	27.0 (0.3–115)

BED_{10} biologically effective dose with α/β = 10 Gy, *PTV* planning target volume, *D* total dose, *d* dose per fraction, *T* total treatment time, *LC* local control, *ns* not specified, *dens inhom corr* density inhomogeneity correction, *PB convol* pencil beam convolution, *CS* convolution superposition

Table 3 Summary of cohort characteristics and clinical follow up for conventionally fractionated and hypofractionated datasets

Dataset	Total No. pats.	% T1	Histology				% histology unknown	% inoperable	Median age (range) [y]	Median follow-up (range) [m]	Median BED_{10} @isoc (range) [Gy]	Median No. Pats (range)
			% Adeno	% SCC	% NOS	% Other						
CF	344	48.0 %	26.3	47.0	15.5	11.2	11.6	86.3	72 (35–90)	28.5 (2–216)	82.0 (67.2-93.5)	43 (31–56)
HF	1975	66.3 %	50.4	31.1	13.5	5.0	35.9	55.2	75 (29–94)	27 (0.3–115)	119.6 (76.8–347.5)	57 (25–177)
Total	2319	63.6 %	45.8	34.1	13.9	6.2	31.9	59.8	74 (29–94)	27 (0.3–216)	105.6 (67.2–347.5)	53 (25–177)

Adeno adenocarcinoma, *SCC* squamous cell carcinoma, *NOS* carcinoma not otherwise specified, *HF* hypofractionated treatment regime, *CF* conventionally fractionated treatment schedule

either on addition of GTV from 3D-CT scans in expiration/inspiration and free breathing in 4 cases, on slow CT scans in 5 cases, and on 4D-CT scans in 4 cases. Nine out of 23 studies did not apply any ITV concept. The most frequently used CTV-to-PTV (planning target volume) margins were 0.5 cm in axial and 1 cm in cranio-caudal directions. A minimal margin of 0.2 cm was added in one patient cohort treated with the Cyber-Knife where tumor tracking was used to correct for intrafractional target motion. In 2 out of 23 series the PTV margin definition was patient-specific.

Different dose reporting concepts were found throughout the selected references. Only 5 CF reports out of 8 explicitly mentioned that the dose was prescribed to the isocenter. When not specified, prescription to the isocenter was assumed. In the case of the hypofractionated SBRT data, 9 references reported the prescribed dose to isocenter and 11 to the isodose line encompassing the PTV, which ranged from the 50 to the 100 % isodose, most frequently to the 80 % isodose line. Only one of the SBRT cohorts was treated with IMRT, and in this case the dose was prescribed to the 95 % isodose line enclosing the PTV. More information can be found in the Additional file 1.

Median [min - max] applied BED at the isocenter, calculated with an α/β ratio of 10 Gy (BED_{10}), was 82.0 [67.2–93.5] and 119.8 [76.8–347.5] Gy for the CF and HF groups, respectively. At the PTV edge, values of 77.2 [62.9–87.5] and 89.9 [56.8–211.2] Gy were applied in the CF and HF groups.

Median value of the documented median follow-up times were 28.5 and 27 months for the CF and HF groups, respectively. Very few of these publications state explicitly the number of patients at risk at each follow-up time point (four cohorts). In only 5 of the selected studies an estimation of the 95 % CI of the calculated actuarial local control rates was reported and one publication presents the standard error. Therefore, no information could be collected about the precision of the estimated actuarial local control rates, apart from the cohort size and the median follow-up time.

3- and 5- year clinical outcomes for stage I NSCLC

The median value [range] for the 3-year LC was 86 [range: 55–100] % for the HF, and 63 [range: 50–91] %, for the CF series, respectively. Twenty-two out of 26 HF 3-year LC data points lie above the 80 % level, while all except two of the CF datasets lie below. All except one HF treatments delivered a BED_{10} of 100 Gy or higher at the isocenter but none of the CF treatments reached a BED_{10} of 100 Gy.

Spearman's correlation coefficients between dosimetric parameters (total absorbed dose and BED_{10}) and the different clinical outcomes were calculated. For the complete dataset and the total BED_{10} at the isocenter, a significant Spearman's correlation of 0.716 for the local control with BED_{10} was found. For the BED_{10} evaluated at the PTV edge, a significant correlation of 0.638 was found between LC and BED_{10}. The total absorbed dose at either dose point however did not correlate with LC.

Modeling local control versus BED

Linear-quadratic (LQ) model with α/β ratios fixed to 10 Gy (two-parameter fit)

All 3-year LC data points for both the HF and CF treatments were fitted to a logistic model coupled with BED_{10} at both isocenter and PTV edge. For the isocenter, the TCD_{50} [68% CI] was 48.3 [23.8–62.4] Gy, k was 44.7 [32.1–64.8] Gy, and the calculated γ_{50} (std error) was 0.27 ± 0.1. A logistic fit under the same assumptions, based on the CF subset alone was made, and resulted in the values: TCD_{50} of 68.9 [50.7–74.4] Gy, k was 20.5 [13.1–50.0] Gy and γ_{50} was 0.84 ± 0.5. The same approach applied to the HF dataset showed a TCD_{50} of −60.2 [−189–3.2] Gy, k of 113.3 [73.4–190.1] Gy, and γ_{50} of -0.13 ± 0.17. These three logistic models are represented in Fig. 1a, and all fit parameter values are summarized in Table 5. The p value was found to be < 0.05 for both TCD_{50} and k simultaneously only for the model based on the full dataset.

The model for the complete dataset based on BED_{10} at PTV edge yielded a TCD_{50} of 28.0 [−0.7–43.1] Gy, and k was equal to 39.7 [28.1–60.5] Gy. These values were 64.2 [48.6–69.3] and 19.5 [12.5–44.6] Gy respectively for

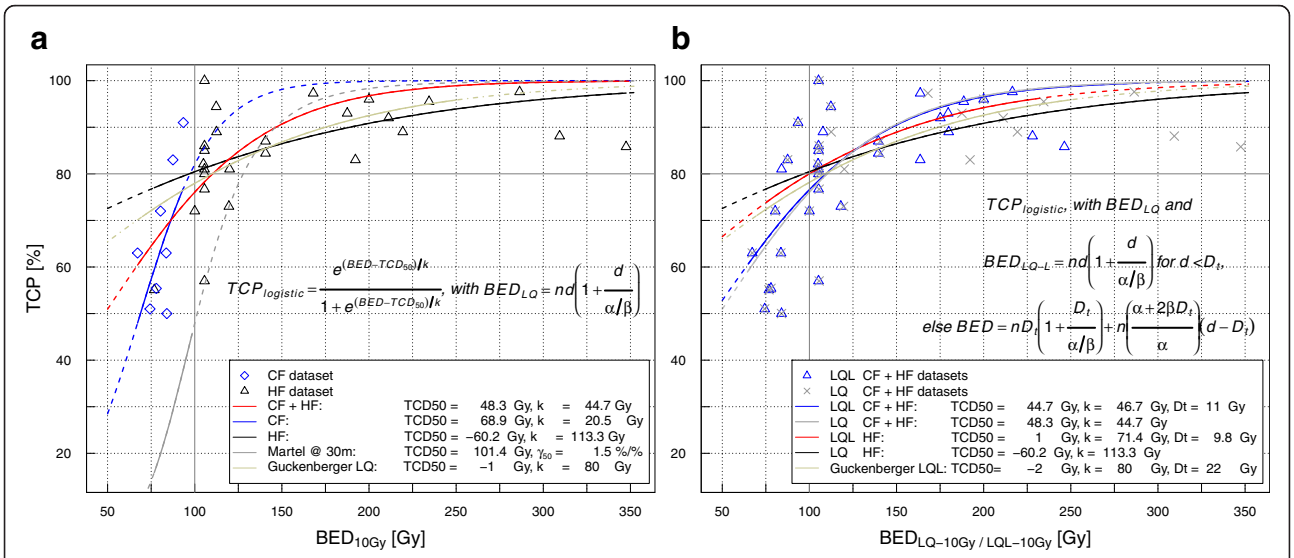

Fig. 1 **a** Clinical 3-year LC data points for the conventionally fracionated and hypofractionated datasets versus BED_{10} at isocenter with corresponding logistic regression fits of the joint CF + HF dataset, and the CF and HF subsets. Previously published related models are included for comparison: Martel et al. [28] and Guckenberger et al. [61]. **b** Comparison between the BED_{10} (isocenter) data points obtained with the LQ and LQ-L fits for the complete dataset and for the hypofractionated subset. The range of experimental data of every model is shown with a continuous line and the extrapolation regions with dashed lines. The levels 80 % TCP and 100 Gy BED_{10} are also shown for reference

the CF, and −19.9 [−93.5–14.5] and 64.4 [42.9–108.1] Gy for the HF group alone. Only the parameter values for the CF dataset yielded significant p values simultaneously. Model summaries and calculated γ_{50} values together with their standard errors obtained with propagation of uncertainties are also presented in Tables 5. These models are represented in Fig. 2a.

Linear-quadratic-linear (LQ-L) model with α/β fixed to 10 Gy (three-parameter fit)

The alternative BED definition including a linear portion in the dose-effect beyond a certain fraction dose was tested, according to Eq. 3, with an α/β ratio fixed to 10 Gy. Fits were performed either based on the full dataset or on the HF subset alone.

For the models based on BED_{10} at the isocenter, the fit based on the full dataset generated a D_t value of 11.0 [8.4–16.7] Gy, together with a TCD_{50} value of 44.7 [24.2–58.2] Gy, and k equal to 46.7 [35.1–63.2] Gy. The calculated γ_{50} value was 0.24 ± 0.11. All of the parameter estimates yielded significant p values. 13 out of 34 data points represented a dose per fraction below the estimated D_t. This fit is shown in Fig. 1b, together with the LQ fit for comparison, and their respective BED_{LQ} and $BED_{LQ\text{-}L}$ data points.

For the fit based on the HF dataset alone, D_t was equal to 9.8 [5.2–15.0] Gy, TCD_{50} was 1.0 [na-23.8] Gy, and k equal to 71.4 [54.2–79.6] Gy. Only two data points were found to be below this D_t, which was too few to obtain a reliable estimate. Thus, the fit parameters did not produce significant p values. This fit is shown in Fig. 2b, together with the LQ fit for comparison.

When BED_{10} doses at PTV edge were used, similar D_t values were found, namely, 12.4 Gy for the complete dataset, and 9.9 Gy for the HF dataset (this fit is shown in Fig. 2b). Likelihood ratio tests showed no difference between LQ-L and LQ fits, independently of which BED_{10} doses were used, at isocenter or PTV edge (see Table 5).

Correlation of local control with BED

To complete the modeling study, the correlation of the 3-year LC with BED under different assumptions for α/β equal to 5, 8.6, 10, 15 and 20 Gy was investigated (see Table 4). For the complete dataset and BED_{10} values at isocenter, a Spearman's correlation of 0.716 ($p < 0.0001$) with BED_{10} was found. For all other α/β ratios, correlation values increased marginally from BED_5 ($r = 0.706$) to a maximum at BED_{10} and decreased again for BED_{20} ($r = 0.706$), in all cases being significant. The Spearman's correlations based on the BED values at the PTV edge decreased with growing α/β values for the complete dataset, from 0.680 to 0.510, all of them being significant and consistently lower than the respective values for the BED_{10} at the isocenter (see Table 4).

In contrast, for the HF subset, the correlation of the LC with the same series of $BED_{\alpha/\beta}$ at isocenter increased minimally from 0.575 to 0.618, and also the values for $BED_{\alpha/\beta}$ at PTV edge, from 0.531 to 0.601, all of them being statistically significant.

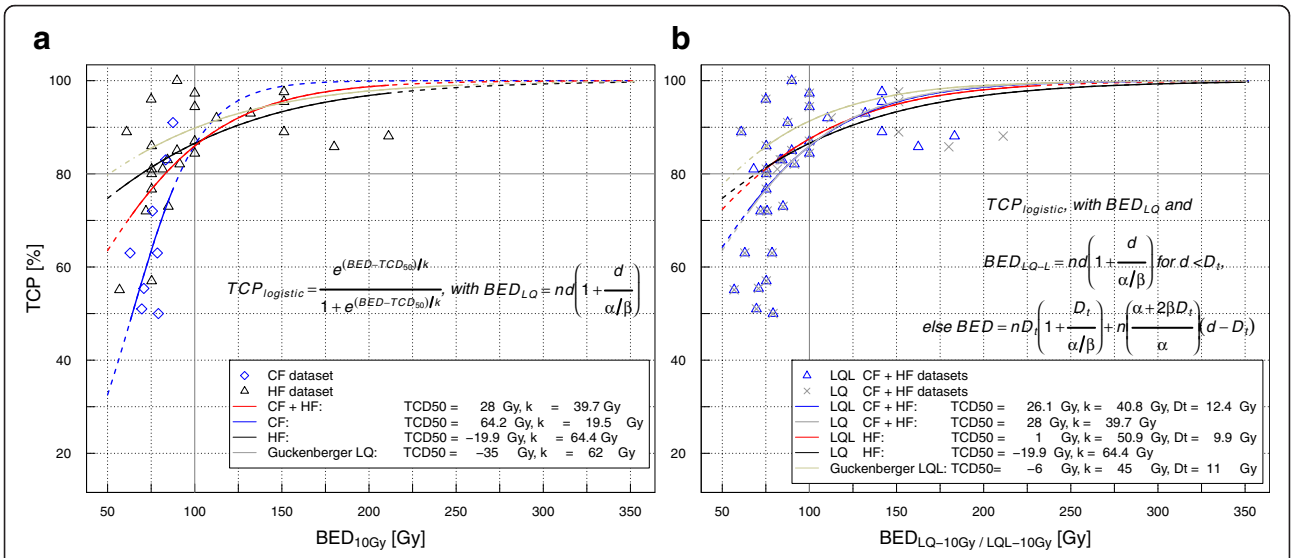

Fig. 2 a Clinical 3-year LC data points for the CF and HF datasets versus BED_{10} at PTV edge, with corresponding logistic regression fits of the joint conventionally and hypofractionated dataset, and the conventionally fractionated and hypofractionated subsets. A previously published related model is included for comparison, Guckenberger et al. [61]. **b** Comparison between the BED_{10} (PTV edge) data points obtained with the LQ and LQ-L fits for the complete dataset and for the hypofractionated subset. The range of experimental data of every model is shown with a continuous line and the extrapolation regions with dashed lines. The levels 80% TCP and 100 Gy BED_{10} are also shown for reference

LQ model with three-parameter logistic fit

Additionally, we attempted to estimate the α/β ratio for NSCLC from the complete data set, fitting all three model parameters simultaneously: TCD_{50}, k and α/β. We obtained for the BED doses at isocenter an α/β value of 3.9 [2.2–9.0] Gy, TCD_{50} of 17.8 [na-56.4] Gy, and k of 130.9 [50.1-na] Gy, with only TCD_{50} yielding a p value < 0.05. For the CF dataset alone we found a similar α/β of 3.8; however, it was not possible to determine confidence intervals. These fits are represented in Fig. 3b. In order to check plausibility of the fit results and to compare our results with published values we calculated γ_{50} and found a value of 0.0 ± 0.15. For the models based on BED_{10} at PTV edge we found values for alpha/beta of 1.7 [1.3–4.1] Gy for the complete dataset and 4.1 [na] Gy for the CF dataset with no significant p values (Table 5).

Table 4 Spearman's correlations of the local control with the biologically effective dose at the isocenter and the planning target volume edge, calculated with different α/β values, for the complete dataset and exclusively for the hypofractionated dataset (all of them significant, $p > 0.05$)

Spearman's r	vs BED @ Isocenter		vs BED @ PTV edge	
α/β [Gy]	All datasets	HF	All datasets	HF
5	0.706	0.575	0.680	0.531
8.6	0.716	0.587	0.680	0.560
10	0.716	0.587	0.638	0.542
15	0.749	0.601	0.572	0.606
20	0.706	0.618	0.510	0.601

BED biologically effective dose, *PTV* planning target volume

Differences in the prediction of isoeffects

In order to translate the impact of the different BED model assumptions on clinical treatment schedules we calculated as an example the doses per fraction which would be necessary to reach selected BED_{10} levels at the isocenter (Fig. 4). Under the assumptions of the LQ model with α/β values of 8, 10, or 15 Gy and the LQ-L model at the isocenter with α/β equal to 10 Gy and a D_t of 11.0 Gy, in order to reach 100 Gy (BED), the maximum differences among models for one and two fractions are 10.5 and 4.5 Gy, respectively. Maximal differences remain below 3.3 Gy for treatments delivered in 3 or more fractions. For 200 Gy (BED), discrepancies between models in fraction size increase to 30.1 and 10.5 Gy for one and two fractions, respectively and remain below 5.6 Gy for 3 fractions and more.

Discussion

Review of clinical outcome data after radiotherapy treatment represents the only possibility to gather long-term information from large numbers of patients, which could serve as basis for statistical analysis for radiobiological modeling. However, this task presents a number of challenges since these datasets are intrinsically heterogeneous. Variability among radiotherapy centers applies to aspects such as target volume definition, dose prescription, planning concepts and delivery techniques with different precision levels. Additional effects hindering

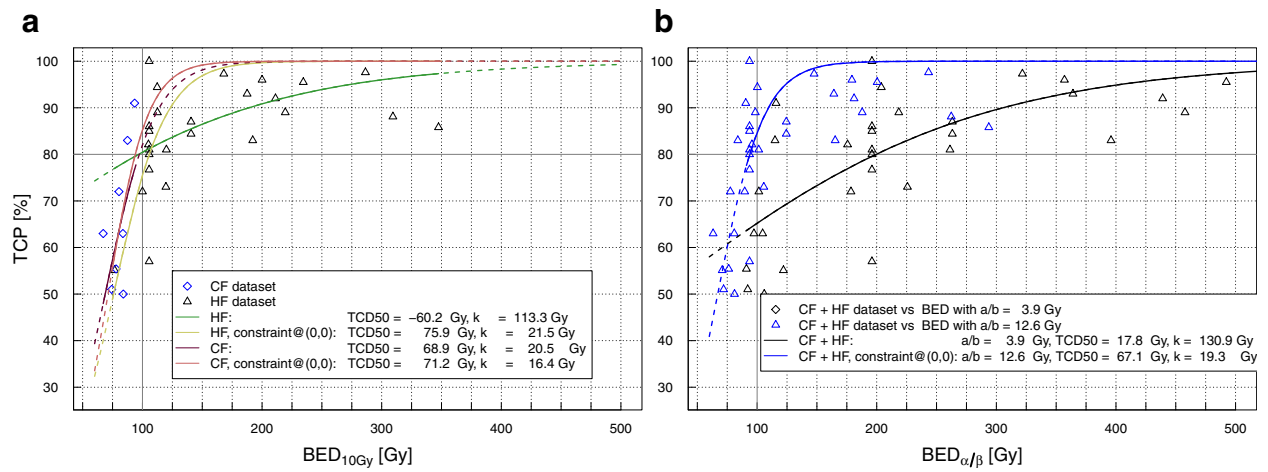

Fig. 3 Logistic fits for LC versus $BED_{\alpha/\beta}$ at isocenter, with constraint to approach the sigmoidal curves to the coordinate origin, **a** with α/β fixed to 10 Gy for the CF and HF datasets separately, and **b** with three free parameters: α/β, TCD_{50} and k, for the combined dataset with conventionally fractionated and hypofractionated treatments. Logistic fits without constraint are provided for comparison

precise dose-effect modeling are: the use of multiple and sometimes less appropriate dose calculation algorithms especially in the case of lung tumors (e.g. with limited heterogeneity correction), which may lead to mis-estimation of the absorbed dose. Additionally, outcome of different tumor stages, dose levels and fractionation schemes are frequently reported together. Furthermore, including historical cohorts implies dealing with changes over time in the standard diagnostic and therapeutic procedures, e.g. for staging, recurrence assessment and radiotherapy image guidance.

To counteract this variability, we applied strict inclusion criteria to the selected publications. The analysis is based on 3-year local control in order to depict the dose-response in mature outcome data, while maintaining a sufficient number of data points. To our knowledge this is one of the largest, most homogeneous patient collectives among similar studies. Through the combination of conventionally fractionated and hypofractionated data, a broad range of doses and fractionation schemes is covered, which is a further requirement in order to achieve conclusive modeling results.

Dosimetric heterogeneity in the PTV can be very pronounced in dose distributions for stereotactic treatments, reaching dose differences between isocenter and PTV edge of up to 50 %. It is not possible to know a priori, which reported dosimetric parameter will describe best the dose-effect relationship: the dose at the PTV edge or the dose at isocenter. Therefore, we calculated models based on both, isocenter and minimum target doses. The TCD_{50} doses estimated for the isocenter doses were in general higher than the ones from the models at PTV edge.

Variability in the estimated doses at PTV edge could arise for instance, from variations in the CTV and PTV margin definitions among institutions, or uncertainties in the dose calculation methods, which in the case of outdated, less accurate dose calculation algorithms for the lung, would produce large dose mis-estimation and underdosage at the PTV edge.

We calculated the Spearman's correlations between outcome parameters and the BED_{10} evaluated at both dose specification points and observed that the correlations with BED_{10} at the PTV edge were without exception lower than the corresponding correlations based on BED_{10} at the isocenter. This could be interpreted as an indication of the isocenter doses being more robust than the doses at the PTV edge for retrospective modeling studies, in agreement with previous studies [61].

The BED_{10} fits based on the CF data and the complete dataset differ in both the TCD_{50} and k values. This can be explained by the fact that the information required defining the slope of the dose-response curve and the TCD_{50}, which together shape the sigmoid region of the logistic function, is provided by the CF data, where generally a lower BED was applied. This explains why TCD_{50} and k are not consistently determined across models, which use different input data: CF + HF, or HF/CF alone. We represented the range of the model input data and the extrapolation regions in all figures, to stress that special care must be taken predicting doses in the extrapolation region.

For comparison, Fig. 1 includes the previously published dose-response models of Martel et al. [28] and Guckenberger et al. [61]. Martel et al. found a TCD_{50}, which is higher as compared to our findings as they

Table 5 Summary of the models for both BED doses calculated at isocenter and PTV edge; all fit parameter values are provided with standard errors (and 68 % CI). This table includes the maximum likelihood ratio tests for comparison between the corresponding LQ and LQ-L models with α/β = 10 Gy

Model concept and dataset		α/β (std error) [Gy]	D_t (std error) [Gy]	TCD_{50} CI 68 % [Gy]	k CI 68 % [Gy]	γ_{50} (std error) [%/%]	AIC	Likelihood ratio test LQ vs LQL: Dataset, Df, LogLik, Df, Chisq, Pr (>Chisq)
ISOCENTER								
LQ fixed α/β	CF + HF	α/β = 10	-	48.3 (23.8–62.4)*	44.7 (32.1–64.8)*	0.27 (0.1)	−4438.1	Isocenter, all data 4, 2223.8, 1, 3.42, 0.064
	CF	α/β = 10	-	68.9 (50.7–74.4)*	20.5 (13.1–50.0)	0.84 (0.5)	−186.4	-
	HF	α/β = 10	-	−60.2 (−189–3.2)	113.3 (73.4–190.1)*	−0.13 (−0.17)	−2625.2	Isocenter, HF 4, 1316.4, 1, 1.68, 0.195
LQ-L fixed α/β	CF + HF	α/β = 10	11 (8.4–16.7)*	44.7 (24.2–58.2)*	46.7 (35.1–63.2)*	0.24 (0.11)	−4439.6	
	HF	α/β = 10	9.8 (5.2–15.0)	1.0 (na–23.8)	71.4 (54.2–79.6)	0.0 (0.15)	−2624.8	
LQ: free α/β, TCD50 and k	CF+ HF	3.9 (2.2–9.0)	-	17.8 (na–56.4)	130.9 (50.1–na)	0.0 (0.15)	−4441.6	
	CF	3.8 (na)	-	90.7 (na)*	19.7 (na)	1.15 (0.64)	−186.6	
PTV EDGE								
LQ fixed α/β	CF + HF	α/β = 10	-	28.0 (−0.7–43.1)	39.7 (28.1–60.5)*	0.18 (0.13)	−4430.1	PTV Edge, all data 4, 2218.3, 1, 0.614, 0.433
	CF	α/β = 10	-	64.2 (48.6–69.3)*	19.5 (12.5–44.6)*	0.82 (0.47)	−186.6	
	HF	α/β = 10	-	−19.9 (−93.5–14.5)	64.4 (42.9–108.1)*	−0.08 (−0.16)	−2625.9	PTV Edge, HF 4, 1315.9, 1, 0.009, 0.925
LQ-L fixed α/β	CF + HF	α/β = 10	12.4 (8.3–na)	26.1 (na)	40.8 (na–60.2)	0.16 (0.13)	−4428.7	
	HF	α/β = 10	9.9 (5.5-na)	1 (na–18.0)	50.9 (40.0–55.3)	0 (0.15)	−2623.9	
LQ: free α/β, TCD50 and k	CF+ HF	1.7 (1.3–4.1)	-	29.8 (na–68.2)	161.1 (60.4–na)	0.0 (0.13)	−4443.5	
	CF	4.1 (na)	-	81 (na)	20.4 (na)	0.99 (na)	−186	

D_t dose threshold, *TCD_{50}* tumor control dose 50 %, *AIC* Akaike information criterion, *Df* degrees of freedom, *LogLik* log-likelihood, *Chisq* chi-square, *PTV* planning target volume
*p value < 0.05

compiled stage I/II data whereas our dataset included stage I tumors only. The values for the slope γ_{50} that we obtained for the complete dataset and the CF subset are lower than the value in Martel et al. [28] and further values in the literature. For instance, Stuschke et al. [11] reported a value of 1.5, and Okunieff et al. [26] found a value of 1.6 on average.

Our fit based on the HF data alone shows a shallower curve than the fits including CF data, since the outcomes after hypofractionation are well above the inflection point of the sigmoidal curve. Our HF fit results for both BED_{10}(isocenter) and BED_{10}(PTV edge) are graphically similar to the findings by Guckenberger et al. [61], which were based on a multicentric compilation of individual patient SBRT data.

The LQ-L model was proposed to account for the experimental observation that curves of the (log cell survival) versus radiation dose often show a more straightened portion at doses beyond 10 Gy than predicted by the LQ model. This effect is in the majority of cases due to heterogeneity of the radiosensitivity distribution of the cells. This is partly due to differences in the stage of cells in the proliferation cycle, but can also be due to partially hypoxic conditions. Resistant cells tend to survive even at larger doses, which causes the survival curve to become less steep than predicted by the LQ model. This explanation implies that the straightening in the curve is not caused by a fundamental mechanism but by a simple to explain heterogeneity in the distribution of sensitivity. Both models converge at dose of less than about 6 Gy.

Applying state-of-the-art fitting methods to compare the performance of the LQ versus the LQ-L models for different fractionation schemes, we did not find significant differences. Therefore, it was not possible to decide, which model better predicts clinical NSCLC outcome

data. For BED corresponding to doses per fraction below 11.0 Gy, the BED points for both concepts overlap, whereas above D_t there is a contraction in the $BED_{LQ\text{-}L}$ values, which has no consequence in the fit itself, since it takes place in the region where the TCP approaches 100 %. Clinical consequences of using one model or another are only relevant for highly hypofractionated schedules aiming at delivering BED values well above 100 Gy.

The LQ-L model was also fitted to the HF datasets alone, although we could not obtain a 68 % CI for the TCD_{50}, and the *p* values of all three parameters were > 0.05. Fig. 2b clearly demonstrates the similarity of our LQ-L fit for the HF data subset to the LQ fit previously presented, therefore TCP predictions will be similar with either model. Although our LQ-L fit based on HF data did not yield significant estimates, the results suggest a D_t estimate in the same range of magnitude of 10 Gy. This fit was tested previously also on hypofractionated data alone by Guckenberger et al. [61]. Their dataset had a median dose per fraction at isocenter of 20.8 Gy with range [6–41] Gy. This group found a D_t value of 22 Gy with a broad 68 % confidence interval, [14–42] Gy, whose addition to the model did not improve the prediction power.

Estimation of the α/β ratio by fitting three parameters simultaneously on a clinical dataset presenting high dispersion - as is the case of the current work - is challenging. Our LQ model with free α/β did not yield significant values for α/β, nor for TCD_{50} and the slope k, which appears to be too shallow after visual inspection. We concluded that there is no indication for larger α/β values than 10 Gy if the complete range of fractionations is considered. The opposite trend (α/β > 10 Gy) was found for the HF dataset as was also the case in Chi et al. [15], although no significant *p* values could be obtained in this case, neither.

There are few works aiming to the estimation of a clinical α/β for radiotherapy of NSCLC [10, 11, 15]. Thames et al. [10] published an extremely high α/β value for lung tumors but these authors did not obtain a reliable confidence interval and so, their calculations must be regarded with caution. A similar work was also carried out by Stuschke et al. [11], who found an α/β value of 8.2 Gy. They used a fit similar to ours, but set a constraint to force the model to approach the axes origin by adding a point with low BED and null TCP, with a high fit weight. We also tested this approach (full model information in the Additional file 1), adding a data point at 0 Gy ($BED_{\alpha/\beta}$) and 0 % TCP. We observed that this constraint influenced the TCD_{50} value to a small extent only, but could have a strong effect on the slope of the curve, and also on the α/β value, for instance, 3.9 [2.2–9.0] versus 12.6 [10.5–15.0] Gy for the complete dataset and BED_{10}(isocenter). The LQ-based fits with α/β of 10 Gy for the CF data alone did not vary much with and without constraint. In contrast, if the fit was based on the HF dataset alone, adding this constraint on the original fit had a pronounced effect on the steepness and TCD_{50} of the curve, which in the constrained fits approached the curves based on CF data (Fig. 4a). For this reason, we think it is preferable not to set a constraint to the model, which largely influences the estimates for k and α/β, and also their standard errors. It seems reasonable to accept that fits done on the HF dataset alone will not reproduce a realistic fall-off in LC at low doses nor a plausible, clinical TCD_{50}, since the input dose-response data are well above that region in this specific case.

The dispersion in the collected data points was high. Due to this fact, in the hypofractionation range the dose-effect relationship appears to be weaker than in other reports [13, 61]. Specifically, for the fraction of HF data above 100 Gy (BED_{10}), the Spearman's correlation between LC and BED_{10} is low. It can be speculated that in the region of high tumor control probability and highly hypofractionated treatments the relative contribution of non-radiobiological factors to the treatment effect is larger. Such factors are, for instance, subjectivity in target delineation and geographical miss, among others.

The logistic fit was applied also in the study at high dose regions since it is widely used for dose-effect description. However, other functional dependencies of LC with BED might be also appropriate in the high BED range. Concerning the BED concept, it seems likely that more than one approach can fit equivalently well on an inherently noisy dataset like this, for instance the LQ applying a higher α/β ratio, or the LQ-L model with α/β of 10 Gy, even if these models have contrasting radiobiological implications.

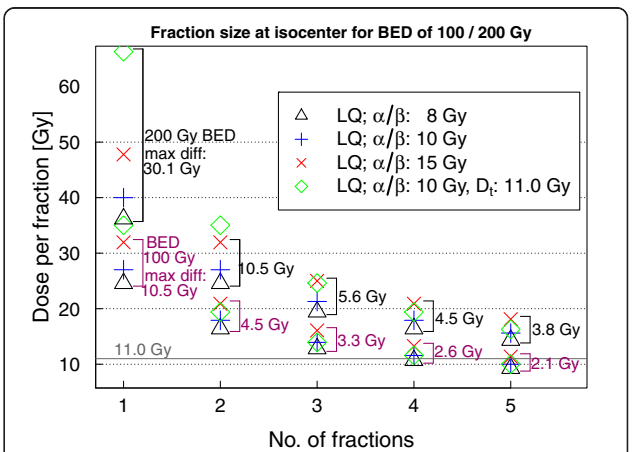

Fig. 4 Fraction dose necessary to deliver a BED equal to 100 and 200 Gy under the assumptions of the LQ model with α/β of 8, 10, and 15 Gy and LQ-L model with α/β equal to 10 Gy and a D_t value of 11.0 Gy, estimated for doses at the isocenter

Conclusion

We found a dose-effect relationship in the studied dataset, which in the high BED region was weaker due to considerable dispersion in the data. Both, the LQ and LQ-L models can be fitted to clinical normo- and hypofractionated NSCLC outcome data. The LQ-L model yielded a significant value for the D_t of 11.0 Gy for the model based on BED_{10}(isocenter); however, it produced a comparable TCP fit to the LQ model. For the application of BED_{10} in the range of 100–150 Gy in three fractions or more, the differences in isoeffects predicted by both models can be neglected. Our findings therefore do not allow us to suggest use of the LQ-L model for an improved fitting compared to the LQ model of local control data in case of hypofractionation. A tentative analysis to establish the optimal α/β ratio in the frame of the LQ model for the full fractionation range did not produce significant estimates, although, it showed a trend for α/β values lower than 10 Gy.

Additional file

Additional file 1: Details of the Pubmed search and of the studies included in this work. (PDF 197 kb)

Competing interests

The authors report no conflicts of interest. The authors alone are responsible for the content and writing of the paper.

Authors' contributions

AW, SB, UJ and RE conceived the study. AS designed the search strategy, collected and assembled the data, analyzed and interpreted the results and drafted the manuscript. AW and SB contributed to define the search strategy and supported the data collection. UJ also contributed to define the search strategy. AW and UJ revised the manuscript and made substantial contributions to the interpretation of the results. All authors read and approved the final manuscript.

Acknowledgements

The study was financially supported by a grant of the Anneliese Pohl Stiftung. The authors thank Iuliana Toma-Dasu for her insightful comments about the modeling methods and Marie-Anne Chanrion for her useful comments and careful manuscript proof-reading.

Author details

[1]Department of Radiotherapy and Radiation Oncology, University Hospital Giessen and Marburg, Philipps-University Marburg, Baldingerstrasse, Marburg 35043, Germany. [2]Present address: Gemeinschaftspraxis Strahlentherapie am St. Agnes Hospital, Bocholt, Germany. [3]Present address: Marburger Ionenstrahl-Therapiezentrum MIT, Marburg, Germany.

Received: 12 February 2016 Accepted: 27 April 2016
Published online: 06 May 2016

References

1. Barendsen GW. Dose fractionation, dose rate and iso-effect relationships for normal tissue responses. Int J Radiat Oncol Biol Phys. 1982;8:1981–97.
2. Joiner MC, van der Kogel AJ. Basic clinical radiobiology. 4th ed. London: Hodder Arnold; 2009.
3. Herrmann T, Baumann M, Dörr W. Klinische Strahlenbiologie – kurz und bündig. 4th ed. Munich: Elsevier; 2006.
4. Bentzen SM, Dörr W, Gahbauer R, Howell RW, Joiner MC, Jones B, et al. Bioeffect modeling and equieffective dose concepts in radiation oncology – terminology, quantities and units. Radiother Oncol. 2012;105:266–8.
5. Guckenberger M, Andratschke N, Alheit H, Holy R, Moustakis C, Nestle U, et al. Definition of stereotactic body radiotherapy: principles and practice for the treatment of stage I non-small cell lung cancer. Strahlenther Onkol. 2014;190:26–33.
6. Guckenberger M, Allgauer M, Appold S, Dieckmann K, Ernst I, Ganswindt U, et al. Safety and efficacy of stereotactic body radiotherapy for stage I non-small-cell lung cancer in routine clinical practice: a patterns-of-care and outcome analysis. J Thorac Oncol. 2013;8:1050–8.
7. Fowler JF. Development of radiobiology for oncology – a personal view. Phys Med Biol. 2006;51:R263–86.
8. Kirkpatrick JP, Brenner DJ, Orton CG. Point/counterpoint. the linear-quadratic model is inappropriate to model high dose per fraction effects in radiosurgery. Med Phys. 2009;36:3381–4.
9. Brown JM, Carlson DJ, Brenner DJ. The tumor radiobiology of SRS and SBRT: are more than the 5 Rs involved? Int J Radiat Oncol Biol Phys. 2014;88:254–62.
10. Thames HD, Bentzen SM, Turesson I, Overgaard M, Van den Bogaert W. Time-dose factors in radiotherapy: a review of the human data. Radiother Oncol. 1990;19:219–35.
11. Stuschke M, Pottgen C. Altered fractionation schemes in radiotherapy. Front Radiat Ther Oncol. 2010;42:150–6.
12. Zhang J, Yang F, Li B, Li H, Liu J, Huang W, et al. Which is the optimal biologically effective dose of stereotactic body radiotherapy for stage I non-small-cell lung cancer? a meta-analysis. Int J Radiat Oncol Biol Phys. 2011;81:e305–16.
13. Mehta N, King CR, Agazaryan N, Steinberg M, Hua A, Lee P. Stereotactic body radiation therapy and 3-dimensional conformal radiotherapy for stage I non-small cell lung cancer: a pooled analysis of biological equivalent dose and local control. Pract Radiat Oncol. 2012;2:288–95.
14. van Baardwijk A, Bosmans G, Bentzen SM, Boersma L, Dekker A, Wanders R, et al. Radiation dose prescription for non-small-cell lung cancer according to normal tissue dose constraints: an in silico clinical trial. Int J Radiat Oncol Biol Phys. 2008;71:1103–10.
15. Chi A, Wen S, Liao Z, Fowler J, Xu J, Nguyen NP, et al. What would be the most appropriate alpha/beta ratio in the setting of stereotactic body radiation therapy for early stage non-small cell lung cancer. Biomed Res Int. 2013;2013:391021.
16. Guerrero M, Li XA. Extending the linear-quadratic model for large fraction doses pertinent to stereotactic radiotherapy. Phys Med Biol. 2004;49:4825–35.
17. Laine AM, Pompos A, Timmerman R, Jiang S, Story MD, Pistenmaa D, Choy H. The role of hypofractionated radiation therapy with photons, protons, and heavy ions for treating extracranial lesions. Front Oncol. 2016;5:302.
18. Bush DA, Cheek G, Zaheer S, Wallen J, Mirshahidi H, Katerelos A, et al. High-dose hypofractionated proton beam radiation therapy is safe and effective for central and peripheral early-stage non-small cell lung cancer: results of a 12-year experience at Loma Linda University Medical Center. Int J Radiat Oncol Biol Phys. 2013;86:964–8.
19. Nihei K, Ogino T, Ishikura S, Nishimura H. High-dose proton beam therapy for stage I non-small-cell lung cancer. Int J Radiat Oncol Biol Phys. 2006;65:107–11.
20. Hata M, Tokuuye K, Kagei K, Sugahara S, Nakayama H, Fukumitsu N, et al. Hypofractionated high-dose proton beam therapy for stage I non-small-cell lung cancer: preliminary results of a phase I/II clinical study. Int J Radiat Oncol Biol Phys. 2007;68:786–93.
21. Krämer M, Scholz M. Treatment planning for heavy-ion radiotherapy: calculation and optimization of biologically effective dose. Phys Med Biol. 2000;45:3319–30.
22. Astrahan M. Some implications of linear-quadratic-linear radiation dose-response with regard to hypofractionation. Med Phys. 2008;35:4161–72.
23. Park C, Papiez L, Zhang S, Story M, Timmerman RD. Universal survival curve and single fraction equivalent dose: useful tools in understanding potency of ablative radiotherapy. Int J Radiat Oncol Biol Phys. 2008;70:847–52.
24. Wang JZ, Huang Z, Lo SS, Yuh WTC, Mayr NA. A generalized linear-quadratic model for radiosurgery, stereotactic body radiation therapy, and high-dose rate brachytherapy. Sci Transl Med. 2010;2:39–48.
25. Moher D, Liberati A, Tetzlaff J, Altman DG. Preferred reporting items for systematic reviews and meta-analyses: the PRISMA statement. BMJ. 2009;339:b2535.
26. Okunieff P, Morgan D, Niemierko A, Suit HD. Radiation dose-response of human tumors. Int J Radiat Oncol Biol Phys. 1995;32:1227–37.

27. Bentzen SM, Tucker SL. Quantifying the position and steepness of radiation dose-response curves. Int J Radiat Biol. 1997;71:531–42.
28. Martel MK, Ten Haken RK, Hazuka MB, Kessler ML, Strawderman M, Turrisi AT, et al. Estimation of tumor control probability model parameters from 3-D dose distributions of non-small cell lung cancer patients. Lung Cancer. 1999;24:31–7.
29. R version 2.15.0, 2012-03-30, Copyright (C) 2012, The R Foundation for Statistical Computing, ISBN 3-900051-07-0.
30. Kaskowitz L, Graham MV, Emami B, Halverson KJ, Rush C. Radiation therapy alone for stage I non-small cell lung cancer. Int J Radiat Oncol Biol Phys. 1993;27:517–23.
31. Jeremic B, Shibamoto Y, Acimovic L, Milisavljevic S. Hyperfractionated radiotherapy alone for clinical stage I nonsmall cell lung cancer. Int J Radiat Oncol Biol Phys. 1997;38:521–5.
32. Hayakawa K, Mitsuhashi N, Saito Y, Nakayama Y, Furuta M, Sakurai H, et al. Limited field irradiation for medically inoperable patients with peripheral stage I non-small cell lung cancer. Lung Cancer. 1999;26:137–42.
33. Cheung PCF, Yeung LTF, Basrur V, Ung YC, Balogh J, Danjoux CE. Accelerated hypofractionation for early-stage non-small-cell lung cancer. Int J Radiat Oncol Biol Phys. 2002;54:1014–23.
34. Langendijk JA, Aaronson NK, de Jong JMA, ten Velde GPM, Muller MJ, Slotman BJ, et al. Quality of life after curative radiotherapy in stage I non-small-cell lung cancer. Int J Radiat Oncol Biol Phys. 2002;53:847–53.
35. Bradley JD, Wahab S, Lockett MA, Perez CA, Purdy JA. Elective nodal failures are uncommon in medically inoperable patients with stage I non-small-cell lung carcinoma treated with limited radiotherapy fields. Int J Radiat Oncol Biol Phys. 2003;56:342–7.
36. Bogart JA, Alpert TE, Kilpatrick MC, Keshler BL, Pohar SS, Shah H, et al. Dose-intensive thoracic radiation therapy for patients at high risk with early-stage non-small-cell lung cancer. Clin Lung Cancer. 2005;6:350–4.
37. Zehentmayr F, Wurstbauer K, Deutschmann H, Fussl C, Kopp P, Dagn K, et al. DART-bid: dose-differentiated accelerated radiation therapy, 1.8 Gy twice daily: high local control in early stage (I/II) non-small-cell lung cancer. Strahlenther Onkol. 2015;191:256–63.
38. Onimaru R, Shirato H, Shimizu S, Kitamura K, Xu B, Fukumoto S, et al. Tolerance of organs at risk in small-volume, hypofractionated, image-guided radiotherapy for primary and metastatic lung cancers. Int J Radiat Oncol Biol Phys. 2003;56:126–35.
39. Xia T, Li H, Sun Q, Wang Y, Fan N, Yu Y, et al. Promising clinical outcome of stereotactic body radiation therapy for patients with inoperable stage I/II non-small-cell lung cancer. Int J Radiat Oncol Biol Phys. 2006;66:117–25.
40. Fritz P, Kraus HJ, Blaschke T, MAhlnickel W, Strauch K, Engel-Riedel W, et al. Stereotactic, high single-dose irradiation of stage I non-small cell lung cancer (NSCLC) using four-dimensional CT scans for treatment planning. Lung Cancer. 2008;60:193–9.
41. Onimaru R, Fujino M, Yamazaki K, Onodera Y, Taguchi H, Katoh N, et al. Steep dose-response relationship for stage I non-small-cell lung cancer using hypofractionated high-dose irradiation by real-time tumor-tracking radiotherapy. Int J Radiat Oncol Biol Phys. 2008;70:374–81.
42. Baumann P, Nyman J, Hoyer M, Wennberg B, Gagliardi G, Lax I, et al. Outcome in a prospective phase II trial of medically inoperable stage I non-small-cell lung cancer patients treated with stereotactic body radiotherapy. J Clin Oncol. 2009;27:3290–6.
43. Brown WT, Wu X, Fayad F, Fowler JF, García S, Monterroso MI, et al. Application of robotic stereotactic radiotherapy to peripheral stage I non-small cell lung cancer with curative intent. Clin Oncol (R Coll Radiol). 2009;21:623–31.
44. Fakiris AJ, McGarry RC, Yiannoutsos CT, Papiez L, Williams M, Henderson MA, et al. Stereotactic body radiation therapy for early-stage non-small-cell lung carcinoma: four-year results of a prospective phase II study. Int J Radiat Oncol Biol Phys. 2009;75:677–82.
45. Kopek N, Paludan M, Petersen J, Hansen AT, Grau C, Hoyer M. Co-morbidity index predicts for mortality after stereotactic body radiotherapy for medically inoperable early-stage non-small cell lung cancer. Radiother Oncol. 2009;93:402–7.
46. Stephans KL, Djemil T, Reddy CA, Gajdos SM, Kolar M, Mason D, et al. A comparison of two stereotactic body radiation fractionation schedules for medically inoperable stage I non-small cell lung cancer: the Cleveland clinic experience. J Thorac Oncol. 2009;4:976–82.
47. Baba F, Shibamoto Y, Ogino H, Murata R, Sugie C, Iwata H, et al. Clinical outcomes of stereotactic body radiotherapy for stage I non-small cell lung cancer using different doses depending on tumor size. Radiat Oncol. 2010;5:81.
48. Crabtree TD, Denlinger CE, Meyers BF, El Naqa I, Zoole J, Krupnick AS, et al. Stereotactic body radiation therapy versus surgical resection for stage I non-small cell lung cancer. J Thorac Cardiovasc Surg. 2010;140:377–86.
49. Timmerman R, Paulus R, Galvin J, Michalski J, Straube W, Bradley J, et al. Stereotactic body radiation therapy for inoperable early stage lung cancer. JAMA. 2010;303:1070–6.
50. Videtic GMM, Stephans K, Reddy C, Gajdos S, Kolar M, Clouser E, et al. Intensity-modulated radiotherapy-based stereotactic body radiotherapy for medically inoperable early-stage lung cancer: excellent local control. Int J Radiat Oncol Biol Phys. 2010;77:344–9.
51. Andratschke N, Zimmermann F, Boehm E, Schill S, Schoenknecht C, Thamm R, et al. Stereotactic radiotherapy of histologically proven inoperable stage I non-small cell lung cancer: patterns of failure. Radiother Oncol. 2011;101:245–9.
52. Hamamoto Y, Kataoka M, Yamashita M, Nogami N, Sugawara Y, Kozuki T, et al. Factors affecting the local control of stereotactic body radiotherapy for lung tumors including primary lung cancer and metastatic lung tumors. Jpn J Radiol. 2012;30:430–4.
53. Lagerwaard FJ, Verstegen NE, Haasbeek CJA, Slotman BJ, Paul MA, Smit EF, et al. Outcomes of stereotactic ablative radiotherapy in patients with potentially operable stage I non-small cell lung cancer. Int J Radiat Oncol Biol Phys. 2012;83:348–53.
54. Shibamoto Y, Hashizume C, Baba F, Ayakawa S, Manabe Y, Nagai A, et al. Stereotactic body radiotherapy using a radiobiology-based regimen for stage I non-small cell lung cancer: a multicenter study. Cancer. 2012;118:2078–84.
55. Shirata Y, Jingu K, Koto M, Kubozono M, Takeda K, Sugawara T, et al. Prognostic factors for local control of stage I non-small cell lung cancer in stereotactic radiotherapy: a retrospective analysis. Radiat Oncol. 2012;7:182.
56. Takeda A, Kunieda E, Sanuki N, Aoki Y, Oku Y, Handa H. Stereotactic body radiotherapy (SBRT) for solitary pulmonary nodules clinically diagnosed as lung cancer with no pathological confirmation: comparison with non-small-cell lung cancer. Lung Cancer. 2012;77:77–82.
57. Inoue T, Katoh N, Onimaru R, Shimizu S, Tsuchiya K, Suzuki R, et al. Stereotactic body radiotherapy using gated radiotherapy with real-time tumor-tracking for stage I non-small cell lung cancer. Radiat Oncol. 2013;8:69.
58. Takeda A, Sanuki N, Eriguchi T, Kaneko T, Morita S, Handa H, et al. Stereotactic ablative body radiation therapy for octogenarians with non-small cell lung cancer. Int J Radiat Oncol Biol Phys. 2013;86:257–63.
59. Hamaji M, Chen F, Matsuo Y, Kawaguchi A, Morita S, Ueki N, et al. Video-assisted thoracoscopic lobectomy versus stereotactic radiotherapy for stage I lung cancer. Ann Thorac Surg. 2015;99:1122–9.
60. Rwigema JC, Chen AM, Wang PC, Lee JM, Garon E, Lee P. Incidental mediastinal dose does not explain low mediastinal node recurrence rates in patients with early-stage NSCLC treated with stereotactic body radiotherapy. Clin Lung Cancer. 2014;15:287–93.
61. Guckenberger M, Klement RJ, Allgauer M, Appold S, Dieckmann K, Ernst I, et al. Applicability of the linear-quadratic formalism for modeling local tumor control probability in high dose per fraction stereotactic body radiotherapy for early stage non-small cell lung cancer. Radiother Oncol. 2013;109:13–20.

Details of the search made in PubMed (July 2015):

(early stage[Title] OR early-stage[Title] OR stage I[Title] OR stage II[Title]) AND (non-small cell lung cancer[Title] OR non-small-cell lung cancer[Title] OR non-small cell lung cancer[Title] OR NSCLC[Title] OR lung cancer[Title] OR lung tumors[Title] OR lung tumor[Title] OR lung carcinoma[Title]) AND (radiother*[Title] OR SBRT[Title] OR stereotactic[Title] OR irradiation[Title] OR radiation[Title])

Number of records identified through database searching: 441
Number of records after duplicates removed: 441
Number of records screened: 441
Number of records excluded: 441-192=249
Number of full-text articles assessed for eligibility: 192
Number of full-text articles excluded, with reasons: 192-31=161 did not fulfill the selection criteria
Number of additional records identified through other sources: Four files found: Hamamoto12 , Onimaru03 , Takeda12 , Takeda13.
Number of studies included in this quantitative analysis: 31 studies, 8 3DCRT + 23 SBRT.

Table 1: Detailed characteristics of included studies with conventionally fractionated treatment schedules

Reference	Tumor Stage	No. Pats	Histology	Location	Schedule, Total Treatment Time Prescription	Total Dose at isocenter [Gy]	Volume Definition	LC [%]	CSS [%]	OS [%]	FU median (range) [m]
Kaskowitz	stage IA/IB 20 T1 - 33 T2, N0	53	11 ade, 32 scc, 4 lc, 6 nos	ns	median 63 (40 - 80) Gy, conv. fractionation, dose point not specified	63$	target: tumor + 1.5 cm (estimated from port films), elective nodal RT	3y: 51	3y: 33 5y: 13	3y: 19 5y: 6	ns
Jeremic	stage IA/IB 25 T1 - 24 T2, N0	49	18 ade, 23 scc, 7 lc, 1 nos	25 p 24 c	69.6 Gy in 1.2 Gy/f (twice a day), 40 days, to isocenter	70	PTV: tumor + ipsilateral hilus + 2 cm	3y: 55 5y: 55		3y: 47 5y: 30	ns
Hayakawa	stage IA/IB 7 T1 – 29 T2, N0	36	16 ade, 19 scc, 1 lc	p	60 - 81 Gy in 2 Gy/f, 48 days, to isocenter	67§	target not specified, 28 % patients elective nodal RT to 38 - 50 Gy	3y: 72 5y: 72	3y: 56 5y: 39	3y: 42 5y: 23	(36 - 216)
Cheung	stage IA/IB 18 T1 - 15 T2, N0	33	10 ade, 13 scc, 5 lc, 5 nos	27 p 6 c	48 Gy in 4 Gy/f, maximum 3 weeks, to isocenter	48	target: GTV + 1 - 1.5 cm, no elective nodal RT	3y: 63	3y: 36	3y: 32	23&
Langendijk	stage IA/IB 26 T1 - 20 T2, N0	46	2 ade, 23 scc, 10 undiff, 11 unknown	37 p 9 c	70 Gy in 2 Gy/f, 7 weeks to isocenter, Dmin(PTV)= 90 %	70	CTV: GTV + 1.5 cm; PTV_{46Gy}: CTV + 0.5 cm, PTV_{70Gy}: GTV + 1 cm; elective nodal RT	3y: 50		3y: 22	36&
Bradley	stage IA/IB 31 T1 - 25 T2, N0	56	14 ade, 25 scc, 6 lc, 11 nos	p	60 - 84 Gy in 1.8 - 2 Gy/f, 6 - 8 weeks to isocenter	70$	PTV: GTV + 1 cm (increased if tumor moved) 39 % patients elective nodal RT	3y: 63	3y: 51	3y: 34	20 (6 - 72)
Bogart	stage IA/IB 19 T1 - 12 T2, N0	31	9 ade, 8 scc, 1 lc, 13 nos	ns	median 70 Gy in 2.25 - 3.7 Gy/f, 5.5 weeks, 95 % dose covering PTV	70$	PTV: GTV + 1 - 1.5 cm (increased if tumor moved), no elective nodal RT	3y: 83 5y: 83		3y: 64 5y: 19	29&
Zehentmayr	stage I	40 +14 stage II	16 ade, 33 scc, 7 nos* 14 stage II reported together, but not in LC	36 p 2 c	Median 79.2 (73.8-90.4) Gy in 1.8 Gy/f twice daily in 2-3 weeks, dose point not specified	79	Slow CT, PTV: GTV + 7mm	3y: 91			28.5 (2-108)
Median		**43**				**70**		**3y: 63 5y: 72**	**3y: 43.5**	**3y: 34 5y: 21**	**28.5 (2 - 216)**

FU: follow-up, §: mean value, $: median value, ade: adenocarcinoma, scc: squamous cell carcinoma, ba: bronchio-alveolar, lc: large cell carcinoma, nos: not otherwise specified, undiff: undifferenciated, non-scc: non-squamous cell carcinoma, ns: not specified, &: pats alive at the end of follow up, p: peripheral, c: central.
Kaskowitz: 54% of total patients received total doses between 60 and 70 Gy, with a median difference in total treatment time of 5 days, the maximal difference was 28 days. Hayakawa: Standard deviation of 7 Gy in the total dose and 8 days in total treatment time.
Cheung: included 4 patients with N1. Bradley: A majority of patients (42%) were receiving between 70 and 83 Gy. Bogart: Total doses range from 60 to 80 Gy, “most frequently 70 Gy” (sic).

Table 2: Detailed summary of hypofractionated data.

Reference	Tumor Stage	No Pats	Histology	Location	Schedule, Total Treatment Time Prescription	Total Dose at isocenter [Gy]	Volume definition	LC [%]	CSS [%]	OS [%]	FU median (range) [m]
Onimaru '03	stage IA/IB 17 T1 - 8 T2, N0	25	14 ade, 8 scc, 3 nos	p	48 Gy in 6 Gy/f or 60 Gy in 7.5/f, 2 weeks, to isocenter, Dmin(PTV) = 80 %	48[$]	CTV = GTV, ITV: CTV in free breathing, exhale, and inhale, PTV: ITV+ 0.5 cm	3y: 55	2y: 60	2y: 47	18 (2-44)[#]
Xia	stage IA/IB 25 (T1 + T2), N0	25	all with pathological confirmation	p, c	50 Gy in 5 Gy/f in 2 weeks 50 % isodose to PTV edge	100	CTV = GTV PTV: GTV + 1 cm	3y: 96		3y: 91	27 (24 - 54)
Fritz	stage IA/IB 22 T1 - 18 T2, N0	40	ade 17, scc 8, lc 13, nos 2	p	30 Gy in 1 single fraction, to isocenter, to cover 80 % of PTV, 90 % of GTV	30	CTV: GTV, ITV: CTV, mid-cycle, inhale, exhale, PTV: ITV + 1 cm axial, 1.5 cm cc	3y: 81	3y: 57	3y: 66	20 (6 - 62)
Onimaru '08	stage IA/IB 13 T1 - 28 T2, N0	41	30 ade, 10 scc, 1 lc	p	40 Gy in 10 Gy/f or 48 Gy in 12Gy/f, 1 week, to isocenter, Dmin(PTV) = 80 %	48[$]	CTV = GTV (CT end exhale)+6-8 mm, PTV: CTV+ 0.5 cm	3y: 57	3y: 53	3y: 47	27[&] (9 - 62)
Baumann	stage IA/IB 40 T1 - 17 T2, N0	57	19 ade, 8 scc, 1 lc, 10 nos, 19 ns	ns	45 Gy in 15 Gy/f, in median 5 (4-15) days to 67 % isodose to PTV edge	66	CTV: GTV +2mm PTV: CTV + 0.5-1.0cm axial, 1 cm cc	3y: 92	3y: 88	3y: 60	35 (4 - 47)
Brown	stage IA/IB 20 T1 - 11 T2, N0	31	8 ade, 1 scc, 1 ba, 21 nos	p	60 - 67.5 Gy in 3 or 5 fractions, prescribed to the 60-80% isodose line	88[$]	CTV: GTV + 0.6 cm, PTV: CTV + 0.2 cm, tumor tracking mit CyberKnife	3y: 86		3y: 84	28 (24 - 53)
Fakiris	stage IA/IB 34 T1 - 36 T2, N0	70	ns	22 c 48 p	60 Gy in 20 Gy/f or 66 Gy in 22Gy/f, to 80 % isodose at PTV edge	83[$]	CTV = GTV PTV: CTV + 0.5-1 cm axial, 1 cm cc	3y: 88	3y: 82 5y: 70	3y: 43 5y: 17	50 (1 - 65)
Kopek	stage IA/IB 51 T1 - 36 T2, N0	88	30 ade, 34 scc, 24 nos	62 p 26 c	45 Gy in 15 Gy/f or 67.5 Gy in 22.5 Gy/f to isocenter in 5-8 days, minD(PTV)=67%	45[$]	CTV = GTV PTV: CTV + 0.5 cm axial and 1 cm cc	3y: 89	3y: 70	3y: 37	44 (2 - 97)
Stephans	stage IA/IB 42 T1 - 14 T2, N0	56	9 ade, 20 scc, 7 undiff/other, 20 ns	p, c	50 Gy in 10 Gy/f in 11 (8 - 14) days, 97 - 100 % isodose to PTV egde	70	ITV: GTV in free breathing, inhale, ex-hale, PTV: ITV + 0.5 cm axial + 1 cm cc	3y: 97		3y: 50	20 (2 - 48)
Baba	T1 87, T2 37	124	66 ade, 35 scc, 13 nos, 10 unproven	nn	48/52 Gy in 12/13 Gy/f in 11 (8 – 14) days, to isocenter, Dmin(95% PTV) =80%	48[$]	CTV = GTV, ITV: CTV in 3 breathing phases, PTV: ITV + 0.5 cm axial, 1 cm cc	3y: 80			26 (7 - 66)
Crabtree	stage IA/IB 57 T1 - 19 T2, N0	76	ns	ns	54 Gy in 18 Gy/f, in 8 to 14 days, to the 80 % to 85 % isodose line	68	ns	3y: 89	3y: 67	3y: 32	19
Timmerman	stage IA/IB 44 T1 - 11 T2, N0	55	19 ade, 17 scc, 16 nos, 3 lc undiff	p	54 Gy in 18 Gy/f in maximum 2 weeks 100 % isodose to PTV edge	79	CTV = GTV PTV: CTV + 0.5 cm axial, 1 cm cc	3y: 98	3y: 55	3y: 48	34 (5 - 50)
Videtic	stage IA/IB 22 T1 - 6 T2, N0	26	13 ade, 4 scc, 3 nos, 8 ns	25 p 3 c	50 Gy in 10 Gy/f, 5 days, PTV enclosed by 95 % isodose line, IMRT planning	54	ITV: GTV in free breathing, exhale, and inhale, PTV: ITV(=CTV) + 0.3-0.5 cm	3y: 94		3y: 52	31 (10 - 51)
Andratschke	stage IA/IB 31 T1 - 61 T2,	92	35 ade, 49 scc, 2 ba, 6 nos	24 c 68 p	24-45 Gy in 3-5 fractions in 5-12 days, to 60 % isodose to PTV edge	62[$]	CTV = GTV, ITV: CTV in slow CT PTV: ITV + 0.5 cm axial and 1 cm cc	3y: 83 5y: 83	3y: 64 5y: 48	3y: 38 5y: 17	21 (3 - 87)

	N0										
Hamamoto	stage IA/IB 101 T1 - 27 T2, N0	128	ns	ns	48 or 60 Gy in 9.2-14 Gy/f ,in 4 to 10 days, to isocenter, Dmin(PTV) = 90 %	48$	ITV: GTV with slow CT, PTV: ITV + 0.5 cm	3y: 85			18 (1 - 60)
Lagerwaard	stage IA/IB 106 T1 - 71 T2, N0	177	20 ade, 16 scc, 24 nos, 117 ns	p, c	5 × 12 Gy, 3 × 20 Gy, or 8 × 7.5 Gy in 2 weeks, to 80 % isodose at PTV edge	75$	CTV = GTV, ITV: GTV from 10 resp. phases, PTV: ITV + 3mm	3y: 93 5y: 93		3y: 85 5y: 51	32
Shibamoto	T1 - T2		104 ade, 60 scc, 16 nos	35 c 145 p	dosage depended on size, T1: 48 Gy, T2: 52 Gy		CTV = GTV, ITV: CTV in 3 resp. phases PTV: ITV + 0.5 cm axial + 1 cm cc	3y: 83 5y: 83	3y: 83 5y: 69	3y: 69 5y: 52	36 (42[&])
Shibamoto d2	124 T1, N0	124			48 Gy in 12 Gy/f, in 9 to 21 days, 95 % of the ITV > 94 % of presc. dose	48		3y: 86			
Shibamoto d3	52 T2, N0	52			52 Gy in 13 Gy/f, in 9 to 21 days, 95 % of the ITV > 94 % of prescribed dose	52		3y: 73			
Shirata	stage IA/IB 63 T1 - 18 T2, N0	80	33 ade, 22 scc, 5 lc, 20 nos		prescription to isocenter, Dmin(PTV) = 90 %		CTV: GTV + 0-0.5 cm, PTV: CTV + 0.5-1 cm, individualized margins	3y: 89	3y: 97	3y: 90	30 (0.3 - 79)
Shirata, d1		45			48 Gy in 12 Gy/f	48		3y: 100			
Shirata, d2		29			60 Gy in 7.5 Gy/f	60		3y: 82			
Takeda			ade 64, scc 38, nos 13, ns 58	p, c	in one week, to 80 % isodose at PTV edge		ITV: GTV in slow CT (6-8 s/slice) PTV: ITV + 0.6-0.8 cm (indiv. margins)				
Takeda, d1	27 (10 T1 + 17 T2)~	27			40 Gy in 8 Gy/f	50		3y: 72			21 (6 - 64)
Takeda, d2	138 (91 T1 + 47 T2)~	138			50 Gy in 10 Gy/f	63		3y: 87			21 (6 - 64)
Inoue	stage IA/IB 79 T1 - 30 T2, N0	109	65 ade, 29 scc, 1 lc, 8 nos, 6 ns	ns	45 Gy in 15 Gy/f or 48 Gy in 12 Gy/f in 4 to 7 days, to isocenter	48$	CTV: GTV + 5 – 8mm PTV: CTV + 5mm	3y: 81 5y: 78		3y: 69 5y: 64	25 (4 - 72)
Takeda	stage IA/IB 67 T1 - 42 T2, N0	109	41 ade, 13 scc, 8 nos, 47 ns	34 c 75 p	40 or 50 Gy in 8 or 10 Gy/f, in 5 days, to 80 % isodose at PTV edge	63$	ITV: GTV in slow CT PTV: ITV + 0.6-0.9 cm	3y: 84.4	3y: 71	3y: 54	24 (3 - 65)
Hamaji	75 T1, 29 T2	104	ade: 54, scc: 34, large cell ca 4, others 0, nos 12	nn	48 Gy in 12 Gy/f in 5 days, to isocenter	48	ITV= GTV w/ slow CT/4DCT, PTV= ITV + 5mm	3y: 76.7			43 (6 - 115)
Rwigema	40 Ia, 6 Ib	46	ade 35, scc 4, adenosquamous 2, nos: 5	41 p 5 c	54 Gy in 18 Gy/f in 5 days, to PTV edge	70	4DCT, ITV-MIP 8 phases, PTV=ITV+3mm transv+6mm in long direction	3y: 95.5			16.8 (0.6 – 38.9)
Median		**57**				**57.0**		**3y: 85.9 5y: 83**	**3y: 70 5y: 69**	**3y: 54 5y: 51**	**27 (0.3 - 115)**

FU: follow-up, §: mean value, $: median value, ade: adenocarcinoma, scc: squamous cell carcinoma, ba: bronchialveolar, lc: large cell carcinoma, nos: not otherwise specified, undiff: undifferenciated, non-scc: non-squamous cell carcinoma, ns: not specified, #: includes the patients with metastases, &: patients alive at the end of follow-up, p: peripheral, c: central.
Onimaru03: local control for the NSCLC group only, 12 Gy difference in total dose among patients, 17 patients got 48 Gy versus 8 patients who got 60 Gy in total with the same number of

fractions.
Onimaru08: 8 Gy difference in total dose among patients, 13 patients received 40 Gy and 28 patients 48 Gy both with four fractions.
Baba: 8 Gy difference in total dose among patients. All 30 stage IA lesions were treated with 48 Gy, and 12 stage IB lesions were treated with 52 Gy, all in 4 fractions.
Xia: stage I pats 25/43.
Brown: 26 out of 31 patients received 60 Gy, most frequently in 3 fractions (24/31).
Kopek: plus one patient T3 N0. Total dose to isocenter was 45 Gy for 62/88 patients, or 67.5 Gy for 26/88 patients who beared peripheral lesions, all delivered in three fractions.
Andratschke: large cohort with most tumors receiving total doses of 24 - 45 Gy in 3 - 5 fractions.
Hamamoto: large cohort of 128 NSCLC patients, the majority received 48 Gy in 4 fractions.
Lagerwaard: 177 patients in total, 82/177 (46%) got 12 Gy per fraction. Maximal difference in the number of fractions is 5.
Takeda: proportion T1-T2 tumors, via personal communication with the authors.

Table 3: Summary of the models for biologically effective doses calculated at isocenter and PTV edge with a constraint to make the logistic curves approach the coordinate origin; all fit parameter values are provided with standard errors (and 68% CI).

Model concept and dataset		**α/β (std error) [Gy]**	**D_t (std error) [Gy]**	**TCD_{50} CI 68% [Gy]**	**k CI 68% [Gy]**	**γ_{50} (std error) [%/%]**	**AIC**
			ISOCENTER				
LQ with constraint at (0,0)	**CF + HF**	**α/β = 10**	-	72.6 (68.2-74.9)*	22.8 (20.1-25.5)*	0.79(0.11)	-4773.8
	CF	**α/β = 10**	-	71.2 (67-74.9)*	16.4 (12.0-20.8)*	1.08(0.36)	-267.1
	HF	**α/β = 10**	-	75.9 (71.0-81.0)*	21.5 (17.9-24.8)*	0.88(0.17)	-2875.8
LQ: free α/β with constraint at (0,0)	**CF + HF**	12.6(10.5-15.0)*	-	67.1(62.4-71.7)*	19.3(15.7-23.0)*	0.87(0.17)	-4780.1
	CF	3.9(2.4-6.6)	-	90.8(77.4-110.0)*	18.3(12.7-27.0)	1.24(0.59)	-270.1
			PTV EDGE				
LQ with constraint at (0,0)	**CF + HF**	**α/β = 10**	-	54.6 (51.5-57.6)*	18.3 (16.1-20.6)*	0.74(0.12)	-4761.9
	CF	**α/β = 10**	-	66.5 (62.7-69.9)*	15.5 (11.6-19.5)*	1.07(0.33)	-266.8
	HF	**α/β = 10**	-	51.5 (48.3-54.7)*	17.2 (15.1-17.2)*	0.75(0.12)	-5294.6
LQ: free α/β with constraint at (0,0)	**CF + HF**	5.8(4.7-7.1)*	-	69.7(63.1-77.0)*	23.2(19.6-27.5)	0.75(0.16)	-4764.7
	CF	4.2(2.4-8.0)	-	81.3(68.8-99.4)	17.7(12.5-25.5)	1.15(0.62)	-267.8

* p value < 0.05

Table 4: Doses per fraction at isocenter and PTV edge, calculated according to the information provided in the references (prescription in bold characters).

Reference	d @ Isocenter	d @ PTV edge	Comment
Conventionally fractionated treatment schedules			
Kaskowitz 1993	**1.8**	1.7	If no minimal dose to the PTV was explicitly reported, it was assumed to be 95% dose, according to ICRU recommendations. This was done for all the conventional treatments. Ratios deviate from 0.95 because of rounding error.
Jeremic 1997	**1.2**	1.1	
Hayakawa 1999	**2**	1.9	
Cheung 2002	**4**	3.8	
Langendijk 2002	**2**	1.9	
Bradley 2003	**1.9**	1.8	
Bogart 2005	**2.5**	2.4	
Zehentmayr 2015	**1.8**	1.7	
Hypofractionated treatment schedules			
Onimaru 2003	**6**	4.8	The dose was prescribed at the isocenter, with the 80% line encompassing the PTV
Xia 2006	10	**5**	The 50% isodose line covered 100% PTV, therefore it was assumed that dose at isocenter was twice the prescription
Fritz 2008	**30**	24	The dose prescribed to the isocenter was 30 Gy. Of the prescribed isocenter dose, at least 90% covered the gross tumor volume (GTV = CTV) and at least 80% the PTV.
Onimaru 2008	**12**	9.6	The dose was prescribed at the center of the PTV, aim was the inclusion of the PTV in the 80% isodose
Baumann 2009	22	**15**	The patients were treated with a dose of 15 Gy times three at about the 67% isodose to the periphery of the PTV, resulting in a central dose of about 22 Gy x 3. More specifically the mean of the maximum dose/fraction to PTV was 22.8 Gy (SD, 3.1 Gy) and the average value of the mean dose/fraction to CTV was 21.6 Gy (SD, 3.0 Gy).
Brown 2009	29.4	**20**	A 60-67.5 Gy dose was prescribed to the 60-80% isodose line (median 65%) and given in three to five fractions
Fakiris 2009	27.5	**22**	The treatment dose was prescribed to the 80% isodose volume
Kopek 2009	**15**	10.1	The prescription dose (45 Gy or 67.5 Gy in three fractions) was delivered to the isocenter. The CTV was encompassed by the 95% isodose surface while the PTV was completely covered by the 67% isodose surface. This corresponds to a minimum dose to the PTV of 30 Gy or 45 Gy in three fractions, depending on the central prescribed dose.
Stephans 2009	14	**10**	Patients treated to 60 Gy were typically planned using three or more dynamic arcs without heterogeneity corrections prescribed to the 81 to 90% isodose line (as allowed by RTOG 0236).
Baba 2010	**12**	9.6	The dose was prescribed at the isocenter; 95% of the PTV was ensured to be covered with at least 80% of the prescribed isocenter dose.
Crabtree 2010	22.5	**18**	The dose is typically prescribed to the 80% to 85% isodose line, meaning that the center of the tumor received a dose that is 15% to 20% higher than the prescription.
Timmerman 2010	26.3	**18**	Edge of the PTV, 95% of PTV received 100% of prescribed dose; from Xiao and Papiez related publication: isocenter dose ranges from 71.3 Gy to 88.9 Gy (mean 78.8 Gy, SE 1.1 Gy, ie 26.3 Gy per fraction). This was a s study based on a subset of 20 patients of the RTOG 0236 trial.

Videtic 2010	10.8	**10**	Prescription: minimum dose in median to the PTV was 9.9Gy (~10Gy), and max dose in median was 10.8Gy. It was assumed that the dose at the isocenter was similar to the maximum dose inside the PTV (stage I, small tumor volumes).
Andratschke 2011	20.8	**12.5**	Doses were prescribed to the 60% isodose covering the planning target volume (PTV)
Hamamoto 2012	**12**	10.8	Leaf margins were arranged so that the 90–95 % isodose line covered the PTV. The dose calculation algorithm was the pencil beam method; this algorithm did not use heterogeneity correction. In SBRT, 48–60 Gy in 4–5 fractions was delivered to the isocenter
Lagerwaard 2012	15	**12**	All fractionation schemes used were prescribed to the encompassing 80% isodose
Shibamoto d2	**12**	9.6	The prescribed dose represented the dose delivered to the isocenter. It was recommended to cover 95% of the PTV with at least 90% of the isocenter dose; in all patients, 95% of the PTV received at least 80% of the prescribed dose. Consequently, 95% of the ITV was covered with !94% of the prescribed dose in all but 1 patient.
Shibamoto d3	**13**	10.4	
Shirata 2012 d1	**12**	10.8	The target reference point was defined as the center of the PTV, and the dose was prescribed for its point. PTV was encompassed by the minimum 90% dose line of the reference point dose as possible.
Shirata 2012 d2	**7.5**	6.8	
Takeda 2012 d1	**10**	8	The prescribed dose was defined as 80% of the maximal dose and its isodose line encompassed the PTV surface. Then the median D95 was consistent with the prescribed dose. For peripheral tumors, a total of 50 Gy/5 fractions/ 5 days was prescribed. For tumors adjacent to critical organs such as trachea, main bronchus, pulmonary artery and esophagus, the total dose was decreased to 40 Gy/5 fractions/ 5 days.
Takeda 2012 d2	**12.5**	10	
Inoue 2013	**12**	9.6	Using a superposition algorithm, they administered 48 Gy in 4 fractions at the isocenter in 2005–2006 (n = 30) and 40 Gy in 4 fractions to the 95% volume of PTV in 2007–2010 (n = 79) with a treatment period of 4 to 7 days. Isocenter dose of 40 Gy in 4 fractions to the 95% volume of PTV was approximately ranged from 45 to 50 Gy. Therefore it was used 12 Gy at isocenter and 9.6 Gy (80%) at edge. Good approximation (min dose 38.4 Gy)
Takeda 2013	12.5	**10**	80% isodose of the maximum dose at PTV periphery
Hamaji 2015	**12**	9.6	Prescription to the isocenter, it was not specified which isodose line surrounds the PTV. It was assumed the 80%.
Rwigema 2015	23.4	**18**	To PTV edge, coverage at 95% of PTV normalized to prescription dose. Heterogeneity in PTV of 15-40%

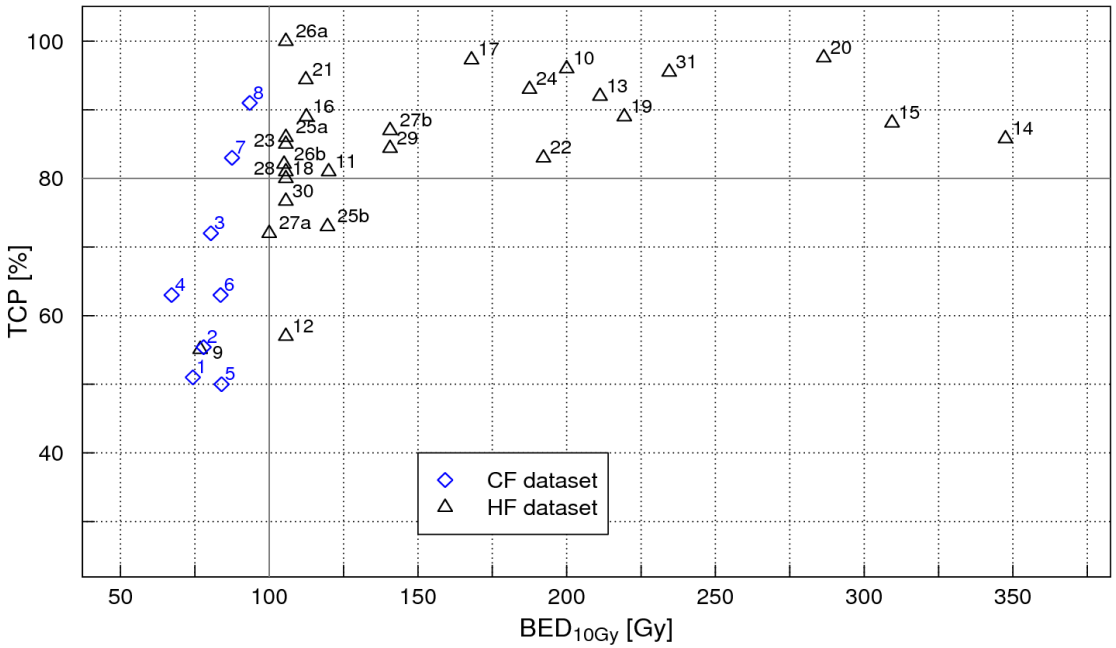

Figure 1: Local control of the conventionally fractionated dataset (blue) and hypofractionated dataset (black) versus BED_{10} calculated at the isocenter, with reference numbers.

7 Appendix

7.1 Academic Faculty

In Dresden

Abolmaali

Abramyuk

Baumann

Cordes

Dörr

Enghardt

Geyer

Helm

Henniger

Herrmann

Hietschold

Hoinkis

Just

Koch

Krause

Kunz-Schughart

Laniado

Lehmann

Pawelke

Steinbach

Zips

In Marburg

Engenhart-Cabillic

Wittig

Zink

7.2 Acknowledgments

I would like to thank everybody who in one way or another contributed to the creation of this work. In first place, I want to thank my supervisor, Prof. Dr. Andrea Wittig for entrusting me with this project as well as for her continuous support and insightful comments. I equally want to thank Prof. Dr. Rita. Engenhart-Cabillic for her continuous encouragement.

My sincere thanks to Prof. Dr. Peter Fritz and Dr. Werner Mühlnickel for giving me access to their clinical data and for answering all my related questions. I want to acknowledge Dr. Urszula Jelen and Filippo Ammazzalorso for their help in both technical and scientific aspects in the initial phases of this project, and Dr. Steffen Barzcyk for the enriching scientific discussions on modeling for the second part of this work. Warmest thanks to the staff and secretariat of the Radiotherapy Clinic for their kind support whenever it was needed.

I acknowledge the funding of the Anneliese Pohl Stiftung granted to Prof. Dr. Wittig, which made this work possible.

I am deeply grateful to Prof. Klaus R. Trott for his trust in me and for giving me the chance to enter the field or radiotherapy research, and to Prof. Dr. Michael Baumann, working with whom helped me to acquire a wider perspective of the same.

My gratitude also goes to all the colleagues that helped me along the way, especially Marie Anne Chanrion, the perfect office mate with whom I shared and enjoyed endless discussions about topics related to our respective projects as well as about everything else.

I would also like to thank my friends and my sister for their understanding and support during these years. My last recognition goes out to Toke for encouraging me throughout this experience and for balancing the difficult moments with his natural optimism, and to our son Leo, who had a very inspiring way of eating my papers while sitting on my lap at the computer.